Designing a Next-generation Epstein-Barr Virus Vaccine

Harman Malhi

A dissertation

submitted in partial fulfillment of the

requirements for the degree of

Doctor of Philosophy

University of Washington

2022

Reading Committee:

Andrew McGuire, Chair

Richard James

Neil P. King

Program Authorized to Offer Degree:

Molecular Medicine and Mechanisms of Disease

University of Washington

Abstract

Designing a Next-generation Epstein-Barr Virus Vaccine

Harman Malhi

Chair of the Supervisory Committee:

Andrew McGuire

Vaccine and Infectious Disease Division

Fred Hutchinson Cancer Center

Epstein-Barr virus (EBV) is a cancer-associated pathogen responsible for 165,000 deaths per year. EBV is also the etiological agent of infectious mononucleosis and is associated with multiple sclerosis and rheumatoid arthritis. Thus, an EBV vaccine could alleviate significant morbidity and mortality. EBV is orally transmitted and has tropism for both epithelial cells and B cells. Therefore, a vaccine would need to prevent infection of both cell types in the oral cavity. I describe how the passive transfer of AMMO1, a dual-tropic neutralizing monoclonal antibody targeting the viral gH/gL glycoprotein complex, prevents experimental EBV infection in humanized mice and rhesus macaques, suggesting that gH/gL is an attractive vaccine candidate. Spurred by these findings, we produced and evaluated the immunogenicity of several nanoparticle immunogens displaying gH/gL with distinct valencies and geometries. After one or two immunizations, all nanoparticles elicited superior binding and neutralizing titers relative to monomeric gH/gL. Antibodies elicited by a computationally designed self-assembling nanoparticle that displays 60 copies of the gH/gL protein conferred protection against a lethal dose of EBV in a humanized mouse challenge model, whereas antibodies elicited by monomeric gH/gL did not. Taken together, these data motivate further development of nanoparticle vaccine candidates for EBV which target the gH/gL glycoprotein.

Dedication

I dedicate this dissertation to my family. It is just as much theirs as it is mine.

To my mother, Pirtpaul, for teaching me to value education. Her life is a testament to how education can open doors for you that you never thought possible.

To my father, Gurcharan, for instilling in me the value of hard work. You embody the American ethos that with hard work and determination, anybody can succeed. I hope I can accomplish even a fraction of what you and mom have in your lifetimes.

To both my parents for leaving behind the only life they ever knew and coming to the United States. It is because of your sacrifices that I can live out my dream. I stand on the shoulders of giants.

To my sister Prabhjeet, for showing me the value in living life on your own terms. No matter what you do, others will have something to say. Happiness comes from being true to yourself.

To my sister Inderpal, for always reminding me of the importance of family. It is easy to get caught up in our own lives, but when we forget about our roots, we lose ourselves.

To my sister Simarjeet, for reminding me to always take care of myself. When life gets too stressful, it's always okay to step away and re-evaluate what is truly important to you.

Acknowledgements

Thank you to everyone in the McGuire lab, both past and present, not only for your contributions to my project, but for your support over the last three and a half years. First, thank you Andy for your mentorship over the last few years, and for being so supportive as I transition into the next stage of my career. With your help, I have grown a ton as a scientist, and I couldn't have hoped for a better environment to have done my PhD. There were bumps in the roads for both of us, sure, but I wouldn't change any of it. I also want to give a special thanks to Leah, who more than earned her spot as second author on the multimer paper. Leah, you deserve a ton of recognition for making all the protein I got to play with. It did not always look easy, but you rarely (if ever) complained about it. Keep being awesome. A big thank you to Kristina for all her help over the years, and more recently for taking over my project. Thank you to Yu-Hsin for the mouse training and to Bibhav for all his help with the humanized mouse work. And thank you to everyone in the lab for being there to bounce ideas off and for making the lab such a fun place to be.

Thank you to all our collaborators from the King Lab (Brooke, Andrew, Jing Yang, Carl, and Lauren), from the Olson Lab (Jason, Colin, and Simran), from the Pancera Lab (Suruchi), as well as Zoe Moodie, Barry Stoddard, and David Veesler. You were all instrumental in the publication of my manuscript.

And thank you to my committee members Richard James, Neil King, Jenny Lund, and Thomas Uldrick. Your guidance has helped me to identify and improve upon my weaknesses, play to my strengths, and ultimately to meet many of my thesis project aims.

Table of Contents

Chapter 1: Introduction x

I. Clinical Relevance x

a. Overview

b. Infectious Mononucleosis

c. Cancer

d. Multiple Sclerosis and Autoimmune Disease

e. Treatments

II. Viral Entry x

a. Overview

b. Viral Tropism

c. Proteins Involved in Viral Entry

III. Animal Models x

a. Overview

b. Non-human Primate Models

c. Mouse Models

d. Rabbit Model

e. Chinese Tree Shrew Model

IV. Vaccines x

a. Overview

b. Pre-existing Antibodies

c. Potential Vaccine Antigens

d. Recent Innovations

V. Summary x

Chapter 2: Immunization with a self-assembling nanoparticle vaccine displaying EBV gH/gL protects humanized mice against lethal viral challenge x

I. Summary x

II. Introduction x

III. Results x

a. Generation and Characterization of Multimeric gH/gL Vaccine Constructs

b. Immunogenicity of gH/gL nanoparticles

c. Plasma epitope mapping

d. Passive transfer of nanoparticle-elicited gH/gL mAbs protects against lethal challenge in humanized mice

IV. Discussion x

V. Figures x

a. Figure 1. Biochemical and Biophysical Characterization of multimeric gH/gL nanoparticles.

b. Figure 2. Immunogenicity of gH/gL nanoparticles.

c. Figure 3. Plasma competition against monoclonal anti-gH/gL antibodies.

d. Figure 4. Depletion of AMMO1-KO insensitive antibodies from pooled plasma.

e. Figure 5. gH/gL nanoparticle elicited antibodies protect humanized mice from lethal EBV challenge.

f. Figure S1. Related to Figure 1. 3D reconstruction of gH/gL-I3 60-mer.

g. Figure S2. Related to Figure 2. Inhibition of EBV infection of epithelial cells by gH/gL immune plasma.

h. Figure S3. Related to Figure 2. Inhibition of EBV infection in B cells by gH/gL immune plasma.

i. Figure S4. Related to Figure 3. Competitive binding between immune plasma and monoclonal antibodies.

j. Figure S5. Related to Figure 5. hCD19+ and hCD8+cell frequencies in humanized mice challenged with EBV.

k. Figure S6. Related to Figure 5. ELISA of pooled purified IgG used in transfer studies.

l. Figure S7. Related to Figure 5. Photographs of spleens from humanized mice challenged with EBV were taken at the time of necropsy.

m. Table S1. Yields of various gH/gL nanoparticles.

n. Table S2. Multimerization domains and observed and expected nanoparticle sizes.

VI. Methods x

a. Experimental Models

b. Cell Lines

c. Plasmids

d. Lentiviral Production

e. Lentiviral Transduction

f. Purification of Polyhistidine Tagged Proteins gH/gL His, gH/gL-KO, and gH/gL-cTRP(6)ss

g. Purification of gH/gL-4-mer (gH/gL-IMX313) and gH/gL-ferritin

h. Purification of gH/gL-I3

i. Size exclusion chromatography with multi-angle light scattering

j. Recombinant Antibodies

k. Negative-Stain Electron Microscopy

l. Immunizations in C57BL/6 Mice

m. IgG Purification from Murine Plasma

n. EBV-Reporter Virus Production

o. B cell Neutralization Assay

p. Epithelial Cell Neutralization Assay

q. Measurement of Plasma Antibody Endpoint Binding Titers by Anti-His Capture ELISA

r. Measure of Competitive Binding Titers by ELISA

s. Biotinylation of recombinant proteins

t. Neutravidin Capture ELISA

u. Measurement of total plasma IgG

v. Bead Depletion Assays

w. EBV Challenge in Humanized Mice

x. Quantitative PCR Analysis of Human Cells in HuCD34 Engrafted Mice

y. Biolayer Interferometry

z. Quantification and Statistical Analysis

Chapter 3: Neutralizing antibodies protect against oral transmission of lymphocryptovirus …….. x

I. Summary x

II. Introduction x

III. Results x

a. AMMO1 confers protection against high-dose EBV challenge in humanized mice

b. Compared to other neutralizing mAbs, AMMO1 provides superior protection against EBV challenge in humanized mice

c. AMMO1 cross-reacts with and neutralizes rhLCV

d. AMMO1 confers sterilizing immunity against rhLCV challenge in macaques

IV. Discussion x

V. Figures x

a. Figure 1. Biochemical and Biophysical Characterization of multimeric gH/gL nanoparticles.

VI. Methods x

a. Experimental Models

b. Cell Lines

c. EBV Infection in Humanized Mice

d. Antibody Expression Plasmids

e. Antibody Production

f. Rhesus macaque PBMC Isolation

g. Rhesus macaque Oral Swabs

h. Quantitative PCR Analysis of Human Cells in huCD34 Engrafted Mice

i. Digital Droplet PCR

j. rhLCV Viral Capsid Antigen ELISA

k. Detection of AMMO1 and VRC01 in Plasma

l. EBV Neutralization Assay in B cells:

m. rhLCV gH/gL Cell Surface Staining:

n. Virus-free Fusion Assay

o. rhLCV Virus Production:

p. rhLCV Titration

q. rhLCV Neutralization Assay

r. Quantification and Statistical Analysis

Chapter 4: Conclusions and Future Directions x

Appendix A: Bibliography x

Chapter 1: Introduction

I. Clinical Relevance

Overview

Epstein-Barr virus (EBV) is one of the most common human viruses, infecting about 95% of people worldwide.[1] It is a herpesvirus with tropism for both B cells and epithelial cells and is associated with several malignancies of these two cell types including Hodgkin lymphoma, Burkitt lymphoma, diffuse large B cell lymphoma, post-transplant lymphoproliferative disease, nasopharyngeal carcinoma and gastric carcinoma.[2-6] It is estimated that EBV is responsible for ~265,000 new cases of cancer and ~164,000 cancer deaths globally per year.[7] EBV is also the causative agent of infectious mononucleosis (IM), and has been linked to multiple sclerosis and rheumatoid arthritis.[8-14]

Infectious Mononucleosis

Acquisition of EBV as an adolescent or young adult typically results in infectious mononucleosis (IM). In one study of undergraduates aged between 18 and 22, 89% of study participants developed symptomatic infectious mononucleosis after primary infection with EBV.[15] IM is caused by an overreactive cytotoxic lymphocyte (CTL) response resulting from an initial failure of the immune system to control viral replication, which leads to highly elevated inflammatory cytokine release and resulting symptoms.[16-18] IM resolves after the CTL response eliminates most EBV infected cells. In fact, EBV is responsible for at least 90% of cases of infectious mononucleosis (IM).[19] Although IM is not considered to be a serious illness, IM symptoms can pose great physical limitations to those infected. These symptoms typically include extreme fatigue, fever, sore throat, head and body aches, swollen lymph nodes, and rash.[20] In most cases patients recover in 2 to 4 weeks, however for some the symptoms of fatigue can persist for months.[20] About 50% of IM cases result in splenomegaly, in which case patients are prevented from performing intense physical activity for up to 4 weeks after onset of symptoms in order to avoid splenic rupture. Following primary infection, EBV enters a latent state within resting memory B cells, allowing it to evade the immune system and, as a result, most infected individuals carry the virus asymptomatically.[3,18,21] Occasionally, EBV infected cells will reactivate the expression of lytic genes, however surveilling CTLs will eliminate these cells and prevent symptomatic infection from occurring in immunocompetent individuals.

Cancer

EBV infection can promote cancer in infected cells through translational and transcriptional programming which promote latency and are anti-apoptotic in nature.[22] These changes are thought to contribute to oncogenesis.

Between 1990 and 2017, EBV-attributed cancer rates increased by 36% and EBV-attributed cancer mortality increased by 17%, due in large part to population growth in East Asia, where the vast majority of EBV-associated malignancies, namely gastric and nasopharyngeal carcinoma, occur.[7] This burden is expected to increase further as populations and life expectancy continue to increase in these regions of the world. EBV-associated carcinogenesis occurs at significantly elevated levels in other subpopulations as well. For example, human immunodeficiency virus (HIV) infected individuals experience much higher rates of EBV-linked cancers than the general population.[23] These rates are even higher among persons living with HIV in Sub-Saharan Africa, and can result in Non-Hodgkin's Lymphomas (NHL) as well as classic Hodgkin's Lymphoma (HL).[23] In fact, HIV-infected individuals overall live with a 60-200-fold higher relative risk of developing NHL and an 8-10-fold higher relative risk of developing HL compared to those that are uninfected.[23] Additionally, patients who have recently received an organ or hematogenic stem cell transplant may develop post-transplant lymphoproliferative disorders, an often-lethal complication, because of the proliferation of EBV-infected cells due to CTL suppression.[3]

Multiple Sclerosis and Autoimmune Disease

EBV is also associated with the development of rheumatoid arthritis and multiple sclerosis (MS). EBV has long been implicated in MS. Most recently, a 20-year longitudinal study of 10 million young adults of which 955 developed MS showed that EBV infection preceded the onset of MS symptoms and was linked to a 32-fold higher risk of developing MS.[14] This study is the strongest piece of evidence that EBV is the leading cause of MS. Despite this, the pathological mechanism for how EBV causes MS is unclear. Recently, it has been suggested that antibodies against the EBV EBNA1 protein may cross-react with human GlialCAM protein, which Is expressed on cells in the central nervous system.[24] Since MS is characterized by lymphocytes attacking central nervous system cells, the presence of this cross-reactivity may be one mechanistic explanation for this phenomenon.

Treatments

To date, no prophylactic or approved treatment for EBV exists. Thus, a vaccine that prevents EBV infection and/or associated pathologies would have a significant global health impact.[2,6,25] In the following sections of this chapter, I am going to summarize progress towards the development of an EBV vaccine, including what we know about EBV infection, which antigens may need to be included in a vaccine, the type of immune response a vaccine may need to elicit, and the animal models which allow us to test vaccines.

II. Viral Entry

Overview

When designing an EBV vaccine, it is important to consider which antigens will be included in your vaccine construct. When developing a vaccine, researchers typically include viral proteins that are involved in cell entry. The rationale being that if immunization can elicit antibodies against these proteins which block them from functioning, this would prevent viral entry and subsequent infection from occurring in the first place. This type of neutralizing antibody response is the correlate of protection for most licensed vaccines.[26,27] In this section, I am going to give a brief overview of EBV viral entry, including which cell types are infected and which proteins are involved in the cell entry process. In later sections, I will also discuss other important aspects of vaccine design, such as the immune response that a protective EBV vaccine would likely need to elicit.

Viral Tropism

EBV is orally transmitted through saliva. In the oropharynx, the site of infection, both oral epithelial cells and infiltrating B cells are present. Both cell types are capable of being infected by EBV, but it is unknown which is infected first. It is possible that epithelial cells are infected first, followed by lytic replication and the infection of B cells. Vice versa, B cells may be infected first, followed by infection of epithelial cells.[18] It is also possible that both cell types are infected simultaneously. Since each scenario is possible, a protective vaccine would likely need to prevent infection of both cell types at the oral mucosa. Because the correlate of protection for most approved vaccines is neutralizing antibodies, an effective EBV vaccine would likely need to prevent or severely limit infection in both cell types.[3,18]

Proteins Involved in Viral Entry

The dual tropism of EBV infection is accomplished through the orchestrated function of multiple glycoproteins.[28] gH, gL and gB constitute the core fusion machinery and are essential for viral entry irrespective of cell type. gB is a transmembrane fusion protein that promotes the merger of the viral and host membranes.[29] gB activity depends on the heterodimeric gH/gL complex, which is essential for infection and regulates fusion.[30-33] Epithelial cell infection is initiated by the binding of the viral BMRF-2 protein to β1 integrins on the cell surface.[34] Following attachment, binding of gH/gL to one or more cell surface receptors is thought to induce a conformational change that triggers gB activation. αvβ6, and αvβ8 integrins, neuropilin 1, non-muscle myosin heavy chain IIA and the ephrin A2 receptor have all been implicated as gH/gL receptors.[35-40]

Viral attachment to B cells is mediated by gp350, which binds to complement receptors (CR) 1 and 2.[41-43] The triggering of gB during B cell entry depends on the tripartite complex of gH/gL and the viral glycoprotein gp42. Binding of gp42 to the B chain of human leukocyte antigen class II leads to activation of gB through the gH/gL/gp42 complex.[44-46]

In Section IV – Vaccines, I will revisit each of these viral entry proteins and explore their use in vaccine development.

III. Animal Models of Epstein-Barr Virus Infection

Overview

To design and test new therapies, researchers rely on the use of pre-clinical animal models of infection.[47-51] These animal models allow vaccine researchers to evaluate the ability of vaccine candidates and other therapeutics to protect against viral challenge. Because EBV is a human virus which has limited tropism for other species, there are few tractable animal models of EBV infection, and many of these models do not fully capitulate human EBV infection or require the use of non-human viruses which are related to EBV. [52-55]. Here, I will briefly describe animal models which have been used to evaluate EBV infection and vaccines:

Non-Human Primate Models

Because many new- and old-world non-human primates (NHPs) are infected by lymphocryptoviruses (LCVs) that are closely related to EBV, NHPs have been seen as an attractive challenge model for the evaluation of EBV vaccines.[56] One of the first uses of NHPs by EBV researchers

involved the use of cotton-top tamarins and common marmosets for the evaluation of vaccine-induced neutralizing antibody titers, as well as protection against challenge by EBV. However, due to the endangered or red-list status of these species, they are no longer viable options for researchers.[57]

Unlike the cotton-top tamarin and common marmoset, rhesus macaques have a relatively large population, are more closely related to humans so have more comparable immune systems and physiology, and can be bred artificially, resulting in the extensive use of these macaques as an animal model of infection. While EBV cannot stably infect and immortalize B cells in rhesus macaques, these NHPs are still attractive to researchers because there is a high level of genetic similarity between EBV and Rhesus Lymphocryptovirus (RhLCV), which is an ortholog of EBV that infects rhesus macaques. Like EBV, RhLCV is orally transmitted, has a similar course of infection as EBV, and causes cancer in immune suppressed animals.[58,59] This similarity allows researchers to use RhLCV as proxy for EBV in challenge studies. In our lab, we demonstrated the protective efficacy of AMMO1, an antibody against the EBV glycoprotein gH/gL, to protect against oral infection by RhLCV in rhesus macaques.[60] In the study, animals with high levels of AMMO1 in their serum were protected against challenge with RhLCV.[60] See Chapter 3 - Neutralizing antibodies protect against oral transmission of lymphocryptovirus for additional detail and data regarding this study.

Mouse Models

Mice remain the most widely used animal model for researchers due to their relatively low-cost and wide availability. Many EBV vaccine studies have used mice as a model for assessing serum or plasma antibody titers in response to various immunization regimens. However, wild-type mice cannot naturally be infected with EBV. For this reason, researchers use humanized mice when conducting EBV challenge experiments.

Humanized mice are immunocompromised mice, typically non-obese diabetic [NOD] Rag1-/-, Il2rg-/-, engrafted with human CD34+ hematopoietic stem cells. These stem cells develop into human B cells which can become infected by EBV, which makes humanized mice especially suitable as an animal model of EBV infection.[61,62] This model has been used to evaluate the ability of monoclonal, or polyclonal antibodies elicited by either vaccination or infection to protect against controlled viral challenge, including a study by our lab which showed passive transfer of AMMO1 protects 11 of 13 humanized mice from

viremia after EBV challenge.[60,63-65] However, because humanized mice do not efficiently generate an antibody response after immunization, evaluating the protective efficacy of vaccine-elicited antibodies requires passive transfer.[66] Additional limitations of this model are that humanized mice a) only have mouse epithelial cells, which cannot be infected by EBV, and b) are not capable of being infected via the natural oral route; thus, these mice do not fully recapitulate two very important aspects of EBV infection.[67] As part of my own research, I passively transferred gH/gL 60-mer vaccine-elicited IgG to humanized mice and demonstrated full protection against lethal challenge with EBV.[68]

Rabbit Model

Several studies have used rabbits as models for the evaluation of EBV vaccine immunogenicity.[69-73] Researchers have also explored the use of rabbits as an EBV challenge model. Challenging rabbits via intravenous, intranasal, or peroral inoculation with EBV leads to the detection of some EBV DNA in the blood of most rabbits, but only a smaller portion of rabbits have detectable levels of EBV DNA transcripts in the spleen, and even fewer rabbits display sustained EBV infection.[74-76] For this reason, rabbits do not see widespread use as EBV challenge models.

Chinese Tree Shrew Model

Recently, the Chinese tree shrew was shown to display symptoms of EBV infection early in challenge, however only a small subset of shrews showed EBV positivity in spleens or lymph nodes, and none had EBV markers in lung or nasopharyngeal epithelial cells, indicating epithelial cells may not become infected in this model.[77,78]

IV. Vaccines

Overview

In this section, I will explore the current state of EBV vaccine development, building upon the information mentioned in earlier sections on EBV viral entry and EBV animal models. I will first talk about whether a vaccine is likely to work given what we know about pre-existing antibodies against EBV in naturally infected individuals. I will then discuss which antigens might be included in an EBV vaccine, looking to animal data and prior EBV vaccine research. Finally, I will review recent advances in EBV vaccines.

Pre-existing Antibodies

Each of the viral entry proteins involved in viral entry (see Section 2 – Viral Entry and Section IV – Vaccines - *Potential Vaccine Antigens* (below)) are targeted by neutralizing antibodies.[34,79-81] Neutralizing antibodies are the correlate of protection for most effective vaccines.[26,27] It is therefore likely that they will be an important component of an immune response elicited by an EBV vaccine. Serum from naturally infected individuals can neutralize EBV infection of B cells and epithelial cells,[34,82-84] however it is unknown whether these antibodies would be able to protect against initial infection.[82-84] There are several pieces of evidence which suggest that this may be possible, as well as some evidence against this being the case. For instance, infected individuals typically have several variants of EBV present in their bodies, which might suggest that pre-existing EBV antibodies cannot protect against secondary infection.[85-88] However, it is possible that these viral variants arose during the lytic replication phase of primary infection, or that the initial virus inoculum contained several viral variants, which is entirely possible given that several variants of EBV can be found in the saliva of IM patients as well as asymptomatic carriers of EBV.[89] Given the fact that there is a long delay between the onset of IM at 4-6 weeks and the peak of neutralizing antibody titers against EBV at 6 months, it is also possible that individuals are exposed to multiple EBV variants before neutralizing antibodies are at sufficient levels for protection.[90] Evidence in support of EBV antibodies being protective include the fact that, newborn infants generally remain EBV negative for 6-8 months until maternal antibody levels wane, again suggesting that EBV antibodies are protective.[91-95] As mentioned in Section III - Animal Models, passive transfer of antibodies targeting certain EBV surface proteins has been shown to protect against viral challenge in both rhesus macaques and humanized mice. Taken together, these studies are strong evidence that pre-existing antibodies can protect against viral challenge, and thus antibodies elicited by an EBV vaccine may be able to protect against EBV infection.

Potential Vaccine Antigens

As mentioned in Section II – Viral Entry, several virally encoded EBV glycoproteins mediate entry and define tropism, and each represent possible targets for an EBV vaccine. The gp350 protein is the most abundant protein on the surface of EBV and mediates attachment of virus to target cells by binding to complement receptors 1 and 2.[79,96-99] However, antibodies against gp350 are ineffective at inhibiting EBV infection of oral epithelial cells lacking these complement receptors, leaving them vulnerable to

infection.[34,100,101] In fact, antibodies against gp350 are ineffective at inhibiting EBV infection of CR^- epithelial cells and can enhance infection of this cell type.[34,100,101]gp350 is capable of adsorbing most of the serum antibodies that neutralize EBV infection of B cells.[79,81] To date, most EBV subunit vaccine efforts have focused on gp350

Mechanistically, neutralizing anti-gp350 monoclonal antibodies (mAbs) block the gp350-CR1/CR2 interaction.[42,102-105] A study in which a gp350 knockout EBV was generated showed that virus lacking gp350 only saw a 1.7-fold reduction in binding to B cells while still retaining infectivity, which indicates gp350 activity may be dispensable.[106] Passive transfer of a neutralizing anti-gp350 mAb protected one of three macaques against high-dose experimental infection with a chimeric rhesus lymphocryptovirus containing the EBV gp350 protein,[107] indicating that gp350 antibodies could be protective *in vivo.* Another study showed that immunization with recombinant RhLCV gp350 protected 2 of 4 macaques from RhLCV challenge, however they did not examine neutralization titers elicited by this vaccine.[108] In one phase II clinical trial, a gp350 vaccine failed to protect against EBV infection, as defined by seroconversion to non-vaccine antigens, despite decreasing the incidence of symptomatic infectious mononucleosis by 78%.[99] This suggests that a gp350 vaccine could be improved upon in order to block EBV infection in the oral cavity. In line with this notion, it has been suggested that the inclusion of additional viral proteins may improve the efficacy of an EBV vaccine.[6,109] Alternatively, it is possible that a vaccine targeting non-gp350 viral proteins could be more efficacious.

One such alternative is the EBV gH/gL glycoprotein complex, which plays an essential role in the infection of both epithelial cells and B cells. Anti-gH/gL antibodies account for most serum antibodies that neutralize EBV infection of epithelial cells, but only a small fraction of antibodies that neutralize infection of B cells.[81] Only a handful of anti-gH/gL monoclonal antibodies (mAbs) have been identified, all of which neutralize EBV infection of epithelial cells with comparable potency, but most have weak, or no neutralizing activity against EBV infection of B cells.[63,100,110-114] We previously described the isolation and characterization AMMO1, an anti-gH/gL monoclonal antibody (mAb) which potently neutralizes EBV infection of epithelial cells and B cells *in vitro* by binding to a discontinuous epitope on gH/gL.[112] The 769B10 mAb also neutralizes EBV infection of both cell types and binds to an epitope that overlaps with AMMO1, confirming this is a critical site of vulnerability on EBV.[81] As mentioned in Section III – Animal

Models, in order to evaluate the ability for AMMO1 to protect against EBV infection *in vivo*, our lab conducted challenge studies using Rhesus lymphocryptovirus (RhLCV), an EBV ortholog, to infect rhesus macaques which had received a passively delivered AMMO1. Passive transfer of AMMO1 severely limits viral infection following high-dose experimental EBV challenge in humanized mice and protects rhesus macaques against oral challenge with RhLCV if present at adequate levels at the time of challenge.[60,63] These studies, which are highlighted in Chapter 3 of this document, provide proof of concept that anti-gH/gL antibodies can protect against EBV infection and indicate that a gH/gL-based vaccine capable of eliciting AMMO1-like antibodies could prevent oral transmission of the virus.

Another antigen, gB, is also essential for both epithelial cell and B cell infection. The gB glycoprotein exists in two conformationally distinct forms: as a pre-fusion trimer prior to cell attachment and entry, and as a post-fusion trimer after gB has fused to host-cell membranes.[35] Immunizing with the pre-fusion trimer could be advantageous since it most likely presents relevant neutralizing epitopes that prevent structural rearrangements that mediate fusion. Immunization of rabbits with altered forms of gB which might mimic the pre-fusion trimer elicit antibodies which are capable of neutralizing titers against EBV infection of B cells *in vitro*. However, these alterations include the removal of a furin cleavage site of the protein, possibly altering the natural folding state of the pre-fusion protein. These alternations to the natural folding of the gB pre-fusion protein trimer could potentially limit this antigen's ability to elicit neutralizing antibodies against natural infection.

Other antigens, such as gp42 and BMRF2, are also potential EBV vaccine antigens. However, these proteins are only implicated in B cell and epithelial cell infection, respectively, and thus are not ideal targets for a vaccine.

Recent Innovations (Multimerization)

Antigen multimerization has been used to improve the immunogenicity of subunit vaccines against several pathogens including malaria, HIV-1, respiratory syncytial virus (RSV), severe acute respiratory syndrome coronavirus 2 (SARS-CoV-2), influenza[115-122] and EBV.[64,69,81] Multimerization can enhance the immunogenicity of subunit vaccines through several mechanisms including more efficient B cell receptor cross linking, triggering of innate B cell responses, lymph node trafficking, and enhanced MHC class II antigen presentation.[123-125] In support of this nation, Cui *et al.* and Bu *et al.* have shown that

immunization with a 3-mer or 24-meric gH/gL, respectively, elicits higher serum neutralizing titers against infection of B cells and epithelial cells than immunization with monomeric gH/gL.[69,81] While promising, both studies only focused on a single multimer platform. In Chapter 2 - Immunization with a self-assembling nanoparticle vaccine displaying EBV gH/gL protects humanized mice against lethal viral challenge, I expand on these by developing several self-assembling gH/gL multimeric constructs of varying valency, size, and geometry to evaluate how different multimerization platforms affect neutralizing antibody titers.

V. Summary

I began this chapter with a brief overview of the clinical significance (See Section I – Clinical Relevance) of Epstein-Barr Virus and its impact on global health. I touched on the causative relationship between EBV and infectious mononucleosis, the role of EBV in cancer cases and deaths, as well as the link between EBV and autoimmune diseases, including multiple sclerosis and rheumatoid arthritis. Prior to any discussion of EBV vaccine development, it is important to overview EBV linked diseases to not only highlight the urgent need for a vaccine, but because our knowledge of EBV disease plays a large role in vaccine development strategies. This is especially apparent when we consider the experimental use of various animal models of EBV infection. For instance, when using animal models to assess the protective efficacy of EBV vaccines, it is necessary to consider how human EBV infection differs from EBV infection in the animal model being used. Because there are differences in the course and mode of infection in animal models, we must acknowledge that vaccine efficacy observed in animal models is not entirely predictive of what will be observed in humans. Some of these limitations of EBV animal models are discussed briefly in Section III – Animal Models. Despite these limitations, there is still a lot we can learn using these models when staying mindful of what they can and cannot tell us.

When discussing EBV vaccine development, we must also consider EBV viral tropism and viral entry. In Section II – Viral Entry, I describe the tropism of EBV for human B cells and epithelial cells and give an overview of the proteins that are involved in viral entry. This knowledge is important for three reasons. First, because, like our understanding of EBV disease, understanding viral tropism informs our use of EBV animal models. As an example, it is important to remember that humanized mice are limited in their ability to recapitulate human EBV infection because mouse epithelial cells are incapable of being

infected by EBV. Second, we must consider tropism and viral entry because it guides the selection of which *in vitro* cell-based models we use to evaluate the immune response to EBV vaccine candidates; as researchers, we focus on B cell and epithelial cell infectivity assays because they are the main cell types for which EBV has tropism. Third, the understanding of which proteins are involved in viral entry is necessary to make rational decisions about which antigens to include in a vaccine. This idea is a topic of discussion in the very next section, in which I cover whether neutralizing antibodies are elicited against viral entry proteins during natural infection, and whether these neutralizing antibodies are capable of neutralizing infection against both B cells and epithelial cells.

In Section IV – Vaccines, I explore both the historical use and potential future use of various EBV viral entry proteins as vaccine antigens. I give an overview of the various EBV glycoproteins that have been explored in the context of EBV vaccine development. First, I touch on gp350 animal studies as well as human clinical trials. Data from gp350 studies suggest that a vaccine targeting additional viral proteins may be more efficacious than one targeting gp350 alone. Complimentary to this idea, I next discuss gH/gL and the various animal studies that suggest an anti-gH/gL vaccine may be protective. Finally, I touch on other glycoproteins, such as gB, gp42, and BMRF2, notably the challenges presented by gB, and the rationale for why gp42 and BMRF2 may not be ideal vaccine antigens as they are only involved in B cell infection. In Section IV – Vaccines, I also explore the several pieces of strong evidence that pre-existing antibodies may be protective against EBV infection. This is important in the context of pre-clinical EBV vaccine development because it shows that an EBV vaccine which elicits high titers of neutralizing antibodies may be protective, and that developing an EBV vaccine with this goal in mind may be an effective strategy. In further support of this idea, neutralizing antibodies are a correlate of protection for most approved anti-viral vaccines, so it is likely that an EBV vaccine will need to elicit neutralizing antibodies.

The selection of *in vitro* cell based models, *in vivo* animal models, and the overall study design in both Chapter 2 and Chapter 3 are informed heavily by the reasoning mentioned earlier in this summary:

In Sections II and III of this chapter, I refer to a study in which AMMO1 is passively transferred to humanized mice and to rhesus macaques, protecting them from challenge with EBV and RhLCV, respectively. This work is included here as Chapter 3 - Neutralizing antibodies protect against oral

transmission of lymphocryptovirus. This study is important to include here because it serves as a proof-of-concept for the work described in Chapter 2. Specifically, the experimental outcomes of this study suggest that passively transferring anti-gH/gL antibody may protect against EBV infection. Additionally, it suggests that a vaccine including the gH/gL antigen could elicit antibodies against the AMMO1-eptiope, the vaccine may confer protection.

In the final paragraph of Section IV – Vaccines, I highlight multimerization, which is a recent innovation in the EBV vaccine field. I mention how recent studies compare a multimeric gH/gL vaccine with monomeric gH/gL vaccine, showing improved immunogenicity in the multimeric format as compared to monomeric. In Chapter 2 - Immunization with a self-assembling nanoparticle vaccine displaying EBV gH/gL protects humanized mice against lethal viral challenge, I expand on these early studies by comparing not just one, but four different multimeric gH/gL vaccines against monomeric gH/gL vaccine and demonstrate protective efficacy in an animal model.

Chapter 2: Immunization with a self-assembling nanoparticle vaccine displaying EBV gH/gL protects humanized mice against lethal viral challenge

This work was published in Cell Reports Medicine on June 21, 2022.

I. Summary

Epstein-Barr virus (EBV) is a cancer-associated pathogen responsible for 165,000 deaths annually. EBV is also the etiological agent of infectious mononucleosis and is linked to multiple sclerosis and rheumatoid arthritis. An EBV vaccine would have significant global health impact. EBV is orally transmitted and has tropism for both epithelial and B cells. Therefore, a vaccine would need to prevent infection of both in the oral cavity. Passive transfer of neutralizing antibodies against the gH/gL glycoprotein complex prevent experimental EBV infection in humanized mice and rhesus macaques, suggesting that gH/gL is an attractive vaccine candidate. Here, we evaluate the immunogenicity of several gH/gL nanoparticle vaccines. All nanoparticles display superior immunogenicity relative to monomeric gH/gL. A nanoparticle displaying 60 copies of gH/gL elicits antibodies that protect against lethal EBV challenge in humanized mice, whereas antibodies elicited by monomeric gH/gL do not. These data motivate further development of gH/gL nanoparticle vaccines for EBV.

II. Introduction

Epstein-Barr virus (EBV) is one of the most common human viruses. It is a herpesvirus with tropism for both B cells and epithelial cells and is associated with several malignancies of these two cell types including Hodgkin lymphoma, Burkitt lymphoma, diffuse large B cell lymphoma, post-transplant lymphoproliferative disease, nasopharyngeal carcinoma and gastric carcinoma.[2-5] It is estimated that EBV is responsible for ~265,000 new cases of cancer and ~164000 cancer deaths globally per year.[2,6,7,126] EBV is also the causative agent of infectious mononucleosis (IM) and is linked to multiple sclerosis and rheumatoid arthritis.[8-14] Thus, a vaccine that prevents EBV infection and/or associated pathologies would have a significant global health impact.[2,6,25]

EBV is orally transmitted and both B cells and epithelial cells are present in the oropharynx. Thus, an effective vaccine would likely need to prevent or severely limit infection in both cell types.[3,18] The dual tropism of EBV infection is accomplished through the orchestrated function of multiple glycoproteins.[28] gH, gL and gB constitute the core fusion machinery and are essential for viral entry irrespective of cell

type. gB is a transmembrane fusion protein that promotes the merger of the viral and host membranes.[29] gB activity depends on the heterodimeric gH/gL complex, which is essential for infection and regulates fusion.[30-33] Epithelial cell infection is initiated by the binding of the viral BMRF-2 protein to β1 integrins on the cell surface.[34] Following attachment, binding of gH/gL to one or more cell surface receptors is thought to induce a conformational change that triggers gB activation. αvβ6, and αvβ8 integrins, neuropilin 1, non-muscle myosin heavy chain IIA and the ephrin A2 receptor have all been implicated as gH/gL receptors.[35-40]

Viral attachment to B cells is mediated by gp350, which binds to complement receptors (CR) 1 and 2.[41-43] The triggering of gB during B cell entry depends on the tripartite complex of gH/gL and the viral glycoprotein gp42. Binding of gp42 to the B chain of human leukocyte antigen class II leads to activation of gB through the gH/gL/gp42 complex.[44-46]

Neutralizing antibodies are the correlate of protection for most effective vaccines.[26,27] It is therefore likely that they will be an important component of an immune response elicited by an EBV vaccine. Serum from naturally infected individuals can neutralize EBV infection of B cells and epithelial cells,[34,82-84] and all the viral proteins involved in viral entry are targeted by neutralizing antibodies.[34,79-81] To date, most EBV subunit vaccine efforts have focused on gp350. gp350 is capable of adsorbing most of the serum antibodies that neutralize EBV infection of B cells.[79,81]

Mechanistically, neutralizing anti-gp350 monoclonal antibodies (mAbs) block the gp350-CR1/CR2 interaction.[42,102-105] However, antibodies against gp350 are ineffective at inhibiting EBV infection of CR^- epithelial cells and can enhance infection of this cell type.[34,100,101] Passive transfer of a neutralizing anti-gp350 mAb protected one of three macaques against high-dose experimental infection with rhesus lymphocryptovirus, the EBV ortholog that infects macaques[107] indicating that gp350 antibodies could be protective *in vivo.* A phase II trial of a gp350 vaccine failed to protect against EBV despite decreasing the incidence of symptomatic infectious mononucleosis by 78%.[99] In light of these results, it has been suggested that a gp350 vaccine could be improved upon with the inclusion of additional viral proteins.[109] Alternatively, it is possible that a vaccine targeting non-gp350 viral proteins could be more efficacious.

gH/gL is a promising antigen for vaccine development. Anti-gH/gL antibodies account for most serum antibodies that neutralize EBV infection of epithelial cells, but only a small fraction of antibodies that neutralize infection of B cells.[81] Only a handful of anti-gH/gL monoclonal antibodies (mAbs) have been identified, all of which neutralize EBV infection of epithelial cells with comparable potency, but most have weak, or no neutralizing activity against EBV infection of B cells.[63,100,110-114] We previously described the isolation and characterization AMMO1, an anti-gH/gL monoclonal antibody (mAb) which potently neutralizes EBV infection of epithelial cells and B cells *in vitro* by binding to a discontinuous epitope on gH/gL.[112] The 769B10 mAb also neutralizes EBV infection of both cell types and binds to an epitope that overlaps with AMMO1, confirming this is a critical site of vulnerability on EBV.[81] Passive transfer of AMMO1 severely limits viral infection following high-dose experimental EBV challenge in humanized mice and protects rhesus macaques against oral challenge with RhLCV if present at adequate levels at the time of challenge.[60,63] These studies provide proof of concept that anti-gH/gL antibodies can protect against EBV infection and indicate that a gH/gL-based vaccine capable of eliciting AMMO1-like antibodies could prevent oral transmission of the virus.

Here we generated several protein subunit vaccines where gH/gL is scaffolded onto self-assembling multimerization domains to produce nanoparticles with well-defined geometries and valency. Relative to monomeric gH/gL, immunization with the gH/gL nanoparticles elicited higher binding titers and neutralizing titers after one or two immunizations in mice. Competitive binding and depletion of plasma antibodies with an epitope-specific gH/gL probe suggested that only a small fraction of vaccine-elicited antibodies targeted the AMMO1 epitope. Consistent with this, depletion of plasma antibodies with an epitope-specific gH/gL knockout reduced plasma neutralizing activity to undetectable levels. Passive transfer of IgG purified from animals immunized with a computationally designed nanoparticle displaying 60 copies of gH/gL protected against high-dose lethal challenge in a humanized mouse model, while IgG purified from animals immunized with monomeric gH/gL did not. Collectively these results demonstrate that gH/gL is an attractive vaccine antigen, but that multivalent display of gH/gL is required to elicit neutralizing antibodies of sufficient titer to protect against EBV infection.

III. Results

Generation and Characterization of Multimeric gH/gL Vaccine Constructs

Cui *et al.* and Bu *et al.* have shown that immunization with multimeric gH/gL elicits higher serum neutralizing titers against infection of B cells and epithelial cells than immunization with monomeric gH/gL.[69,81] However, these studies focused on a single multimerization platform when generating gH/gL constructs, either *Helicobacter pylori* ferritin, a 24-mer, or a T4 fibritin foldon domain, a trimer. Here we sought to develop several self-assembling multimeric gH/gL constructs with differing valencies, sizes, and geometries to evaluate how they differ in their ability to elicit neutralizing antibodies in mice. We generated various expression constructs where different multimerization domains were genetically fused to the C terminus of the gH ectodomain. These included i) a computationally designed circular tandem repeat protein (cTRP) that forms a planar toroid displaying four copies of gH/gL that is stabilized by inter-protomer disulfide bonds;[127] ii) a modified version of the multimerization domain from the C4b-binding protein from *Gallus gallus* (IMX313) which also forms a planar, ring-like structure stabilized by inter-protomer disulfide bonds capable of displaying seven copies of gH/gL [128]; iii) *Helicobacter pylori* ferritin which assembles into a 24-mer nanoparticle with octahedral symmetry and has previously been used to multimerize the EBV gp350 and gH/gL proteins;[81,129] and iv) a secretion-optimized variant of a computationally designed, self-assembling 60-mer with icosahedral symmetry.[130] The gH fusion proteins were co-expressed with gL using the Daedalus lentiviral expression system in HEK293 cells [131]. The gH/gL fusion proteins were purified by affinity chromatography followed by size-exclusion chromatography (SEC). The average yields, in mg/L of each purified gH/gL protein are provided in Table S1. The SEC elution profiles of the gH/gL fusion proteins were consistent with their expected size (Fig. 1A and Table S2). The 4-mer and 7-mer constructs eluted earlier than the monomer. The gH/gL 60-mer eluted in the void volume as expected, while the gH/gL 24-mer eluted near the void volume. SEC-MALS revealed that the molecular weight of the particles were ~540, ~670, ~4420 and ~7400 kDa for the 4-mer, 7-mer, 24-mer and 60-mer, respectively, which are close to their predicted nanoparticle sizes (Table S2). Bands corresponding to the expected sizes of the gH fusion proteins were identified by reducing SDS-PAGE (Fig. 1B). Non-reducing SDS-PAGE revealed higher molecular weight complexes of the 4-mer and 7-mer consistent with the formation of inter-protomer disulfide bonds between the multimerization domain

subunits (Fig.1C). These analyses also revealed a band corresponding to gL and demonstrated that the preparations were highly pure (Fig. 1B and C).

The gH/gL nanoparticles were imaged using negative-stain electron microscopy (nsEM), which demonstrated that all particles were monodisperse and of the predicted size. Density corresponding to gH/gL emanating from the nanoparticle cores was apparent in 2D class averages of the 4-mer, 7-mer and 24-mer (Fig. 1D). Density corresponding to gH/gL was less clearly defined on the 60-mer particles; however, a comparison of 3D reconstructions of the gH/gL-I3 fusions relative to the 60-meric I3 core revealed clear density corresponding to the C terminus of gH, indicating conformational flexibility around the gH-I3 fusion junction (Fig. S1).

To ensure that fusion to the multimerization domains did not alter the antigenicity of gH/gL, we measured the binding of several anti-gH/gL mAbs to each nanoparticle using an ELISA assay where biotinylated monomeric or gH/gL nanoparticles were captured on an ELISA plate coated with streptavidin. Of all the mAbs, AMMO1 binds with the highest affinity to monomeric gH/gL (Fig. 1E).[112] The AMMO1 epitope bridges Domain I and Domain-II (D-I/D-II) and spans both gH and gL.[112] CL40 has the second highest affinity (Fig. 1E),[112] and binds to an epitope spanning the D-II/D-III interface of gH [111]. CL59 binds at the C terminus of gH on D-IV[111] and has lower affinity than CL40 or AMMO1 (Fig. 1E).[112] E1D1 binds exclusively to gL and has the lowest affinity for the complex (Fig. 1E).[112,113]

In general, the mAbs maintained antigenicity to each multimeric construct, and some showed significant improvements in binding to the nanoparticles (Fig. 1E-I). Despite showing the weakest binding of all the mAbs to the gH/gL monomer, E1D1 showed the strongest binding to the 7-mer and the 24-mer (Fig. 1G and H). The E1D1 epitope is most distal to the multimerization domains and is therefore highly exposed on the nanoparticles. Moreover, the spacing of the E1D1 epitope may be optimally presented for bivalent engagement by the E1D1 mAb in some formats. In contrast, CL59 showed the weakest binding to all the gH/gL nanoparticles. CL59 binds closer to the C terminus of the gH ectodomain, which would be in close proximity to the nanoparticle core, potentially limiting exposure of the epitope in the context of the nanoparticles (Fig. 1F-I). With the exception of E1D1,we did not observe a significant improvement in binding for most mAbs in the 60-mer format relative to the monomer.

Immunogenicity of gH/gL nanoparticles

To assess the immunogenicity of the gH/gL nanoparticles, we immunized C57BL/6J mice with 5 μg of gH/gL monomer, 4-mer, 7-mer, 24-mer, or 60-mer formulated with adjuvant at weeks 0, 4 and 12. Plasma was collected two weeks post each immunization (Fig. 2A). Endpoint binding titers to gH/gL were measured by ELISA (Fig. 2B). After the first immunization, the median reciprocal binding titers in the gH/gL 4-mer, 7-mer, 24-mer, and 60-mer groups were higher than those in the monomer group. A second immunization boosted the binding titers in each group 200- to 1000-fold. Again, the median titers in animals immunized with the gH/gL 4-mer, 7-mer, 24-mer, and 60-mer were higher than in those immunized with monomeric gH/gL.

A third immunization with the monomer boosted the gH/gL binding titers such that they were comparable to those elicited by the 4-mer, 7-mer, and 60-mer. A third immunization with the 24-mer also boosted the titers such that they were higher than the monomer 4-mer and 60-mer groups, while the third immunization with the other nanoparticles did not further boost the median binding titers (Fig. 2B).

We next measured the ability of vaccine-elicited plasma to neutralize EBV infection of both B cells and epithelial cells. To monitor neutralization in eptihelial cells we used the SVKCR2 cell line that stably expresses CR2 which promotes cellular attachment of virions via gp350 improving the otherwise poor infectivity of epithelial cells *in vitro* [132]. Neutralizing activity against epithelial cell infection was elicited two weeks after the first immunization in all groups that received multimeric, but not monomeric gH/gL. The median reciprocal half maximal inhibitory dilution (ID_{50}) titers were significantly higher in the 60-mer group compared to the monomer and 24-mer groups (Fig. 2C and S2). Additionally, median titers were significantly higher in the 7-mer group compared to the monomer and 24-mer groups.

The second immunization boosted median neutralizing titers by ~10-100 fold in the epithelial cell infection assay. The median neutralizing titers were higher in all of the gH/gL nanoparticle immunized groups than they were in the monomer group (Fig. 2C and S2). The epithelial cell neutralizing titers in the 7-mer and 60-mer were also higher than those elicited by the 24-mer. The third immunization with the gH/gL nanoparticles did not further boost epithelial cell neutralizing responses, while the third dose of monomeric gH/gL boosted titers to levels that were comparable to those in other groups.

None of the gH/gL antigens elicited antibodies that could neutralize B cell infection two weeks after the first immunization (Fig. 2D and S3). Following the second immunization, neutralizing titers were

present in plasma from all groups immunized with gH/gL nanoparticles, but not in animals immunized with the monomer. Among the nanoparticle-immunized mice, the B cell neutralizing titers elicited by the 60-mer were higher than the 4-mer and 24-mer at this time point. Although the median B cell neutralizing titers elicited by the 60-mer (reciprocal ID_{50} = 436) were higher the 7-mer (reciprocal ID_{50} = 94), the difference was not statistically significant.

As was observed with the epithelial cell neutralizing titers, a third immunization with the gH/gL nanoparticles did not further boost B cell neutralizing responses, while a third dose of monomeric gH/gL boosted titers to levels that were comparable to those in other groups. In general, the neutralizing titers were about 10-fold lower against B cell infection compared to epithelial cell infection in all groups. From these analyses we conclude that all gH/gL nanoparticles displayed superior immunogenicity compared to monomeric gH/gL after one or two immunizations and that a third immunization did not result in a significant titer boost.

Plasma epitope mapping

Each multimeric gH/gL nanoparticle tested here has a unique valency and geometry which differentially affects the exposure of certain epitopes bound by neutralizing anti-gH/gL mAbs (Fig. 1D-H). To test whether the nanoparticle format skewed the epitope-specificity of vaccine-elicited antibodies from each construct, we assessed the ability of pooled immune plasma to compete with the E1D1, CL40, CL59 and AMMO1 mAbs for binding to monomeric gH/gL by ELISA (Fig. 3A-D).

Pooled plasma collected following one immunization with the gH/gL 4-mer and gH/gL 60-mer weakly inhibited E1D1 binding (Fig. 3A and S4A). After the second immunization, plasma from all groups inhibited CL40, CL59, and E1D1 binding (Fig. 3A-C and S4B). Plasma antibodies that inhibited binding of these mAbs were further boosted following a third immunization in most groups. The only exception was that a third immunization with the 7-mer did not boost CL59-blocking plasma antibodies (Fig. 3C and S4C).

Plasma antibodies capable of inhibiting AMMO1 binding were less common. Immune plasmas from the 4-mer and 60-mer groups weakly inhibited AMMO1 binding after two immunizations, and were boosted following a third immunization (Fig. 3D and S4C). All antigens elicited low titers of AMMO1-

blocking antibodies following three immunizations. Among these, titers elicited by the 60-mer were highest at ~1:150.

These experiments demonstrate that each gH/gL nanoparticle readily elicits antibodies that compete with E1D1, and that AMMO1-competing antibodies are rarer. This difference in competition could be attributed to the relative affinities of these mAbs for gH/gL (Fig. 1E), or it could be due to the relative exposure of these epitopes on the nanoparticle.

Although the titers of AMMO1-competing antibodies in the plasma of mice immunized with gH/gL nanoparticles are low, because the epitope boudn by this mAb represents a critical site of vulnerability on gH/gL, we sought to assess the relative contribution of AMMO1-like antibodies to the plasma neutralizing activity of immunized mice. To achieve this, we developed an epitope-specific gH/gL probe and carried out plasma depletions. We previously identified two mutations, K73W and Y76A that reduced binding of AMMO1 to cell-surface expressed gH/gL [112]. We expressed and purified a monomeric gH/gL ectodomain harboring these two mutations (herein called gH/gL-KO) which completely ablated AMMO1 binding while maintaining binding to other gH/gL mAbs as measured by biolayer interferometry (BLI) (Fig. 4 A-D).

Antibodies from pooled plasma collected from each group two weeks after the third immunization were depleted using immobilized gH/gL-KO. ELISA binding of depleted plasma to gH/gL-KO confirmed depletion of gH/gL-KO-specific antibodies (Fig. 4, compare panels E and F). Depletion with gH/gL-KO also reduced binding to wild-type gH/gL (Fig. 4G and H). The binding signal was slightly stronger for gH/gL relative to gH/gL-KO post-depletion (Fig. 4H and F), suggesting that very few plasma antibodies are sensitive to the KO mutations in the serum. Although we cannot completely rule out the presence of antibodies that share the AMMO1 binding footprint but are insensitive to the KO mutations in this assay, these results are consistent with the mAb competition studies which demonstrated that there are very few AMMO1-like antibodies in the plasma of immunized animals (Fig. 3D and Fig. S4).

Depletion of gH/gL-KO-specific antibodies led to a complete loss of neutralizing titers in both the B cell and epithelial neutralization assays (Fig. 4I-L). Collectively these data demonstrate that only a small portion of vaccine-elicited antibodies in each group target the AMMO1 epitope, and that they do not make a measurable contribution to the plasma neutralizing activity.

Passive transfer of nanoparticle-elicited gH/gL mAbs protects against lethal challenge in humanized mice.

Immunocompromised mice engrafted with human hematopoietic stem cells develop human B cells that can become infected by EBV and are used as an *in vivo* model of EBV infection.[61,62] This model has been used to evaluate the ability of monoclonal, or polyclonal antibodies elicited by either vaccination or infection to protect against controlled viral challenge.[60,63-65] Having established that gH/gL nanoparticles display superior immunogenicity, we sought to assess whether the antibodies they elicit confer protection against EBV challenge in this model.

To generate mice for these studies, non-obese diabetic [NOD] Rag1-/-, Il2rg-/- mice were engrafted with mobilized huCD34+ hematopoietic stem cells, hereafter referred to as humanized mice. At 20 weeks post-transplant, 1 day prior to challenge, ~10-25% of peripheral blood mononuclear cells were human cells, of which ~65-80% were huCD19+ B cells (Fig. S5). Since the humanized mouse model used here does not efficiently generate antibody responses to immunization,[66] we opted to passively transfer purified antibodies elicited in wild-type C57BL/6 mice, which allowed us to directly evaluate the protective efficacy of the vaccine-elicited antibodies independent of other vaccine-induced immune responses.

To generate sufficient antibody for these experiments, C57BL/6J mice (n=20) were immunized two times with 5 μg of the gH/gL 60-mer at weeks 0 and 4. This nanoparticle was selected because after two doses it consistently elicited high titers of antibodies that neutralize EBV infection of B cells which are the primary targets of infection in humanized mice. As a comparator, we also immunized a group of mice with gH/gL monomer (n=20). Two weeks after the second immunization, plasma were harvested, pooled, and total IgG was purified using protein A/G resin. As a control IgG was purifed from unimmunized C57BL/6J mice (n=20). The concentration of each pool of purified IgG was measured by spectrophotometry and gH/gL binding activity was measured by ELISA, demonstrating that the anti-gH/gL titers were higher in the 60-mer immunized group (Fig. S6).

IgG from each group were delivered to humanized mice (n=4-5 mice/group) via intraperitoneal injection 2 days prior to challenge at a dose of 500 μg IgG/mouse (Fig. 5A). Total IgG measured in pooled plasma collected 2 days prior to and 1 day after transfer confirmed that that the mice received comparable levels of total IgG (Fig. 5B). However, the levels of anti-gH/gL antibodies were higher in the

mice that received IgG from 60-mer immunized animals compared to those that received plasma from animals immunized with the monomer (Fig. 5C), consistent with the superior immunogenicity of the gH/gL nanoparticle (Fig. 2B). Plasma from animals that received IgG from unimmunized animals (control IgG) did not display any binding activity to gH/gL (Fig. 5C). Two days after IgG transfer (day 0), each mouse was challenged via retro-orbital injection with 33,000 Raji Infectious Units (RIU) of EBV. We also included an infected control group which did not receive antibody pre-treatment and an uninfected control group that received neither antibody pre-treatment nor EBV challenge.

Following challenge, the mice were weighed three times a week and monitored for general health over the course of 10 weeks. Blood samples were collected weekly beginning at 3 weeks post-challenge, and spleens were harvested from each mouse at the day 70 endpoint, or earlier if they met euthanasia criteria. Upon completion of the study, 100% of the animals in the uninfected control and 60-mer treatment groups survived (Fig. 5D). In contrast, 100% of the animals in the infected control and control IgG treatment groups succumbed to infection by 56- and 66-days post-challenge, respectively. 75% of mice in the monomer treatment group did not survive beyond day 60, and only one animal survived the entire 70 days (Fig. 5D). The survival rate of mice in the uninfected control group and 60-mer treatment group were significantly higher than all other groups (Fig. 5D).

EBV DNA was not detected in the blood or spleen of the uninfected control group throughout the duration of the experiment (Fig. 5E and J). In contrast, 100% of mice in the control IgG treatment group (Fig. 5F) and 100% of mice in the infected control group were viremic as early as 21 days post-challenge (Fig. 5E). In the monomer IgG group, EBV DNA was detected in the blood of 100% of mice (Fig. 5G). In the 60-mer IgG group, EBV DNA was undetectable in blood of 40% of mice at any time point tested. One mouse was viremic at weeks 7 and 10, another at weeks 9 and 10, and a third at week 10 (Fig. 5H).

A phenotypic analysis of the peripheral blood lymphocytes revealed a rapid decline in $CD19^+$ B cells (Fig. S3A) and increase in $CD8^+$ T cells (Fig. S3B) in mice that received control IgG or IgG elicited by the monomer, and the infected controls relative to the uninfected controls approximately one-month post-challenge a phenotype consistent with a high dose EBV challenge [133], and consistent with T cell-mediated killing of infected B cells.[134] A more gradual decline in B cell frequencies and increase in CD8+

T cell frequencies was noted in three of the mice that received IgG elicited by the gH/gL 60-mer (Fig. S3 A and B).

At necropsy, spleens from animals in the infected control and control IgG groups were significantly heavier than those in the uninfected control groups (Fig. 5H) and had visible splenic tumors (Fig. S5). Spleens from two of the viremic mice in the 60-mer IgG group were about 3 times heavier than the other three mice in the 60-mer IgG group and 3 of 5 spleens had visible tumors (Fig. S7). Three of the spleens were heavier in the monomer group relative to the uninfected control while the fourth was comparable to the uninfected controls and 3 of 5 of the 60mer IgG-treated animals (Fig. 5I). All mice in the monomer IgG group had visible splenic tumors (Fig. S7). Viral DNA was not detected in the the spleens of all animals in the uninfected control group and from the spleens from one animal in each of the 60-mer IgG and monomer IgG groups (Fig. 5J), but it was detected in the spleens of all remaining mice (Fig. 5J).

Collectively, these data demonstrate that multivalent display of gH/gL elicits higher titers of neutralizing antibodies that protect against lethal EBV challenge in a humanized mouse model. However, they do not confer sterilizing immunity.

IV. Discussion

A safe and effective vaccine could alleviate the global disease burden resulting from EBV infection. Here we developed several multimeric vaccine candidates derived from the gH/gL ectodomain and evaluated their ability to elicit antibodies capable of neutralizing EBV infection of both B cells and epithelial cells in mice and demonstrated that a computationally designed nanoparticle displaying 60 copies of gH/gL elicited antibodies capable of protecting against high-dose, lethal challenge in a humanized mouse infection model.

Antigen multimerization has been used to improve the immunogenicity of subunit vaccines against several pathogens including malaria, HIV-1, RSV, SARS-CoV-2, influenza[115-122] and EBV.[64,69,81] Multimerization can enhance the immunogenicity of subunit vaccines through several mechanisms including more efficient B cell receptor cross linking, triggering of innate B cell responses, lymph node trafficking, and enhanced MHC class II antigen presentation.[123-125] In general we observed that mAb binding as measured by ELISA was generally improved by multimerization (Fig 1E-I), however this was

not always the case as the binding of most mAbs showed comparable binding to monomeric and 60-meric gH/gL. This discrepancy may be related to the efficiency of antigen biotinylation and/or capture on the ELISA plate. Nevertheless, nanoparticle display resulted in a significant improvement in immunogenicity in vivo (Fig. 2).

Previous studies have shown that antigen valency correlates with B cell activation, germinal center recruitment, and B cell differentiation as well as serum binding and neutralizing titers.[118,135,136] Although nanoparticles displaying gH/gL exhibited superior immunogenicity as compared to monomeric gH/gL, we did not observe a strict correlation between antigen valency and binding or neutralizing titers. The differences in the ability of these antigens to elicit neutralizing antibodies could be linked to nanoparticle stability *in vivo* or T cell help directed at MHCII-restricted epitopes that differ between the nanoparticle scaffolds.[137]

Because of its ability to potently neutralize infection of both cell types, the overlapping epitope targeted by AMMO1 and 769B10 represents a critical site of vulnerability on EBV.[81,112] Despite readily eliciting antibodies targeting several other epitopes on gH/gL, our analysis indicates that the AMMO1 epitope is subdominant in the context of immunization. Despite this, immune plasma from gH/gL 60-mer immunized mice was protective *in vivo*. Thus, relative to monomeric gH/gL, the gH/gL 60-mer may have elicited high titers of less potent anti-gH/gL antibodies like CL40 and CL59. Alternatively, the immunogens may have elicited antibodies targeting other potently neutralizing epitopes on gH/gL such as the one defined by the recently identified 1D8 mAb or other yet to be identified epitopes.[63] Gaining a better understanding of the epitopes on gH/gL that are targeted by neutralizing and non-neutralizing antibodies elicited by natural infection or immunization through the isolation and characterization of monoclonal antibodies would enable rational gH/gL vaccine design that could further enhance neutralizing titers when combined with multimeric antigen display. For example, immunogen design strategies could be employed to immunofocus the antibody response to potently neutralizing gH/gL epitopes.

The majority of humanized mice that received IgG elicited by monomeric gH/gL did not survive EBV challenge. Similarly, passive transfer of sera from rabbits immunized with monomeric gH/gL conferred partial protection from lethal EBV challenge in humanized mice.[64] Since EBV infection in

humanized mice is restricted to human B cells,[61,62] the observed lack of protection by IgG raised against monomeric gH/gL in our study is most likely due to the inability of this antigen to elicit antibodies that neutralize infection of B cells following two immunizations. In contrast, IgG purified from animals immunized with the gH/gL 60-mer prevented death within a 10 week window following high dose EBV challenge, demonstrating that multivalent display substantially improves the quality of vaccine-elicited anti-gH/gL antibodies. We note that 3/5 animals in this group were viremic and had obvious tumors at the study endpoint, and a 4th had trace amounts of viral DNA in the spleen thus sterilizing immunity was not achieved in this model and it is possible that some of the animals may have succumbed to infection if observed for a longer period.

In sum, we demonstrate that multivalent display of EBV gH/gL markedly enhanced immunogenicity in mice and that a computationally designed 60-mer nanoparticle elicited antibodies that protected against lethal challenge in a humanized mouse infection model. These results underscore the importance that vaccine-elicited antibodies against gH/gL can play in preventing EBV infection and highlight the utility of cutting-edge vaccine approaches in the development of vaccines against this important cancer-associated pathogen.

Limitations of the Study:

Although we only evaluated the ability of antibodies elicited by the 60-mer in the humanized mouse challenge studies, the other nanoparticles developed here and elsewhere[64,81] have potential for clinical development and additional in vivo comparisons and manufacturing feasibility studies are warranted.

Both B cells and epithelial cells are present in the oropharynx, thus antibodies that can neutralize infection of both types of cells are an important consideration for EBV vaccine development.[138] The gH/gL constructs developed here and by others [64,81] consistently elicit higher epithelial cell neutralizing titers as compared to B cell neutralizing titers. Since murine epithelial cells are not susceptible to infection and oral transmission is not possible in humanized mice,[62,139] this challenge model may underestimate the relative importance of antibodies capable of neutralizing infection of this cell type. Moreover, it is not understood how an intravenous dose of virus in humanize mice compares to the inoculum in a natural oral exposure. Thus, the evaluation of a multivalent gH/gL vaccine to prevent rhesus lymphocryptovirus infection of

macaques, where oral transmission is the natural route of infection,[140] should more accurately predict its ability to protect humans against EBV.

V. FIGURES

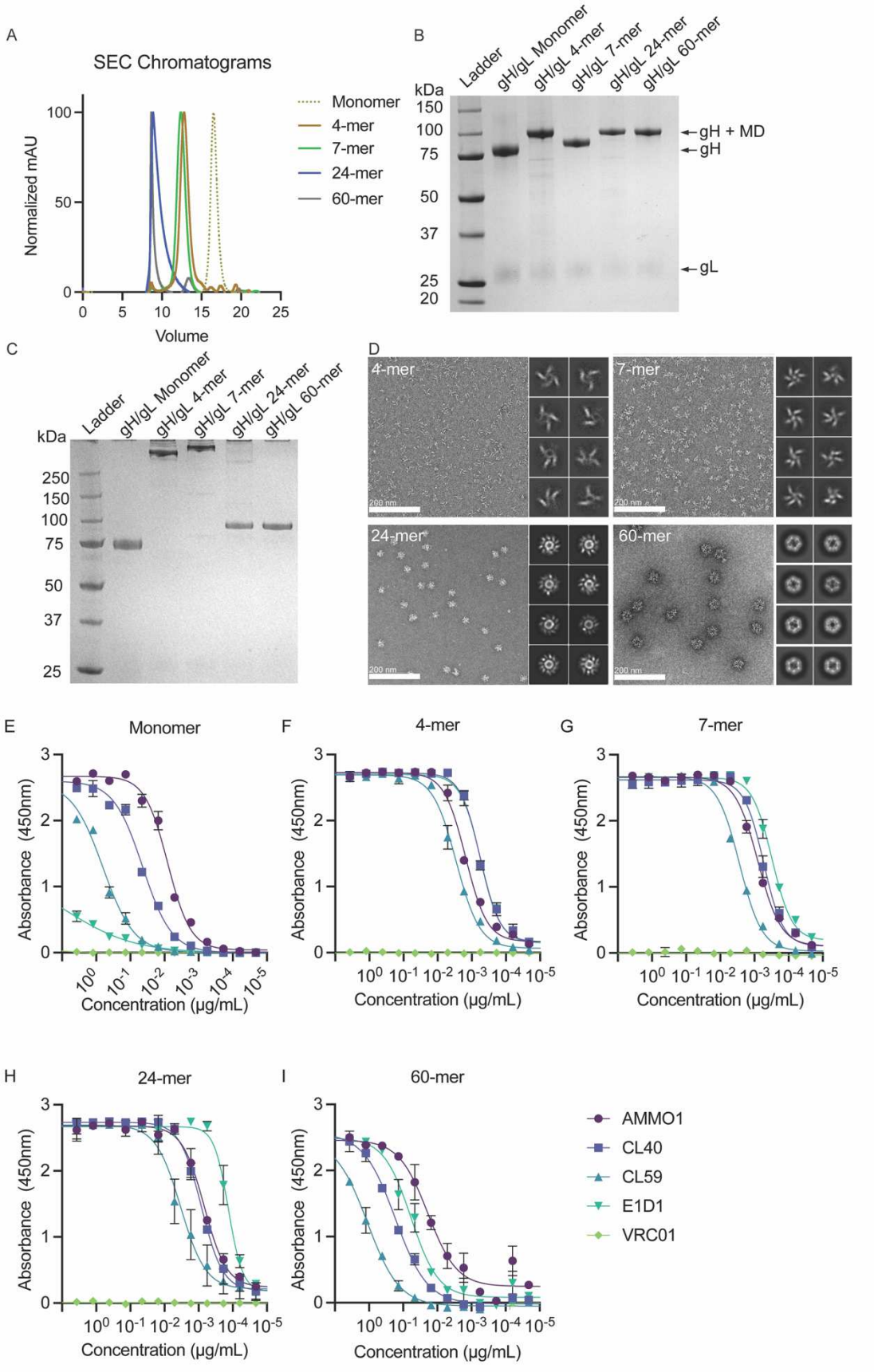
A
SEC Chromatograms
Normalized mAU
Volume
Monomer
4-mer
7-mer
24-mer
60-mer
B
Ladder
gH/gL Monomer
gH/gL 4-mer
gH/gL 7-mer
gH/gL 24-mer
gH/gL 60-mer
kDa
gH + MD
gH
gL
C
D
4-mer
7-mer
24-mer
60-mer
200 nm
E
Monomer
F
4-mer
G
7-mer
Absorbance (450nm)
Concentration (µg/mL)
H
24-mer
I
60-mer
AMMO1
CL40
CL59
E1D1
VRC01

Figure 1. Biochemical and Biophysical Characterization of multimeric gH/gL nanoparticles. (**A**) Monomeric gH/gL and multimeric gH/gL nanoparticles were analyzed by size-exclusion chromatography (SEC) on a Superose 6 column as indicated. (**B**) Reducing SDS-PAGE analysis of 1 µg of monomeric gH/gL or multimeric gH/gL nanoparticles. Bands corresponding to gL, gH, and gH fused to 4-mer, 7-mer, 24-mer or 60-mer multimerization domains (MD) are indicated with arrows. (**C**) Non-Reducing SDS-PAGE analysis of 1 µg of the proteins in **B**. (**D**) Negative stain electron microscopy was performed on 4-mer, 7-mer, 24-mer or 60-mer gH/gL nanoparticles as indicated. The eight most frequent 2D class averages for each particle are shown in the inlay. Scale bars represent 200 nm. Binding of the anti-gH/gL mAbs E1D1, CL40, CL59 and AMMO1 to monomeric gH/gL **(E)** or multimeric gH/gL nanoparticles **(F-I)** were measured by ELISA as indicated. Each data point represents mean and standard deviation of two technical replicates. The anti-HIV-1 Env mAb VRC01 was used as a control for non-specific binding. See also Figure S1.

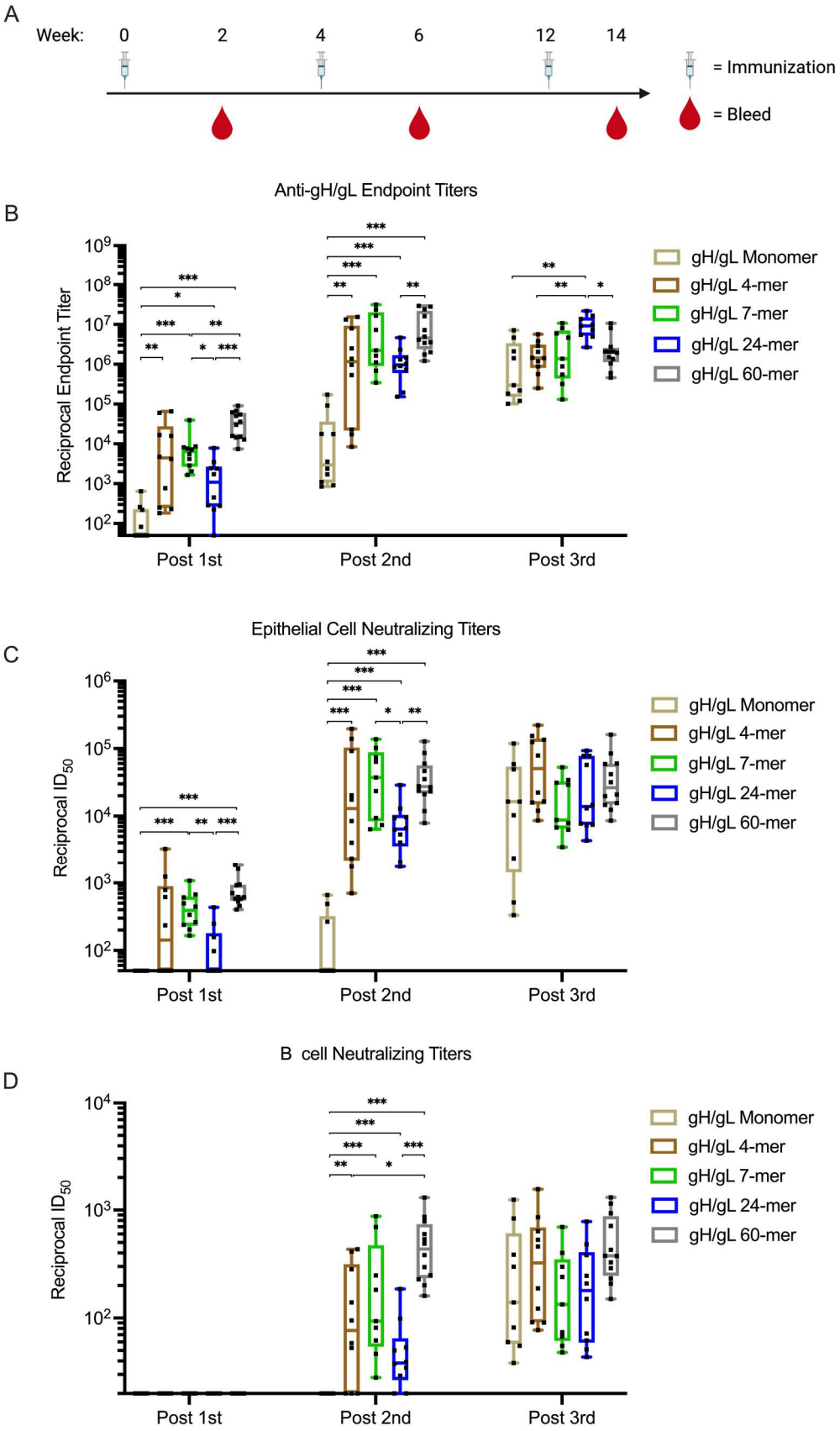
A
Week: 0 2 4 6 12 14
= Immunization
= Bleed
B
Anti-gH/gL Endpoint Titers
Reciprocal Endpoint Titer
Post 1st
Post 2nd
Post 3rd
gH/gL Monomer
gH/gL 4-mer
gH/gL 7-mer
gH/gL 24-mer
gH/gL 60-mer
C
Epithelial Cell Neutralizing Titers
Reciprocal ID50
Post 1st
Post 2nd
Post 3rd
gH/gL Monomer
gH/gL 4-mer
gH/gL 7-mer
gH/gL 24-mer
gH/gL 60-mer
D
B cell Neutralizing Titers
Reciprocal ID50
Post 1st
Post 2nd
Post 3rd
gH/gL Monomer
gH/gL 4-mer
gH/gL 7-mer
gH/gL 24-mer
gH/gL 60-mer

Figure 2. Immunogenicity of gH/gL nanoparticles. (**A**) C57BL/6 mice (n=10 mice for gH/gL monomer, 4-mer, 7-mer, and 24-mer, and n=12 for gH/gL 60-mer) were immunized with monomeric gH/gL or multimeric gH/gL nanoparticles at weeks 0, 4, and 12. Blood was collected 2 weeks after each immunization. (**B**) Endpoint plasma binding titers to gH/gL were measured by ELISA. Each dot represents the reciprocal endpoint titer for an individual mouse measured in duplicate. Box and whisker plots represent the minimum, 25th percentile, median, 75th percentile, and maximum values. The ability of plasma from individual mice to neutralize EBV infection of epithelial cells (**C**), or B cells (**D**). Each dot represents the reciprocal half-maximal inhibitory dilution (ID_{50}) titer of an individual mouse. Plasma that did not achieve 50% neutralization at the lowest dilution tested (1:20) was assigned a value of 10. Box and whisker plots represent the minimum, 25th percentile, median, 75th percentile, and maximum values. Significant differences were determined using Mann-Whitney tests with Holm-adjusted p-values (*$p < 0.05$, **$p < 0.01$, ***$p < 0.001$). See also Figures S2 and S3.

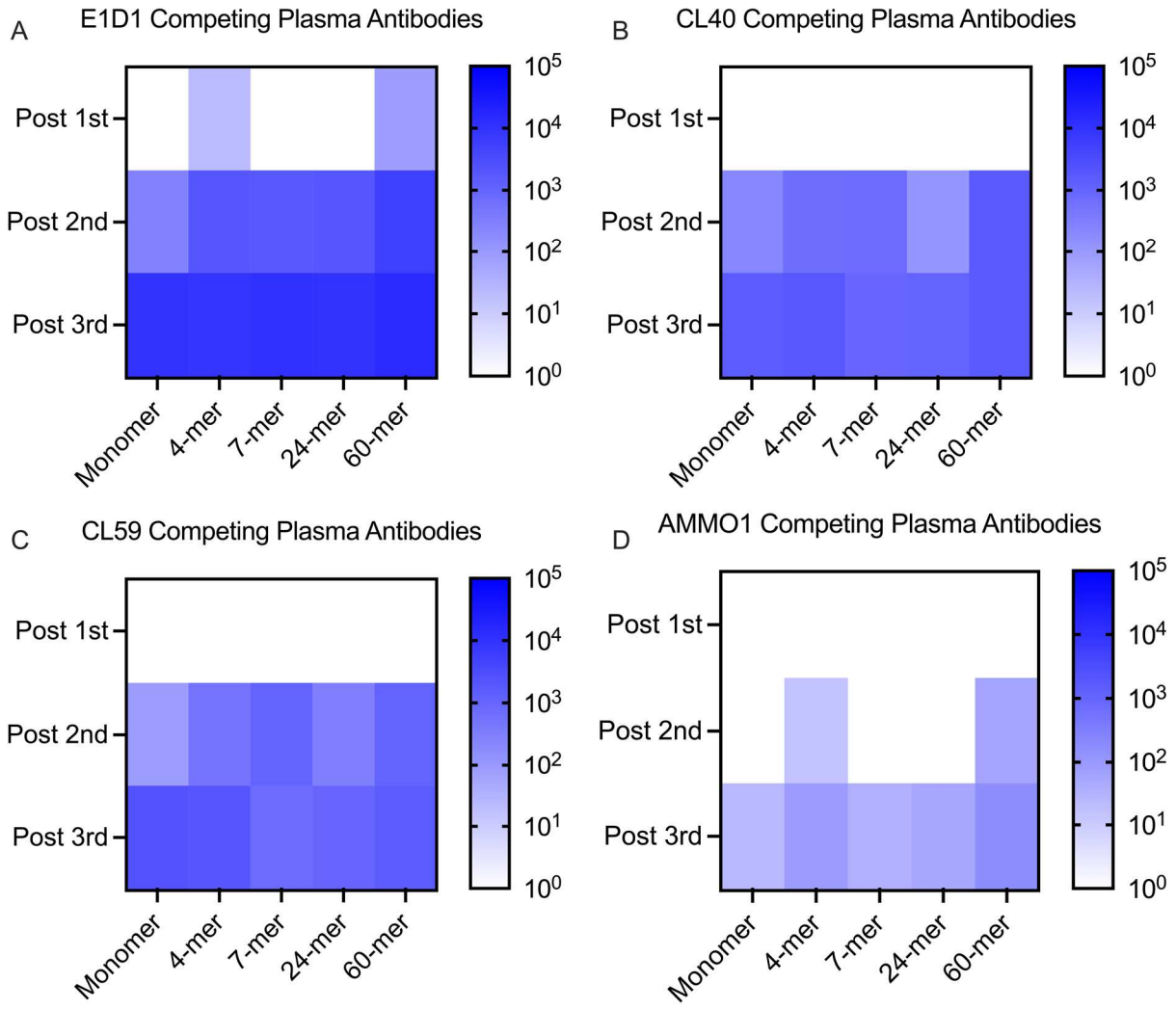

Figure 3. Plasma competition against monoclonal anti-gH/gL antibodies. The ability of plasma pooled from groups of mice immunized with monomeric gH/gL or multimeric gH/gL nanoparticles to inhibit binding to a panel of anti-gH/gL antibodies to monomeric gH/gL was measured by ELISA. The heatmap depicts the log reciprocal plasma dilution titers resulting in a 50% inhibition of (**A**) E1D1, (**B**) CL40, (**C**) CL59, or **(D**) AMMO1 antibodies at each time point. See Supplementary Figure S2 for titration curves. See also Figure S4.

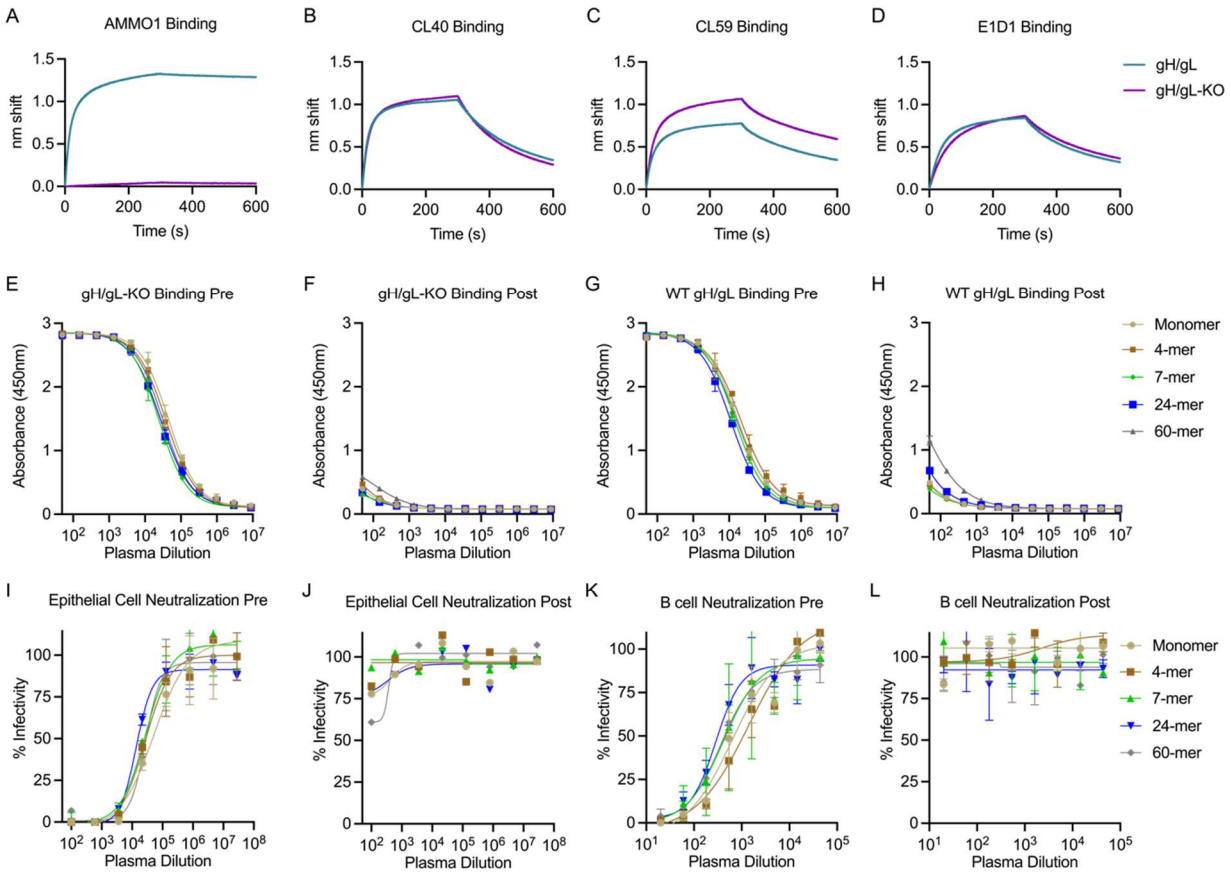

Figure 4. Depletion of AMMO1-KO insensitive antibodies from pooled plasma. The binding of AMMO1 (**A**), CL40 (**B**), CL59 (**C**), and E1D1 (**D**) binding to gH/gL and gH/gL-KO (gH K73W,Y76A/gL) were measured using biolayer interferometry. **(E-H)** Antibodies were depleted from pooled plasma collected following three immunizations with gH/gL or gH/gL nanoparticles using gH/gL-KO conjugated magnetic beads. Pre- and post-depletion plasma samples were then assayed for binding to gH/gL and gH/gL-KO by ELISA as indicated. Each data point represents mean and standard deviation of two technical replicates. **(I-L)** The ability of plasma pre- and post- depletion to neutralize EBV infection was measured in B cells and epithelial cells. Each data point represents mean and standard deviation of two technical replicates.

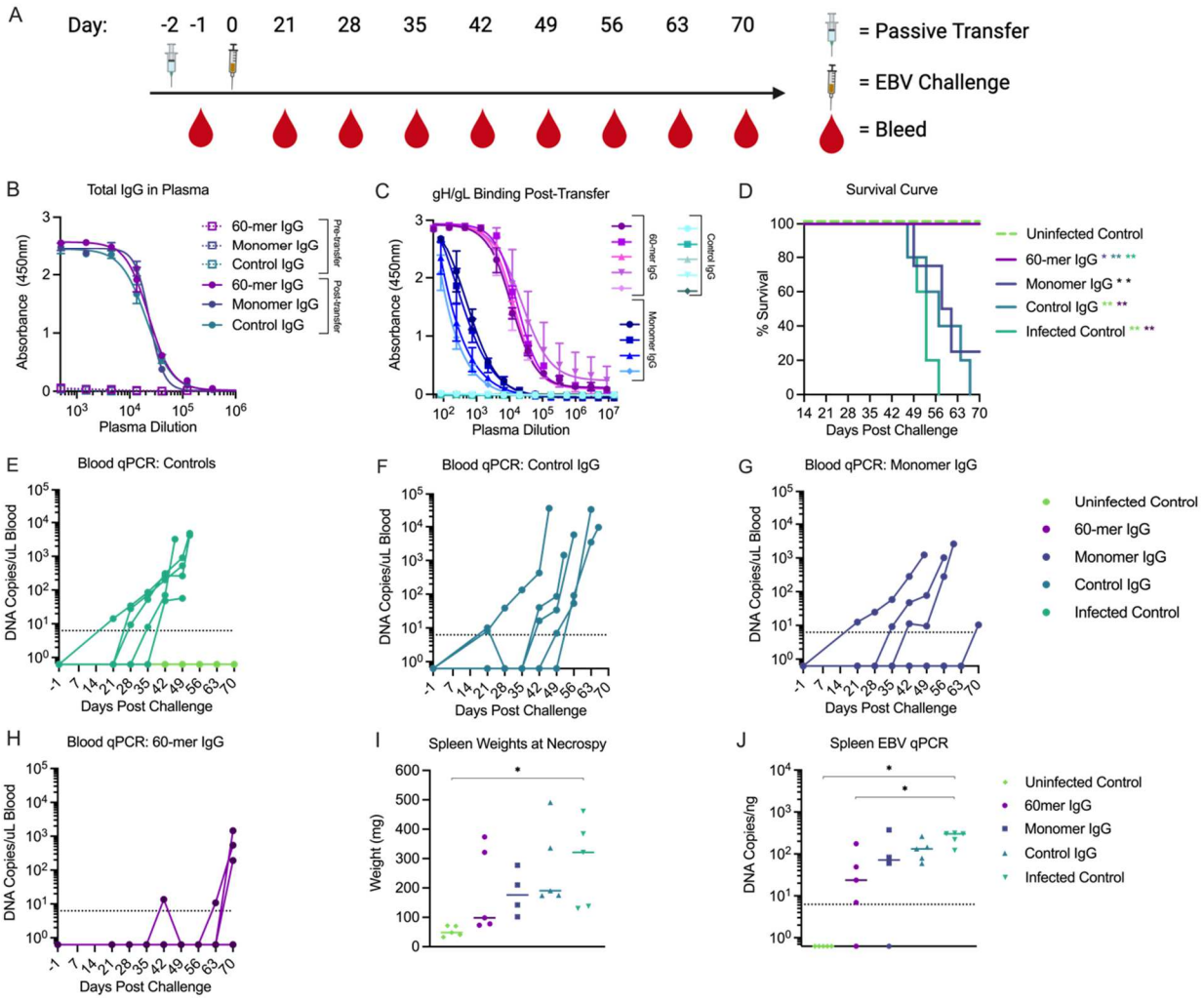

Figure 5. gH/gL nanoparticle elicited antibodies protect humanized mice from lethal EBV challenge. C57 BL6 mice were immunized with either monomeric or gH/gL 60-mer (n=20 per group) at weeks 0, and 4. Blood was collected by cardiac puncture at week 6, pooled and the serum IgG was purified. 0.5 mg of total IgG from monomer (n=4) or 60-mer (n=5) immunized mice was administered to humanized mice (**A**). A control group of mice received 0.5 mg total IgG purified from naïve C57 BL6 mice (n=5). (**B**) Total IgG was measured in pooled plasma from each group collected 3 days prior to and 1 day after IgG transfer. Each data point represents mean and standard deviation of two technical replicates. (**C**) Anti-gH/gL IgG antibodies from plasma collected from individual humanized mice one day after transfer was measured by ELISA as indicated. Each data point represents mean and standard deviation of two technical replicates. (**D**) Survival of humanized mice that received IgG purified from the indicated groups was monitored over a 70-day period following EBV challenge. An infected control group (n=5) did

not receive IgG prior to challenge, and an uninfected control group (n=5) did not receive IgG or viral challenge. Significant differences in the survival data were determined using log-rank tests (*p < 0.05, **p < 0.01). **(E-H)** Viral DNA was quantified in the peripheral blood of infected and uninfected control (**E**), Control IgG (**F**), Monomer IgG (**G**), and 60-mer IgG (**H**) groups collected at the indicated timepoints via qPCR. Each series of connected dots represents an individual mouse at each time point analyzed, and the dashed line represents the limit of detection. (**I**) At necropsy, spleens were harvested and weighed. Each dot represents an individual mouse, and the bar represents the median weight in milligrams. Photographs of individual spleens are shown in Figure S7. (**J**) Viral DNA copy number was quantified in splenic DNA extracts at necropsy. Each dot represents an individual mouse, the bar represents the median copy number, and the dashed line indicates the limit of detection. Significant differences for spleen weight and viral DNA copy number were determined using Mann-Whitney tests with Holm-adjusted p-values (*p < 0.05). See also Figures S5, S6 and S7.

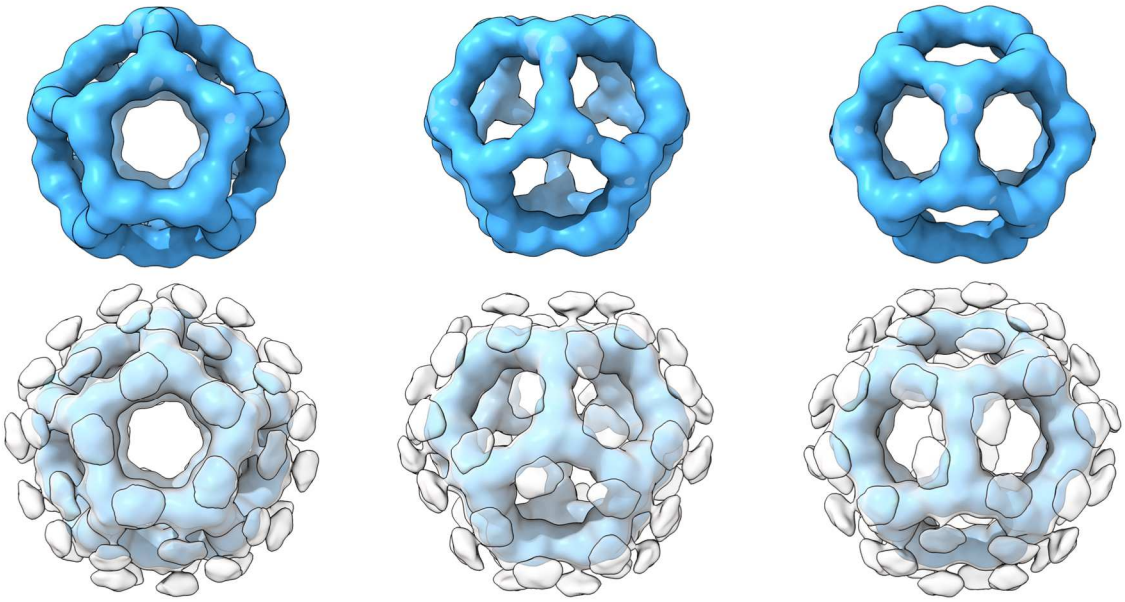

Figure S1. Related to Figure 1. 3D reconstruction of gH/gL-I3 60-mer. Negative stain electron microscopy icosahedral 3D reconstruction of the gH/gL-I3 60-mer displayed at different contour levels. (Top) High contour level depicting the I3 nanoparticle base scaffold. (Bottom) Superimposition of two contour levels of the same 3D reconstruction depicting both the I3 base scaffold (blue; high contour) and

the presence of displayed flexible gH/gL antigen (grey; low contour). All renderings were generated using ChimeraX.

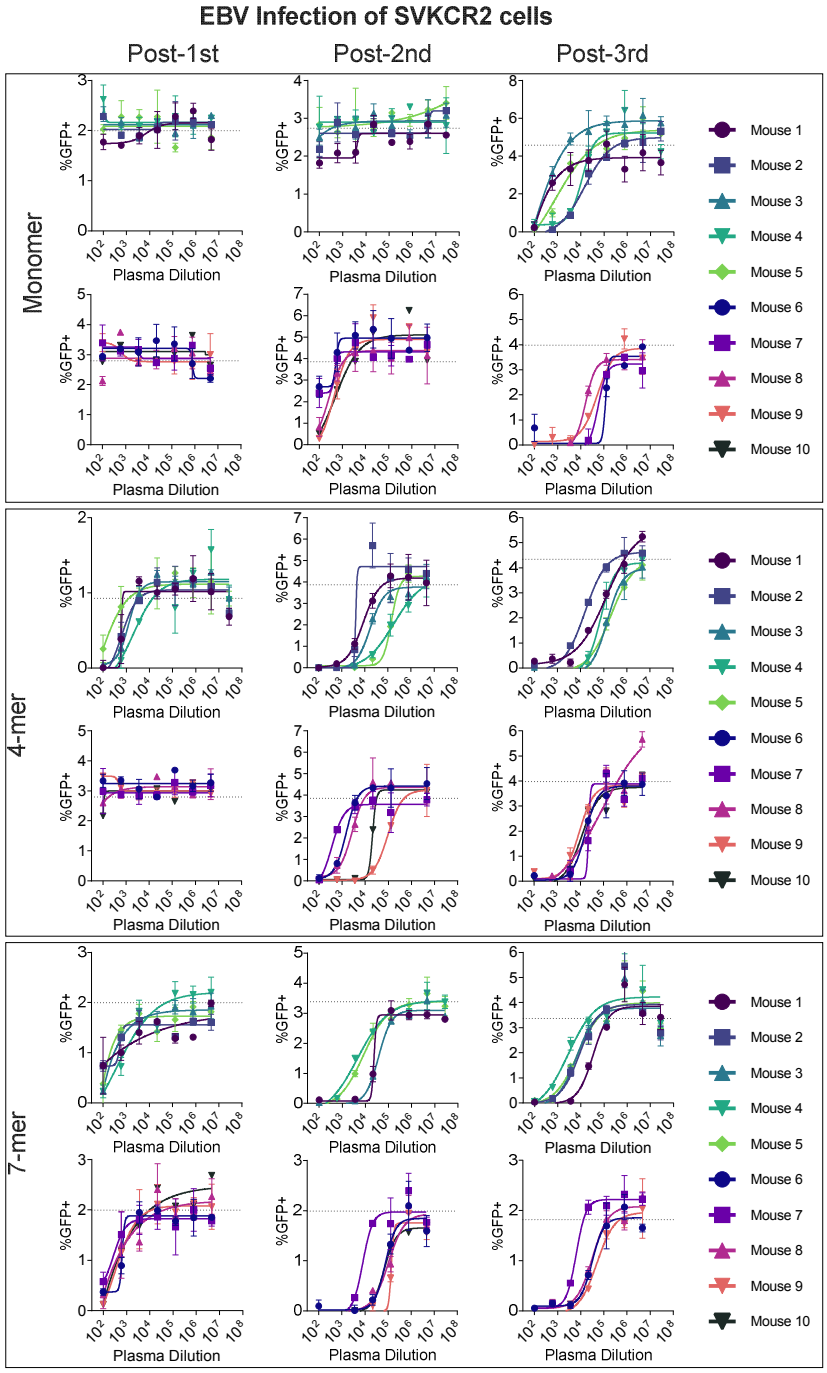

Figure S2. Related to Figure 2. Inhibition of EBV infection of epithelial cells by gH/gL immune plasma. Continued on next page.

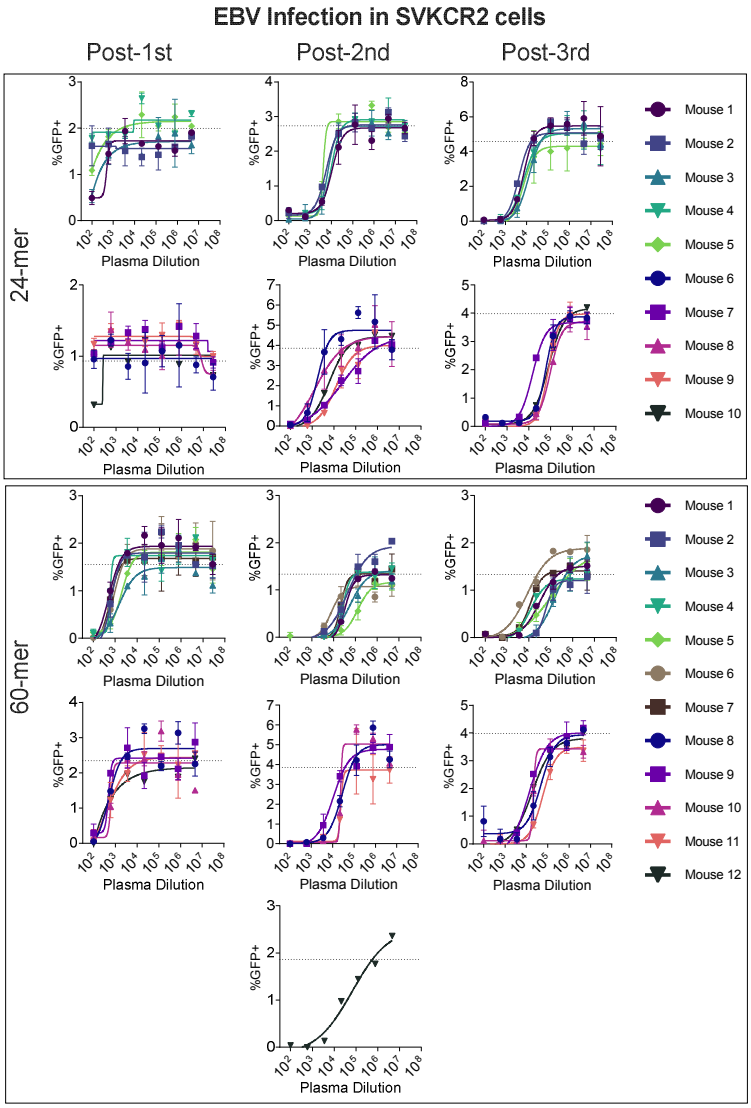

Figure S2 Related to Figure 2. Inhibition of EBV infection of epithelial cells by gH/gL immune plasma. Plasma from C57BL/6 (n=10-12 per group) mice were serially diluted and evaluated for its ability to inhibit AKATA-GFP EBV infection of SVKCR2 cells. Animals immunized with the same monomeric gH/gL or gH/gL nanoparticles are bound by boxes. The y-axis shows the % of background subtracted GFP+ SVKCR2 cells and the y-axis is the plasma dilution. Each data point represents mean and standard deviation of two technical replicates, and the dashed line indicates the % of GFP+ SVKCR2 cells in the absence of plasma.

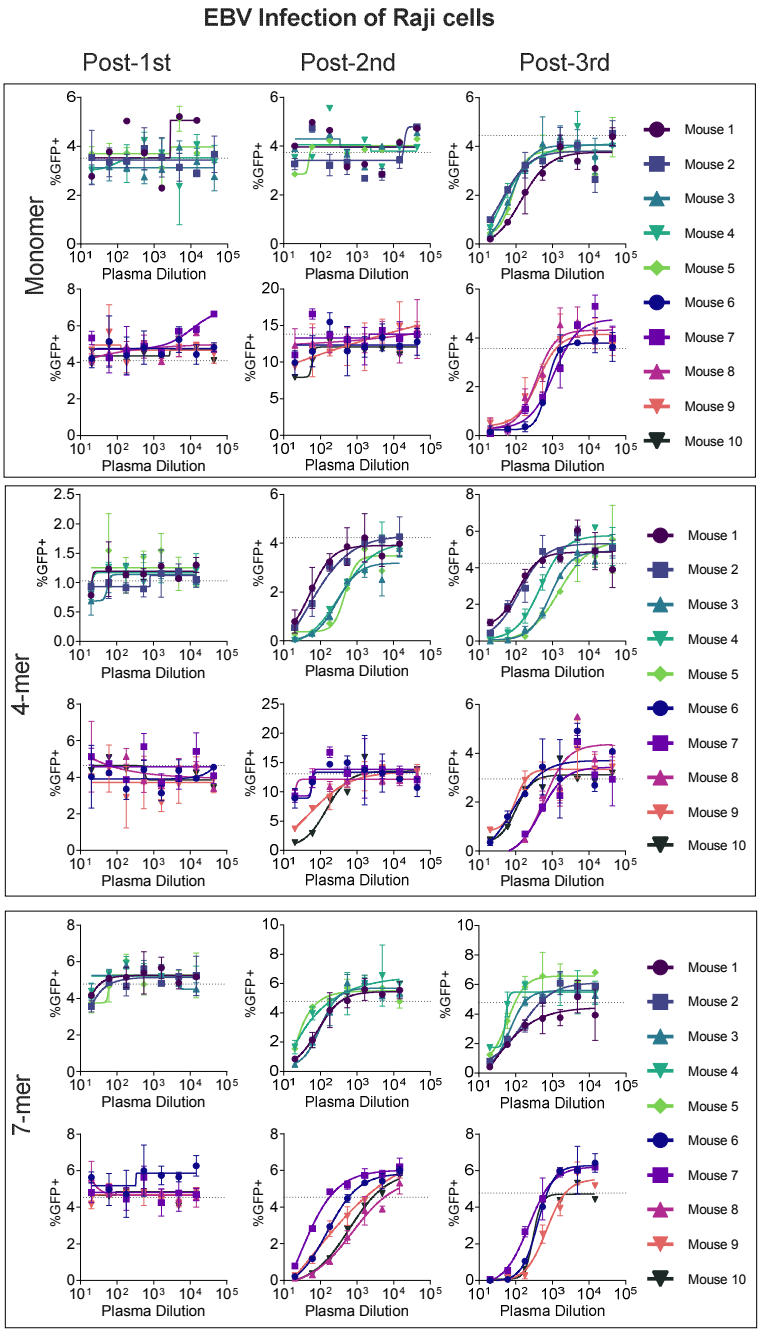

Figure S3. Related to Figure 2. Inhibition of EBV infection in B cells by gH/gL immune plasma.

Continued on next page.

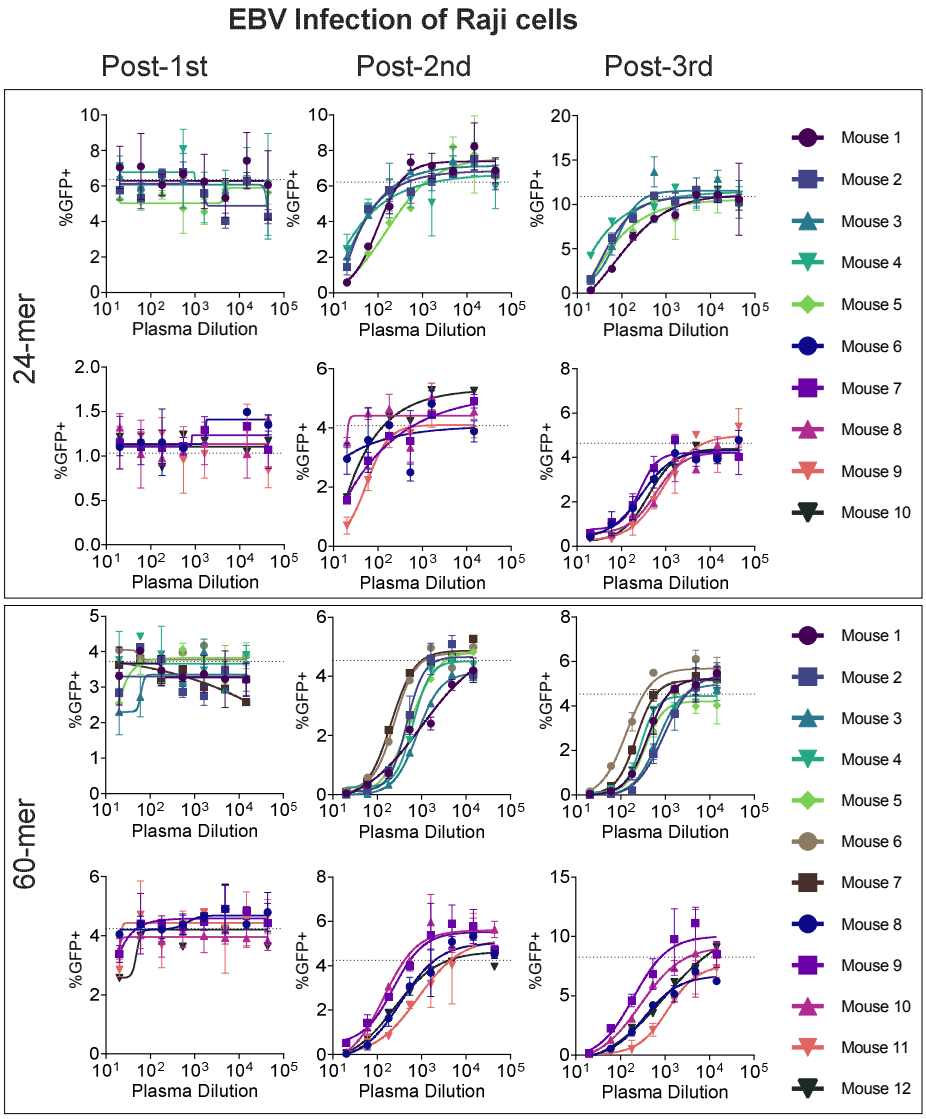

Figure S3. Related to Figure 2. Inhibition of EBV infection in B cells by gH/gL immune plasma.

Plasma from C57BL/6 mice (n=10-12 per group) were serially diluted and evaluated for its ability to inhibit EBV B95.8/F infection of Raji cells. Animals immunized with the same monomeric gH/gL or gH/gL nanoparticles are bound by boxes. The y-axis shows the % of background subtracted GFP+ Raji cells and the y-axis is the plasma dilution. Each data point represents mean and standard deviation of two technical replicates, and the dashed line indicates the % of GFP+ Raji cells in the absence of plasma.

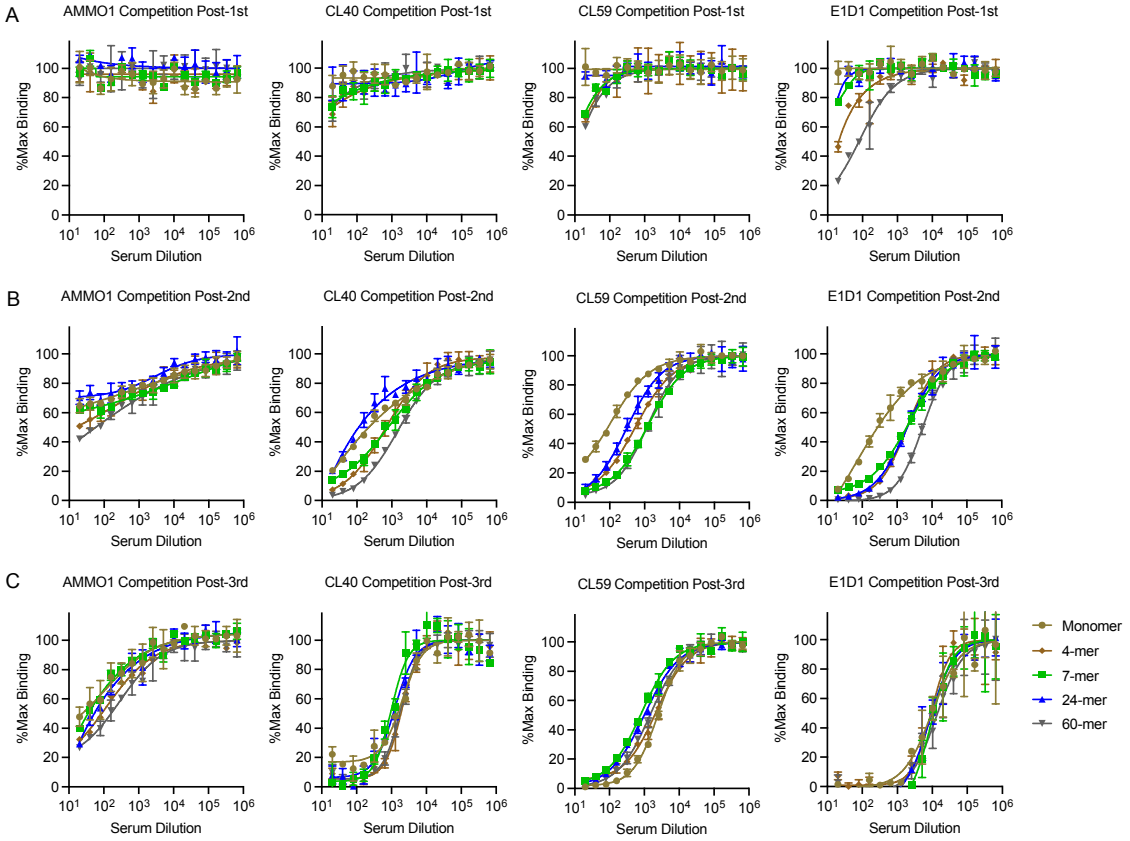

Figure S4. Related to Figure 3. Competitive binding between immune plasma and monoclonal antibodies. Competitive binding ELISAs were performed using pools of plasma from groups of C57BL/6 mice (n=10-12 per group) immunized with monomeric gH/gL or multimeric gH/gL nanoparticles, and a panel of anti-gH/gL antibodies. At each time point, pooled sera from each group were titrated on to gH/gL immobilized on an ELISA plate, after which either AMMO1, CL40, CL59, or E1D1 antibodies were added at a concentration previously determined to achieve half maximal binding. Competitions were performed using plasma pools collected at Post-1st (**A**), Post-2nd (**B**), and Post-3rd timepoints (**C**). Each data point represents mean and standard deviation of two technical replicates.

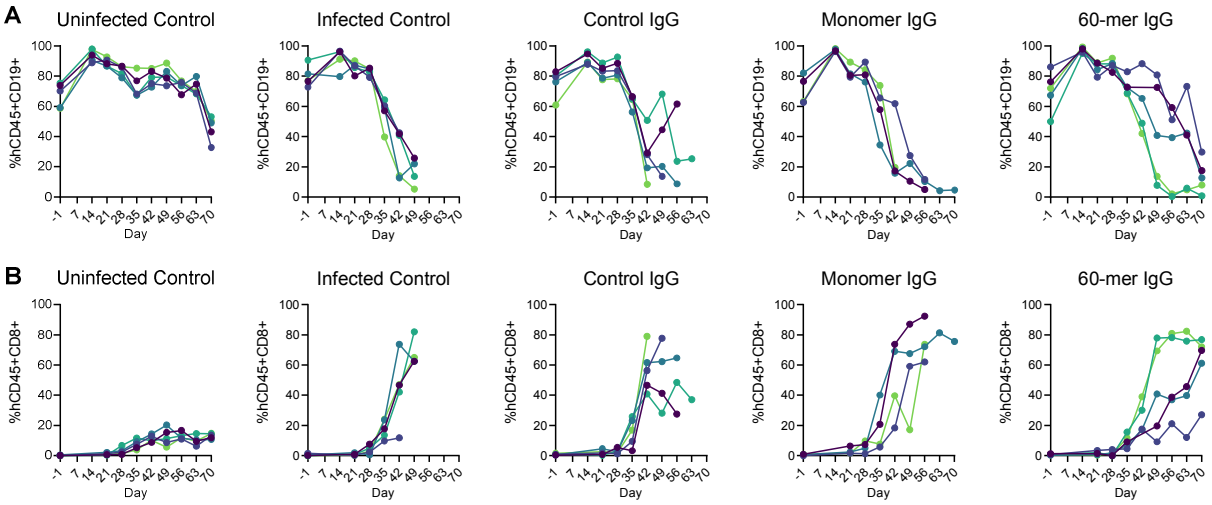

Figure S5. Related to Figure 5. hCD19+ and hCD8+cell frequencies in humanized mice challenged with EBV. hCD45+CD19+ B cells (**A**) and hCD45+CD8+ T cell (**B**) frequencies were measured in the peripheral blood drawn from the mice in Figure 5 at the indicated timepoints via flow cytometry. Individual mice in each group are indicated by different colored symbols. The same color is used to indicate the hCD45+CD19+ and hCD45+CD8+ T cells from the same mouse each group in **A** and **B.** The days indicated on the x-axis are relative to the time of challenge (day 0).

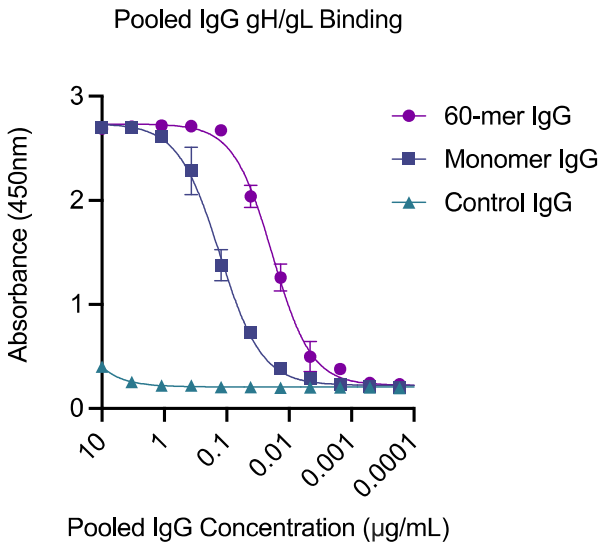

Figure S6. Related to Figure 5. ELISA of pooled purified IgG used in transfer studies. The binding of purified IgG used for adoptive transfer experiments in Figure 5 was measured against gH/gL was measured by ELISA. Each data point represents mean and standard deviation of two technical replicates.

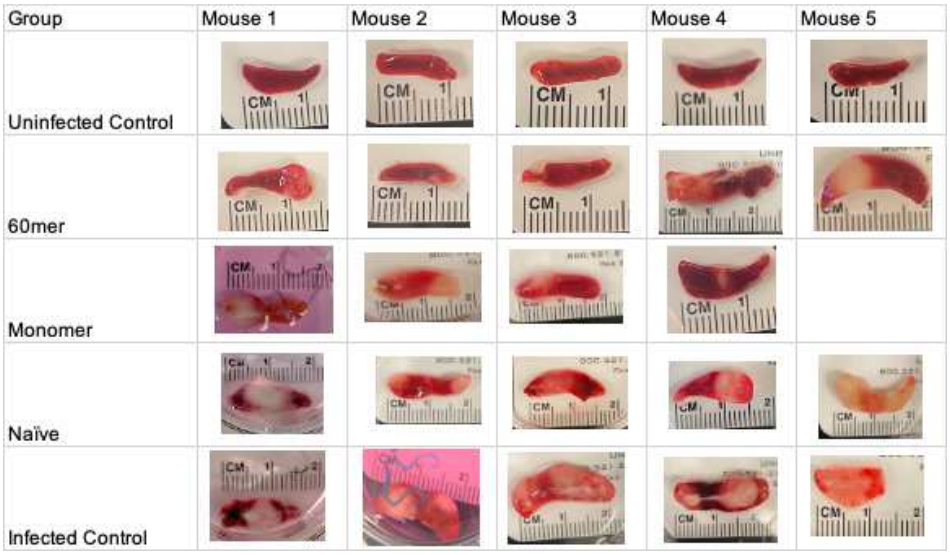

Figure S7. Related to Figure 5. Photographs of spleens from humanized mice challenged with EBV were taken at the time of necropsy.

gH/gL protein	Yield mg/L (mean ± S.D.)	# of production runs
Monomer	8.1	1
4-mer	2.6 ± 0.6	2
7-mer	1.8 ± 0.2	2
24-mer	1.4 ± 0.2	2
60-mer	0.5 ± 0.4	7

Table S1. Yields of various gH/gL nanoparticles.

Multimerization domain	Sequence	Predicted MW of protomer (particle) kDa*	Observed MW of particle by SEC-MALS**
4-mer	GGGGSGGGGSC-(EAIKAAAELGKAGISSEEILELLRAAHELGLDP)X4 ECIKAAAELGKAGISSEEILELLRAAHELGLGGSH HHHHH	115.7 (462.8)	543 ± 76 kDa (S200)
IMX313, 7-mer	GSSKKQGDADVCGEVAYIQSVVSDCHVPTAELR TLLEIRKLFLEIQKLKVELQGLSKE	101 (700.7)	700 ± 89 kDa (S200) 635 ± 69 kDa (Superose 6)
H. pylori Ferritin, 24-mer	GGGGSGGGGSGGSGESQVRQQFSKDIEKLLNE QVNKEMQSSNLYMSMSSWCYTHSLDGAGLFLF DHAAEEYEHAKKLIIFLNENNVPVQLTSISAPEHK FEGLTQIFQKAYEHEQHISESINNIVDHAIKSKDHA TFNFLQWYVAEQHEEEVLFKDILDKIELIGNENHG LYLADQYVKGIAKSRKSGS	114.9 (2757.6)	4418 ± 471 kDa (Superose 6)
Sec Opt I3, 60-mer	GSGSIEELFKKHKIVAVLRANSVEEAKKKALAVFL GGVDLIEITFTVPDADTVIKELSFLKEMGAIIGAGT VTSVEQARKAVESGAEFIVSPHLDEEISQFAKEK GVFYMPGVMTPTELVKAMKLGHTILKLFPGEVVG PQFVKAMKGPFPNVKFVPTGGVNLDNVAEWFKA GVQAVGVGEALNKGTPVEVAEKAKAFVEKIRGA T	155.7 (6942)	7377 ± 943kDa (Superose 6)

Table S2. Multimerization domains and observed and expected nanoparticle sizes.

*Includes the weight of the peptide component predicted by https://web.expasy.org/protparam/ plus the weight of 8 putative N-linked glycosylation sites on gH/gL, each assigned a molecular weight of 1kDa

** the column used for size exclusion chromatography appears in parentheses.

VI. METHODS

Experimental Models:

Comparative immunogenicity studies and the elicitation of polyclonal antibodies for passive transfer studies were performed in an equal mix of male and female C57BL/6 mice between 7-10 weeks of age. C57BL/6 mice were purchased from Jackson Labs and housed in a specific pathogen-free facility at the Fred Hutchinson Cancer Research Center.

6-7 week old NOD-scid Il2rg^{null} (NSG) NSG mice were irradiated with 275 Roentgen and then engrafted with 1×10^6 CD34-enriched PBSCs obtained from granulocyte colony-stimulating factor mobilized healthy donors by intravenous injection (herein called humanized mice). All humanized mice used in this study were female and were engrafted with CD34-enriched PBSCs from the same female donor. Humanized mice were purchased from the Co-operative Center for Excellence in Hematology, Fred Hutchinson Cancer Research Center. Prior to EBV challenge, humanized mice were housed in a specific pathogen-free facility and after EBV challenge the animals were housed in an animal basic safety level 2 facility at the Fred Hutchinson Cancer Research Center. All mice used in our studies were housed with free access to food and water with a 12:12 light:dark cycle. The animal facilities are accredited by the Association for Assessment and Accreditation of Laboratory Animal Care. Mice were handled in accordance with the NIH Guide for the Care and Use of Laboratory Animals. All animal experiments were approved by the Fred Hutch Institutional Animal Care and Use Committee and Institutional Review Board.

Cell Lines:

All cell lines were incubated at 37°C in the presence of 5% CO2 and were not tested for mycoplasma contamination. Raji cells (human male) were maintained in RMPI + 10% FBS, 2 mM L-glutamine, 100 U/ml penicillin, and 100 µg/ml streptomycin (cRPMI). 293-2089 cells (human female) were grown in cRPMI containing 100 µg/ml hygromycin.[141] AKATA (human female) B cells harboring EBV in which the thymidine kinase gene has been replaced with a neomycin and GFP cassette virus (AKATA-GFP) were grown in cRPMI containing 350 µg/ml G418.[100] SVKCR2 cells (human male) were grown in DMEM containing 10% cosmic calf serum, 2 mM L-glutamine, 100 U/ml penicillin, 100 µg/ml streptomycin, 10 ng/ml cholera toxin and 400 µg/ml G418.[132] 293-6E (human female, RRID:CVCL_HF20)

and 293T cells (human female, RRID:CVCL_0063) cells were maintained in Freestyle 293 media with gentle shaking.

Plasmids:

pTT3 plasmids containing cDNA encoding gH (AA 19-679, Genbank AFY97969.1) with a C-terminal His and Avi tag (pTT3-gH-HIS-AVI), and gL AA 24-137 Genbank: AFY97944.1 (pTT3-gL) with a TPA leader peptide have been previously described [112]. Site directed mutagenesis was used to introduce stop codons into gH between the His and Avi tags to produce an expression plasmid without the Avi tag, or 5' of the His tag to produce an expression plasmid with no tags (pTT3-gH). The K73W and Y76A mutations gH (herein called gH/gL-KO), were introduced into pTT3-gH-His using the QuickChange XL II Kit according to manufacturer's instructions.

To create a 7-mer gH expression construct, cDNA encoding a modified version of the C4b-BP protein (IMX313)[128] followed by a stop codon was synthesized and cloned in-frame with the gH ectodomain in pTT3-gH-His-Avi, replacing the His and Avi tags to create pTT3-gH-IMX313. To create a 24-meric gH expression construct, cDNA encoding the gH ectodomain was amplified by PCR with primers that introduced an EcoRI site at the 5' end followed by a $(G_4S)_2$ linker and finally a BamHI site at the 3' end. The PCR amplicon was cloned into pTT3-426cTM4ΔV1-3-ferritin[142] (a kind gift from Dr. Leonidas Stamatatos) replacing the HIV-1 Env gene fused to *Helicobacter pylori* ferritin[129] to create pTT3-gH-ferritin.

cDNA encoding gH-IMX313 and gH-ferritin were amplified by PCR, and then cloned into the XhoI and BamHI restriction sites of pCVL-UCOE0.7-SFFV-muScn-IRES-GFP [131] replacing the muSCN cDNA, to create pCVL-UCOE0.7-SFFV-gH-IMX313-IRES-GFP and pCVL-UCOE0.7-SFFV-gH-ferritin-IRES-GFP. A C153T mutation which replaces an unpaired cysteine in gH was added to pCVL- UCOE0.7-SFFV-gH-IMX313-IRES-GFP using the QuickChange XL II Kit according to manufacturer's instructions.

pCVL-UCOE0.7-SFFV-gH-I3-C153T-IRES-GFP was created by synthesizing a g-block encoding a modified version of I3-01 ([130] and J.Y.W. manuscript in preparation) with homology to the 3' end of the gH ectodomain at the 5' end of the g block and homology to the downstream IRES region at the 3' end of the g block. The plasmid backbone was amplified from pCVL-UCOE0.7-SFFV-gH-IMX313-IRES-GFP using a reverse primer that annealed to the 3' end of the gH cDNA (containing the C153T mutation) and a

forward primer that annealed to the 5' end of the IRES and Platinum SuperFi II DNA polymerase . The g block and linearized plasmid backbone were ligated together using the In-fusion HD cloning kit .

The tetramerization domain from cTRP24$_6$SS[127] was amplified by PCR using primers that added homology to the 3' end of the gH ectodomain at the 5' end homology to the downstream IRES region at the 3' of the amplicon. The amplicon was ligated to the PCR linearized plasmid backbone described above using the In-fusion HD cloning kit to create from pCVL-UCOE0.7-SFFV-gH-C153T-cTRP(6)ss-IRES-GFP.

cDNA encoding gL was amplified by PCR, and then cloned into the XhoI and BamHI restriction sites of pCVL-UCOE0.7-SFFV-muScn-IRES-RFP [131] replacing the muSCN cDNA, to create pCVL-UCOE0.7-SFFV-gL-IRES-RFP.

The sequences of all plasmids were confirmed by Sanger sequencing.

Lentiviral Production:

5.46 µg of psPAX2, 2.73 µg of pMD2.G (both gifts from Didier Trono), and 11.05 µg of each pCVL-derived gH plasmid were mixed in 1.56mL PBS followed by 39 µL of 293-Free Transfection Reagent. The transfection mix was gently agitated, incubated at room temperature for 15 minutes, and added dropwise to 13 mL of suspension-adapted 293T cells at 2×10^6 cells/mL in a 125 mL flask. After 24 hours, an additional 15 mL of 293 Freestyle media containing 15 µg of valproic acid was added to the cell culture. After another 48 hours, the cell culture was centrifuged at 1000 × *g* for 3 minutes, the supernatant was passed through a 0.44 µm filter, aliquoted, and stored at -80ºC.

Lentiviral Transduction:

Polybrene was added to 10 mL of 293-6E cells at 1×10^6 cells/mL to a final concentration of 2 µg/mL in addition to 2-3 mL of supernatant containing lentiviral particles harboring the various gH and gL expression constructs. 24 hours following transduction, 15 mL of 293Freestyle media was added to the culture. A Guava easyCyte Flow Cytometer was used to monitor gH (GFP$^+$) and gL (RFP$^+$) transduction efficiency 72 hours after transduction. Transduced cultures were expanded to a total volume of 1 liter and cultured until cell viability declined to ~80%. The transduced cell cultures were centrifuged at 4000 × *g* for 10 minutes to pellet cells. The supernatant was further clarified by passing through a 0.22 µm filter.

Purification of untagged monomeric gH/gL:

Clarified cell supernatant was adjusted to pH 5.5-6 using 2 M acetic acid. The clarified cell supernatant was incubated with CaptoMMC resin, pre-equilibrated with 30 mM sodium acetate, 50 mM NaCl, pH 5.5 (MMC binding buffer), then washed with 10 column volumes of MMC binding buffer and then eluted with 10 column volumes of 50 mM sodium acetate, 1 M ammonium chloride, pH 7.4. The protein elute was collected and concentrated using an Amicon Ultra-4 Centrifugal Filter Unit , and further purified via size exclusion chromatography (SEC) on a HiLoad 16/600 Superdex 200 pg column with 10 mM Tris, 50 mM NaCl, pH 7.4 as the mobile phase. The protein was further purified by anion exchange chromatography using a HiTrap Q HP column pre-equilibrated with 10 mM Tris, 50 mM NaCl, pH 7.4. The column was washed with 7% elution buffer (10 mM Tris, 1 M NaCl, pH 7.4) until the absorbance at A280 achieved a stable baseline. gH/gL was eluted over a linear gradient from 7% to 25% elution buffer over 20 column volumes. The eluted protein was further purified by SEC with Phosphate-Buffered Saline (PBS) as the mobile phase on the Superose 6 Increase 10/300 GL . Fractions were analyzed by SDS-PAGE to identify those containing gH/gL >95% purity based on Coomassie blue staining. The purified protein was aliquoted, flash frozen in liquid nitrogen and stored long term at -80°C.

Purification of Polyhistidine Tagged Proteins gH/gL His, gH/gL-KO, and gH/gL-cTRP(6)ss:

Clarified cell supernatant was adjusted to a final concentration of 10 mM imidazole and 500 mM NaCl and then incubated with HisPur Ni-NTA resin pre-equilibrated with 10 mM Tris, 500 mM NaCl, 10 mM imidazole, 0.02% azide, pH 7.1 (Ni-NTA binding buffer). The column was then washed with 10 column volumes of Ni-NTA binding buffer and eluted using 10 mM Tris, 500 mM NaCl, 500 mM imidazole, pH 8.0. The NiNTA eluate was subsequently purified by SEC using a Superdex 200 column with PBS as the mobile phase. Purified protein was aliquoted flash frozen in liquid nitrogen and stored at -80ºC.

Purification of gH/gL-4-mer (gH/gL-IMX313) and gH/gL-ferritin:

Clarified cell supernatant was adjusted to a final concentration of 100 mM NaCl and then incubated with Galanthus Nivalis Lectin Agarose , washed with 10 column volumes of 20 mM Tris, 100 mM NaCl, 1 mM EDTA, pH 7.4 and eluted with 20mM Tris, 100 mM NaCl, 1 mM EDTA, 1M methylmannopyranoside, pH 7.4. The eluted protein was further purified by SEC with PBS as the mobile phase on the Superdex 200 column or the Superose 6 Increase 10/300 GL for gH/gL-C4b and gH/gL-

ferritin, respectively. gH/gL-IMX313 was flash frozen and stored at -80ºC. gH/gL-ferritin was expressed and purified within a week of each immunization and stored at 4ºC.

Purification of gH/gL-I3:

To prepare an affinity chromatography resin to purify gH/gL-I3, 4.5 mg E1D1 antibody was incubated with 1 mL Protein A resin with rotation at room temperature for 30 minutes and then washed thoroughly with PBS. 6.5 mg of disuccinimidyl suberate was dissolved in 0.5 mL DMSO, then diluted in 10 mL PBS and added to the Protein A resin. The resin and DSS mixture were incubated at room temperature with rotation for at least 1 hour. The resin was washed thoroughly with PBS, and then incubated overnight with rotation at 4ºC in 10 mL of 1 M Tris, pH 7.5, and washed again extensively with PBS. The resin was then washed with Pierce IgG Elution buffer to remove any E1D1 antibody that was not crosslinked to the resin, and then washed again with PBS. The E1D1 affinity resin was stored in 50 mM Tris, 150 mM NaCl, 0.02% azide when not in use.

Supernatant from cells transduced with gH/gL-I3-was incubated with the E1D1 resin, washed with TBS, eluted with Pierce IgG elution buffer, and neutralized with a 1/10th volume of 1 M Tris pH 8. The eluted protein was further purified by SEC using a Superose 6 Increase column with 50 mM Tris, 150 mM NaCl, 150 mM L-arginine, pH 8 as the mobile phase. Purified protein was flash frozen and stored at -80ºC.

Size exclusion chromatography with multi-angle light scattering:

Fractions containing single predominant species from the initial round of size exclusion chromatography were concentrated down with 10,000 MWCO protein concentrators (Novagen) to a concentration of 1.0-2.0 mg/mL. 100 uL of each sample was then run through a high-performance liquid chromatography system (Agilent 1260) using a Superdex 200 10/300 GL or a Superose 6 Increase 10/300 column gel filtration column at an elution rate of 1 mL/min in Pierce TBS in line with a multi-angle light scattering detector (Wyatt Heleos) and refractive index detector (Wyatt tREX). The data was then analyzed using ASTRA (Wyatt Technologies) to calculate the absolute molecular weights for each designed protein. Accounting for error in light scattering data acquisition, species with calculated molecular weights within 13% of the expected target molecular weight for each design were considered to be forming the anticipated oligomeric state.

Recombinant Antibodies:

Cloning, expression and purification of AMMO1[112], CL40 , and CL59[60] was performed as previously described. For cloning of E1D1, codon-optimized cDNA corresponding to E1D1 VH (GenBank: KX755644) was synthesized (Integrated DNA Technologies) and cloned in-frame with the human IgG1 constant region in pTT3-based expression vectors. Codon-optimized cDNA corresponding to E1D1 VL (GenBank: KX755645) was cloned in-frame with the human kappa constant regions in pTT3-based expression vectors. Recombinant E1D1 was expressed in 293-E cells and purified using Protein A affinity chromatography.

Negative-Stain Electron Microscopy:

For gH/gL 4-mer and 7-mer, 1% uranyl formate negative staining solution and Formvar/carbon grids (Electron Microscopy Sciences) of 300 mesh size were used to perform the negative staining experiment. The protein samples of 4-mer and 7-mer gH/gL were diluted to ~40 µg/ml and ~50 µg/ml, respectively and applied for 60 sec on glow discharged grids. Excess sample was blotted off using Whatman filter paper and the grids were rinsed using water droplets and further stained for additional 60 seconds. Excess stain was blotted off and the grids were air dried for 1-2 min.

For gH/gL 24-mer and 60-mer, sample were diluted to 100 µg/mL and 3 µL was negatively stained using Gilder Grids overlaid with a thin layer of carbon and 2% uranyl formate as previously described [143].

For the gH/gL 4-mer and 7-mer, data were collected using a FEI Tecnai T12 electron microscope operating at 120 keV equipped with a Gatan Ultrascan 4K×4K CCD camera. The images were collected using an electron dose of 45.05 e−/Å^2, a magnification of 67,000 × that corresponds to pixel size of 1.6 Å, and exposure time of 1 sec. The defocus range used was -1.00 µm to -2.00 µm. The data was collected using Leginon interface [144] and processed using cryoSPARC [145]. Particles were further picked from the micrographs and subjected to 2D classification and the best 2D classes were selected.

For the gH/gL 24-mer, data were collected on an FEI Technai 12 Spirit 120kV electron microscope equipped with a Gatan Ultrascan 4000 CCD camera. A total of 150 images were collected per sample by using a random defocus range of 1.1–2.0 µm with a total exposure of 45 e−/A^2. Data were automatically acquired using Leginon, and data processing was carried out using Appion.[146] The

parameters of the contrast transfer function (CTF) were estimated using CTFFIND4,[147] and particles were picked in a reference-free manner using DoG picker.[148] Particles were extracted with a binning factor of 2 after correcting for the effect of the CTF by flipping the phases of each micrograph with EMAN 1.9.[149] The gH/gL 24-mer stack was pre-processed in RELION/2.1[150-152] with an additional binning factor of 2 applied, resulting in a final pixel size of 6.4 Å. Resulting particles were sorted by reference-free 2D classification over 25 iterations.

For the 60-mer, data were collected on an Talos L120C 120kV electron microscope equipped with a CETA camera. A total of ~350 images were collected per sample by using a random defocus range of 1.3–2.3 µm, with a total exposure of 35 e−/A^2, and a pixel size of 3.16 Å/pixel. Data were automatically acquired using EPU (ThermoFisher Scientific). All data processing was performed using CryoSPARC.[145] The parameters of the contrast transfer function (CTF) were estimated using CTFFIND4,[147] and particles were picked initially in a reference-free manner using blob picker, followed by template picking using well-defined 2D classes of intact nanoparticles. Particles were extracted after correcting for the effect of the CTF for each micrograph with a box size of 256 pixels. Extracted particles were sorted by reference-free 2D classification over 20 iterations. 3D ab initio was performed in cryoSPARC with the subsequent homogenous refinement step performed using icosahedral symmetry. The resulting 3D map was displayed at two different contours levels and images were generated using ChimeraX [153].

Immunizations in C57BL/6 Mice:

Comparative immunogenicity studies were performed in groups of 10 C57BL/6 mice (5 male and 5 female) between 7-10 weeks of age. After collecting a pre-bleed, mice were immunized at weeks 0, 4, and 12 with 5 µg (total protein) of monomer, 4-mer, 7-mer, 24-mer, or 60-mer formulated with 20% (v/v) synthetic lipid A in squalene emulsion SLA-SE[154] in PBS or TBS (60-mer only) at a total volume of 100 µL. Mice were immunized via intramuscular injection split into two 50 µL doses split between both rear legs. Blood was collected retro-orbitally 2 weeks after the first and second immunizations and via cardiac puncture at week 14. Blood was collected in tubes containing a 1/10th volume of citrate. Plasma was separated from whole blood via centrifugation and then heat inactivated at 56°C for 30 min. For passive transfer experiments into humanized mice immunizations were performed in groups of 20 C57BL/6 mice (10 male and 10 female) between 7-10 weeks of age. After collecting a pre-bleed, mice were immunized

at weeks 0 and 4 with 5 μg of gH/gL monomer or 60-mer formulated in PBS (monomer) or TBS (60-mer) with 50% (v/v) Sigma Adjuvant System (SAS) for a total volume of 100 μL. Mice were immunized via intramuscular injection split 50 μL each between both rear legs. Blood was collected retro-orbitally via cardiac puncture at week 6 into a separate vial for each mouse containing 100 μL citrate. Plasma was separated from whole blood via centrifugation.

IgG Purification from Murine Plasma:

Plasma was pooled and heat inactivated at 56°C for 1 hour then diluted in protein G binding buffer and passed over a column containing 1mL of protein A/G resin. The column was then washed 3 times with 5 column volumes of binding buffer. Finally, IgG was eluted from the resin in 5 × 2 mL fractions using IgG elution buffer. Fractions were buffer exchanged into PBS, concentrated, filter sterilized, and yields were measured by nanodrop.

EBV-Reporter Virus Production:

To produce B-cell tropic GFP reporter viruses (B95-8/F), 9×10^6 293–2089 cells were seeded on a 15 cm tissue culture plate in cRPMI containing 100 μg/mL hygromycin. 24 hours later the cells were washed twice with PBS, the media was replaced with cRMPI without hygromycin, and the cells were transfected with 15 μg of each of p509 and p2670 expressing BZLF1 and BALF4, respectively, using GeneJuice transfection reagent.[141,155] 72 hours later the cell supernatant was collected, centrifuged at 300 × *g* for 5 min and then passed through a 0.8 μm filter. To produce epithelial cell tropic virus, B cells harboring AKATA-GFP EBV were suspended at 4×10^6 cells/ml in RPMI containing 1% FBS. Goat anti-human IgG was added to a final concentration 100 μg/ml and incubated at 37°C for 4 hours. Cells were then diluted to 2×10^6 cells/ml in RPMI containing 1% FBS and incubated for 72 hours. Cells were pelleted by centrifugation at 300 × *g* for 10 min and then the supernatant was passed through a 0.8 μm filter. Bacitracin was added to a final concentration of 100 μg/mL. Virions were concentrated 25× by centrifugation at 25,000 × *g* for 2 hours and re-suspended in RPMI containing 100 μg/ml bacitracin. Virus was stored at -80°C and thawed immediately before use.

B cell Neutralization Assay:

B cell neutralization assays were carried out in Raji cells essentially as described [82]. Mouse plasma was serially diluted in duplicate wells of 96 well round-bottom plates containing 25 μL of cRPMI.

12.5 µl of B95-8/F virus (diluted to achieve an infection frequency of 1-5% at the final dilution) was added to each well and plates were incubated at 37°C for 1 hour. 12.5 µl of cRPMI containing 4×10^6 Raji cells/ml was added to each well and incubated for another hour at 37°C. The cells were then pelleted, washed once with cRPMI, and re-suspended in cRPMI. Reciprocal plasma dilutions are reported relative to the final infection volume (50 µL). After 3 days at 37°C, cells were fixed in 2% paraformaldehyde. The percentage of GFP+ Raji cells was determined on a BD LSRII cytometer or Luminex Guava HT cytometer.

To account for any false positive cells due to auto-fluorescence in the GFP channel, the average %GFP+ cells in negative control wells (n = 4-6) was subtracted from each well. The infectivity (%GFP+) for each well was plotted as a function of the plasma dilution. The neutralization curve was fit using the log(inhibitor) versus response- variable slope (four parameters) analysis in Prism 9.2.0. The half maximal inhibitory plasma dilution ID_{50} was interpolated from the curve in Prism 9.2.0.

For depletion assays, the average %GFP+ cells in negative control wells (n=4-6) was subtracted from each well. The %Infectivity was calculated for each well by dividing the %GFP+ cells in each well by the average %GFP+ cells in the most dilute plasma dilution wells and multiplying by 100. % Infectivity was plotted as a function of the plasma dilution. The neutralization curve was fit using the log(inhibitor) versus response- variable slope (four parameters) analysis in Prism 9.2.0.

Epithelial Cell Neutralization Assay:

1.5×10^4 SVKCR2 cells per well were seeded into a 96 well tissue culture plate. The following day plasma was serially diluted in duplicate wells containing 20 µL of media in a 96 well flat bottom plate followed by the addition of 20 µL of 25× concentrated epithelial cell-tropic virus and incubated for 15 min. Media was aspirated from the SVKCR2 cells and replaced by the antibody-virus mixture and incubated at 37°C. 48 hours later the cells were detached from the plate using 0.25% trypsin, transferred to a 96 well round bottom plate, washed twice with PBS, and fixed with 10% formalin, and the percentage of GFP+ cells were determined on an BD LSRII cytometer or Luminex Guava HT. Percent neutralization was determined as in the B cell neutralization assay.

Measurement of Plasma Antibody Endpoint Binding Titers by Anti-His Capture ELISA:

30µL/well of rabbit anti-His tag antibody was adsorbed at a concentration of 0.5 µg/mL on to 384 well microplates at 4ºC for 16 hours in a solution of 0.1 M NaHCO3 pH 9.4-9.6 (coating buffer). The next day, plates were washed 4 times with 1 x PBS, 0.02% Tween 20 (ELISA wash buffer) prior to blocking for 1 hour with 80 µL/well of 1× PBS containing 10% non-fat milk and 0.02% Tween 20 (blocking buffer). After blocking, plates were washed 4× with wash buffer and 30 µl/well of a 2 µg/mL solution of monomeric His-tagged gH/gL diluted in blocking buffer was added to the plate and incubated for 1 hour, and then washed 4× with ELISA wash buffer. Plasma was diluted in blocking buffer and three-fold serial dilutions were performed in duplicate followed by a 1-hour incubation at 37°C. 8-16 additional control wells were included that contained immobilized gH/gL but no immune plasma (control wells). Following 4 additional washes with ELISA wash buffer, a 1:2,000 dilution of goat anti-mouse IgG-HRP (SouthernBiotech) in blocking buffer was added to each well and incubated at 37°C for 1 hour followed by 4 washes with ELISA wash buffer. 30 µl/well of SureBlue Reserve TMB Microwell Peroxidase substrate was added. After 5 min, 30µL/well of 1N sulfuric acid was added and the A_{450} of each well was read on a Molecular Devices SpectraMax M2 plate reader. The binding threshold was defined as the average plus 10 times the standard deviation of the determined by calculating the average of A_{450} values of the control wells. Endpoint titers were interpolated from the point of the curve that intercepted the binding threshold using the Prism 9.2.0 package.

Measure of Competitive Binding Titers by ELISA:

Coating, blocking, and gH/gL immobilization steps were performed as described under "Measurement of plasma antibody endpoint binding titers by anti-His capture ELISA." Following capture of monomeric gH/gL, equal amounts of plasma from each mouse in a group were pooled and diluted in blocking buffer and 2-fold serial dilutions were performed, followed by a 1-hour incubation at 37°C. Following 4 additional washes with ELISA wash buffer, monoclonal antibodies AMMO1, CL40, CL59, and E1D1 were added at a concentration that achieves half-maximal binding (EC_{50}; pre-determined in the same assay in the absence of competing sera) to each well containing serially diluted pooled sera from each group, followed by a 1-hour incubation at 37°C. After 4 washes with ELISA washing buffer, a 1:20,000 dilution of goat anti-human IgG-HRP (Jackson ImmunoResearch) in blocking buffer was added to each well and incubated at 37°C for 1 hour followed by 4 washes with ELISA wash buffer. Addition of

SureBlue Reserve TMB Microwell Peroxidase substrate, addition of 1N sulfuric acid, and reading of plates was performed as described above. The average A_{280} values of buffer only control wells were subtracted from each mAb containing well and plotted in Prism 9.2.0. A280 values were plotted as a function of the $\log_{10}$ of the plasma dilution. A binding curve was fit using the Sigmoidal, 4PL, X is log(concentration) least squares fit function. Maximum binding was defined as the best-fit value for the top of each curve computed in Prism. A_{280} values at each dilution on the curve were divided by the maximum binding and multiplied by 100 to calculate the % of max binding ([A_{280} at each dilution/max binding] × 100). The titer at which half-maximal binding was observed was interpolated from the binding curve using the Prism 9.2.0 package (GraphPad Software).

Biotinylation of recombinant proteins:

Recombinant gH/gL proteins were biotinylated using the EZ-Link NHS-PEG4-Biotin Kit according to the manufacturer's instructions. The biotinylation reaction incubated overnight at 4ºC, after which excess biotin was removed using a Zeba Spin Desalting Column.

Neutravidin Capture ELISA

30 µL/well of a 0.3 µg/mL solution of NeutrAvidin in ELISA coating buffer was incubated on 384 well microplates at 4ºC for 16 hours. The next day, plates were washed 4 times with ELISA wash buffer prior to blocking for 1 hour with 80 µL/well of 1X PBS containing 3% bovine serum albumin and 0.02% Tween 20 (neutravidin blocking buffer). After blocking, plates were washed 4 times with ELISA wash buffer and 30 µL/well of a 2 µg/mL solution of biotinylated gH/gL monomer, 4-mer, 7-mer, 24-mer, or 60-mer was added and allowed to incubate 1 hour. After 4 washes with ELISA wash buffer, a panel of monoclonal antibodies were diluted to 10 µg/mL in neutravidin blocking buffer and three-fold serial dilutions were performed in duplicate followed by a 1-hour incubation at 37°C. 8-16 additional control wells were included that contained immobilized the gH/gL but no monoclonal antibodies (control wells). Following 4 additional washes with ELISA wash buffer, a 1:5000 dilution of goat anti-human IgG-HRP (SouthernBiotech) in neutravidin blocking buffer was added to each well and incubated at 37°C for 1 hour followed by 4 washes with ELISA wash buffer. Addition of SureBlue Reserve TMB Microwell Peroxidase substrate, addition of 1N sulfuric acid, and reading of plates was performed as described above.

Measurement of total plasma IgG:

Plasma was serially diluted in ELISA coating buffer in duplicate and incubated on 384-well microplates at 4°C for 16 hours. At least 10 additional control wells were included that contained only coating buffer and no plasma. The next day, plates were washed 4× with ELISA wash buffer prior to blocking for 1 hour with 80 µL/well of ELISA blocking buffer. After blocking, plates were washed 4× with ELISA wash buffer and a 1:4000 dilution of goat anti-mouse IgG Human ads-HRP in ELISA blocking buffer was added to each well and incubated at 37°C for 1 hour followed by 4 washes with ELISA wash buffer. Addition of SureBlue Reserve TMB Microwell Peroxidase substrate, addition of 1N sulfuric acid, and reading of plates was performed as described above.

Bead Depletion Assays:

To conjugate biotinylated gH/gL and gH/gL-KO to beads, streptavidin magnetic beads were washed 2× with PBS using a magnetic separator and then co-incubated with biotinylated gp350, gH/gL, or gH/gL-KO on a rotator overnight at 4°C. The supernatant was collected using a magnetic separator and analyzed via spectrophotometry to ensure protein concentration in supernatant had been reduced and saturation of beads was achieved. Beads were washed 2× to remove excess unbound gp350, gH/gL, or gH/gL-KO and stored at 4°C in PBS.

For depletion of plasma antibodies, beads were resuspended with diluted, pooled plasma and incubated 16 hours at 4°C on a rotator. Beads were then separated from plasma using a magnetic separator and the remaining plasma was collected and transferred to a new tube and subsequently tested for binding to gH/gL and for neutralizing activity.

EBV Challenge in Humanized Mice:

10 weeks post-cell transfer of CD34-enriched PBSCs, successful human cell engraftment in NSG mice was confirmed via immunophenotyping of circulating lymphocytes using antibodies at indicated dilution: hCD45-FITC (1:100), hCD8-BV21 (1:100), L/D-BV506 (1:200,), hCD19-BV711 (1:100), hCD20-BV786 (1:200), mCD45-APC (1:200), hCD4-AF700 (1:250), hCD33-PE (1:100), mCD16/32 (1:200).

12-13 weeks post-human HSPC transfer, 500 µg of total IgG purified from immunized C57BL/6 mice were injected per humanized mouse intraperitoneally (IP). Two days prior to, and one day following transfer, blood was collected to measure the relative levels of total and anti-gH/gL IgG in the plasma.

48 hours after transfer, the mice received a dose of EBV B95.8/F, equivalent to 33,000 infectious units as determined by infection of Raji cells, via retro-orbital injection. Beginning 3 weeks post-challenge (Day 21), peripheral blood samples were collected weekly to determine the presence of EBV DNA in whole blood and to immunophenotype circulating lymphocytes.Mice were weighed three times a week on non-consecutive days. If mice fell below 80% of their starting weight, or met other criteria for symptoms of pain (i.e. hunching, lack of mobility, etc.), they were euthanized.

Levels of EBV in the blood were monitored on a weekly basis using primers specific for BALF5 as described in "*Quantitative PCR analysis of human cells in huCD34 engrafted mice*." Blood samples were collected from mice on day prior to challenges and weekly beginning 3 weeks post-challenge (day 21) through to the end of the experiment at 10 weeks post-challenge (day 70), or until the animals reached euthanasia criteria. Spleens were harvested from each mouse at the day 70 endpoint, or earlier if they met euthanasia criteria.

Ten weeks post-challenge, surviving mice were euthanized and spleens were collected and weighed. DNA was extracted from 5×10^6 total splenocytes, utilizing the DNeasy Blood & Tissue Kit and according to the manufacturer's instructions, for subsequent viral load analysis.

Quantitative PCR Analysis of Human Cells in HuCD34 Engrafted Mice:

A primer-probe mix specific for the EBV BALF5 [156] gene was used to quantify EBV in DNA extracted from blood or spleen in hCD34 engrafted NSG recipient mice at the time points described. Each 25 µL qPCR reaction contained 12.5 µL of 2× QuantiTect Probe PCR Master Mix, 600nM of each primer, 300nM of FAM-labeled probe, 1.25 µL of a TaqMan 20× VIC-labeled RNase-P primer-probe mix. Reactions were heated to 95°C for 15 minutes to activate DNA polymerase followed by 50 cycles of 95°C for 15 s 60°C for 60 s, on an Applied Biosystems QuantStudio 7 Flex Real Time PCR System. Synthetic DNA fragments containing the BALF5 target gene as well as flanking genomic regions were synthesized as double stranded DNA gBlocks, and were used to generate a standard curve with known gene copy numbers ranging from 10^2 -10^7 copies/ml. The copy number in extracted DNA was determined by interpolating from the standard curve. Serial dilutions of reference standard were used to experimentally determine a limit of detection of 6.25 copies, which corresponds to the amount of template that can be

detected in >95% of reactions. For graphical purposes, samples with no amplification or those yielding values below the limit of detection were assigned a value of 0.625 copies.

Biolayer Interferometry:

BLI assays were performed on the Octet Red 96 instrument at 30°C with shaking at 1,000 RPM. Anti-Human Fc Capture (AHC) Biosensors were submerged in wells of black 96-well microplates (containing 250 µL of kinetics buffer (PBS, 0.02%Tween 20, 0.03% azide, 0.1% BSA) for at least 15 minutes prior to any data collection. Biosensors were submerged for 30 seconds in KB to establish baseline response (baseline step 1). Biosensors were submerged in KB containing 10 µg/mL of monoclonal antibodies for 240 seconds (load step). Biosensors were then equilibrated for 60 seconds in kinetics buffer alone (baseline step 2), after which the antibody-bound biosensors were submerged in wells containing a 250 nM solution of gH/gL or gH/gL-KO in KB for 300 seconds (association step) followed by immersion in KB for 300 seconds (dissociation step).

The background signal from each analyte-containing well was measured using empty reference sensors and subtracted from the signal obtained with each corresponding ligand-coupled sensor at every timepoint.

Quantification and Stastical Analysis:

Kruskal-Wallis tests were performed to assess whether the distributions of responses varied across treatment groups, with p-values < 0.05 considered significant. If the Kruskal-Wallis test reached significance, a Mann-Whitney test was used to compare the distribution of outcomes between the pairs of groups considered. Immunogenicity was compared across each pair of treatment groups; for spleen weights and viral DNA copies, each group was compared to the infected control. The Holm method was used to adjust for multiplicity across the Mann-Whitney tests conducted for each outcome, with Holm's adjusted p-values reported. For survival data, significant differences were determined using Log-rank Mantel-Cox test.

Chapter 3: Neutralizing antibodies protect against oral transmission of lymphocryptovirus

I. Summary

Epstein-Barr virus (EBV) is a cancer-associated pathogen for which there is no vaccine. Successful anti-viral vaccines elicit antibodies that neutralize infectivity, however it is unknown whether neutralizing antibodies prevent EBV acquisition. Here we assessed whether passively-delivered AMMO1, a monoclonal antibody that neutralizes EBV in a cell-type-independent manner, could protect against experimental EBV challenge in two animal infection models. When present prior to a high-dose intravenous EBV challenge, AMMO1 prevented viremia and reduced viral loads to nearly undetectable levels in humanized mice. AMMO1 conferred sterilizing immunity to three of four macaques challenged orally with rhesus lymphocryptovirus, the EBV ortholog that infects rhesus macaques. The infected macaque had lower plasma neutralizing activity than the protected animals. These results indicate that a vaccine capable of eliciting adequate titers of neutralizing antibodies targeting the AMMO1 epitope may protect against EBV acquisition and are therefore highly relevant to the design of an effective EBV vaccine.

II. Introduction

Epstein-Barr virus (EBV), a member of the *Lymphocryptovirus genus*, is associated with 200,000 new cases of cancer and 140,000 deaths annually [126]. EBV is also a causative agent of infectious mononucleosis (IM) and can lead to lymphoproliferative disease in immunocompromised individuals, such as those undergoing organ transplant or persons living with AIDS [3]. In addition to its contribution to oncogenesis, EBV infection is also associated with multiple sclerosis [8,9] and rheumatoid arthritis [12]. Thus, a safe and effective vaccine that protects against EBV infection and/or pathogenesis would be of clinical benefit, particularly to those in resource poor settings where the EBV-associated cancer burden is high [25,109,157].

Most effective vaccines elicit antibodies that neutralize infection [26]. However, it is not clear whether pre-existing neutralizing antibodies can protect against EBV infection *in vivo*. Infants generally remain EBV negative for 6-8 months until the presence of maternal antibody wanes, suggesting that neutralizing antibodies are protective [158-162]. However, several studies have demonstrated the presence of

multiple viral variants in infected individuals [163-168], which could indicate that an antibody response elicited by primary infection is not sufficient to protect against superinfection with additional EBV strains.

Primary infection occurs in the nasopharynx, where B cells and epithelial cells are both susceptible to infection. Host cell entry is a complex process mediated by several viral glycoproteins that define tropism and mediate membrane fusion [169]. Sera from infected individuals can neutralize EBV infection of both B cells and epithelial cells *in vitro* [34,82-84]. Multiple viral antigens have been shown to be targeted by serum neutralizing antibodies [34,79,170], but it is not clear which are ideal candidates for an EBV vaccine.

Passive transfer of monoclonal antibodies (mAbs) followed by controlled challenge in susceptible animal models has demonstrated the protective efficacy of neutralizing antibodies and defined relevant protective epitopes against several other viral pathogens [171-180]. Conducting similar proof of concept studies with EBV antibodies have been hampered due to the near-obligate tropism of the virus for humans, and a dearth of mAbs with well-defined neutralizing potentials.

Human B cells in immunocompromised mice engrafted with human lymphocytes can be infected by EBV and provide a small animal model to study EBV infection *in vivo* [67,181-185]. A high dose of EBV delivered intravenously to humanized mice leads to the development of splenomegaly, splenic tumors and an expansion of activated CD8 T cells [182,186].

The viral glycoprotein gp350 facilitates EBV attachment to complement receptors 1 and 2 (CR1 and CR2) [41,42]. The anti-gp350 72A1 mAb neutralizes EBV infection of B cells *in vitro* by disrupting the gp350-CR interaction [41,42,102], but is ineffective a blocking infection of CR^- epithelial cells [100]. Repeated transfer of 72A1 into SCID mice engrafted with PBMC from EBV seronegative donors prevented tumor formation following intravenous (i.v.) challenge with EBV, implying that pre-existing neutralizing antibodies may protect against EBV infection *in vivo* [187].

Rhesus lymphocryptovirus (rhLCV) is an ortholog of EBV that naturally infects rhesus macaques [140,188,189]. RhLCV infection of macaques is considered the best animal model for EBV infection due to the high level of homology between EBV and rhLCV, the oral transmission of the virus, and the similar courses of infection in their respective hosts [140]. RhLCV infection of rhesus macaques therefore represents a highly relevant animal model to evaluate the protective efficacy of neutralizing antibodies in

a controlled setting. However, no neutralizing mAbs specific for rhLCV have been isolated. Two mAbs, CL40 and E1D1 that bind the EBV gH/gL glycoprotein complex, an essential component of the viral fusion machinery, also bind to rhLCV gH/gL, although it is not known whether the neutralize rhLCV [190]. The 72A1 mAb which showed protection in mice does not cross-react with the rhesus gp350 protein [191]. A chimeric rhLCV virus expressing gp350 from EBV is infectious in macaques and susceptible to neutralization by 72A1 [191], yet passive transfer studies of neutralizing mAbs against rhLCV have not been reported to date.

We previously isolated an anti-gH/gL mAb, AMMO1, that neutralizes EBV infection of both B cells epithelial cells [192]. Herein we show that AMMO1 cross-reacts with and neutralizes rhLCV. We took advantage of the cross-reactivity of AMMO1 between EBV and rhLCV to evaluate its protective efficacy against *lymphocryptovirus* challenge in complementary animal models, humanized mice and rhesus macaques.

III. RESULTS

AMMO1 confers protection against high-dose EBV challenge in humanized mice

72A1 and AMMO1 neutralize EBV infection of B cells with comparable potency [192]. Since 72A1 has previously been shown to protect against EBV-driven tumor formation in humanized mice [187], we sought to address whether AMMO1 could also prevent lymphoproliferation in a similar humanized mouse model. To this end, NOD-*scid* Il2rg^{null} (NSG) mice were engrafted with healthy human donor-derived mobilized peripheral blood hematopoietic stem cells (PBSC), herein referred to as humanized mice. At 12 weeks post-transplant ~10-15% of the peripheral blood mononuclear cells were of human origin (fig. S1, A and B). Among these ~80% were hCD19$^+$ B cells, with very few hCD4$^+$ or hCD8$^+$ T cells (Fig. S1, A and B).

As shown in Fig. 1A, humanized mice received an intravenous injection (i.v.) containing 500μg of purified, recombinant AMMO1 or as a control, the anti-HIV-1 mAb VRC01 [193]; followed at 48 hours by an i.v. injection of EBV B95.8/F [82] equivalent to ~33000 Raji infectious units. Infected control mice received the same dose of virus without antibody pre-treatment and uninfected control mice did not receive antibody or viral challenge. Mice were bled weekly and euthanized 8-9 weeks following challenge. At 6-7 weeks following challenge, while all mice retained equivalent proportions of total human cells and hCD4$^+$ cells (Fig. 1, B and C), mice from the infected control and VRC01 groups showed a marked decrease in

the frequency of peripheral hCD19^{+} B cells (Fig. 1D), concurrent with an increase in hCD8^{+} T cells (Fig. 1E) as compared to the uninfected control mice and mice that received AMMO1. Viremia was detectable in the peripheral blood of the infected control and VRC01 groups and in 2 of 13 mice that received AMMO1 at 4 to 6 weeks post-challenge (Fig.1, F and G). The remaining animals from the AMMO1 group and the uninfected controls remained aviremic (Fig.1 F&G).

Splenic lymphocytes were analyzed at the study endpoint. While the proportion of total human cells and hCD4+ T cells were similar in all animals (Fig. 1, H and I), the infected control and VRC01 groups exhibited a decrease in hCD19^{+} cells (Fig. 1J) and this population contained an increased frequency of hCD24^{-}hCD38^{hi} cells (Fig. 1K). Concurrent with the decline of hCD19^{+} cells, there was a significant increase in the frequency of total (Fig. 1L) and activated (Fig. 1M) hCD8^{+} T cells in the control infected and VRC01 groups, consistent with T-cell mediated killing of infected peripheral human B cells.

Spleens from 11 of 13 animals that received AMMO1 were comparable in weight to the uninfected controls, while the spleens from the 2 animals that were viremic were enlarged (indicated by blue triangles on Fig. 1N), as were the spleens from the infected control and VRC01 groups.

Mice from the infected control and VRC01 groups had 100-1000 fold higher levels of EBV DNA in the spleen compared to the uninfected controls (Fig. 1O). Low amounts of viral DNA were detectable in splenic DNA extracts from 8 of the 11 aviremic mice in the AMMO1 group. Comparable amounts were detected in splenic extracts from half of the uninfected control mice (Fig. 1O). In contrast, splenic DNA from the two viremic mice in the AMMO1 group harbored higher levels of EBV DNA (indicated by blue triangles on Fig. 1O). Collectively, these data indicate that AMMO1 prevented viremia and splenomegaly in 11/13 mice. Due to the trace amount of DNA detected in the spleens of both AMMO1 challenged mice and the uninfected controls we cannot conclude that AMMO1 conferred sterilizing immunity in these animals. However, AMMO1 prevented the splenomegaly, viremia, increase in hCD8^{+}, and decline in hCD19^{+} cells observed in the positive control and VRC01 groups, which are consistent with high-dose EBV infection in this model [182].

Compared to other neutralizing mAbs, AMMO1 provides superior protection against EBV challenge in humanized mice

We next evaluated whether passive transfer of the CL40 and CL59 mAbs that target distinct epitopes on gH/gL [113,194] could similarly limit or prevent *in vivo* EBV infection in this humanized mice model. To bridge our studies with previous work [187], we also included the anti-gp350 72A1 mAb. CL40, CL59 and 72A1 are murine mAbs while AMMO1 is human, so to mitigate potential differences in kinetics and/or effector function, all mAbs were administered as purified recombinant variants with human IgG1 constant regions [195]. As in Fig. 1A, mice received 500μg of each mAb/animal followed 48 hours later by an i.v. injection of ~33000 Raji infectious units of EBV B95.8/F. At 1 week post-viral challenge, the mean concentrations of AMMO1, 72A1, CL40 and CL59 in the plasma were 49μg/ml, 34μg/ml, 261μg/ml, and 22μg/ml, respectively (Fig. 2A).

At 4 weeks post-viral challenge, one of the animals in the 72A1 group died. At 9 weeks post-viral challenge, the study endpoint, mice from the infected control group had larger spleens than the uninfected control, AMMO1, CL40 and CL59 groups (Fig. 2B). One of the remaining animals from the 72A1 group displayed extreme splenomegaly (Fig. 2B) and a large splenic tumor (not shown). Relative to the uninfected controls, the frequency of $hCD19^{+}$ cells was lower (Fig. 2C), while the frequencies of $hCD19^{+}hCD24^{-}hCD38^{hi}$ B cells (Fig. 2D), as well as total and activated $hCD8^{+}$ T (Fig. 2, E and F) cells were higher in the 72A1, CL59 and infected control groups, a phenotype consistent with infection in prior challenge experiments (Fig. 1). In contrast, the animals that received AMMO1 or CL40 had frequencies of $hCD19^{+}$ and $hCD8^{+}$ cells indistinguishable from uninfected controls (Fig. 2, C to F). EBV viral DNA was present in splenic extracts from all mice in the 72A1 and infected control groups, three of four mice in the CL59 group, one mouse from the CL40 group and one mouse from the AMMO1 group (Fig. 2G). These data indicate that among anti-gH/gL mAbs, AMMO1 confers superior protection against i.v. EBV challenge in humanized mice, as predicted by the relative potency of each antibody in a B cell neutralization assay [192]. The efficacy of CL40 is likely over-estimated in this experiment considering that it was present at approximately 5× higher levels in the blood than AMMO1 at the time of challenge.

Considering that AMMO1 and 72A1 neutralize B cell infection with comparable potency *in vitro*[192], the complete lack of protection by 72A1 was unexpected. AMMO1 was present at slightly higher levels than 72A1 in the plasma 9 days post-transfer (Fig. 2A) and plasma from the AMMO1 group had higher *in vitro* neutralizing capacity than plasma from the 72A1 group (Fig. 2H). Thus, the difference in protection

between 72A1 and AMMO1 may reflect differences in the effective *in vivo* plasma neutralizing titer. However, the previous demonstration that 72A1 prevented EBV-driven tumor formation in vivo utilized repeated mAb dosing [187] suggesting that other factors may explain the differences in *in vivo* functional activity of 72A1 vs. AMMO1. Taken together, our *in vivo* challenge studies demonstrate that passive transfer of AMMO1 limits EBV to levels detected in control animals in 16/18 humanized mice indicating robust capacity for protection in this setting.

AMMO1 cross-reacts with and neutralizes rhLCV

In addition to B cells, epithelial cells present in the human nasopharynx are also susceptible to EBV infection [196], thus the viral dose and kinetics of infection are likely to differ between i.v. challenge in humanized mice and oral transmission in humans. To address whether AMMO1 can also limit EBV infection in a more physiologic challenge setting, we sought to assess whether passively transferred AMMO1 could prevent oral transmission in a non-human primate model. To achieve this goal, we utilized rhesus lymphocryptovirus (rhLCV) in a rhesus macaque model.

EBV and rhLCV gH and gL share 85.4% and 81.8% amino acid identity, respectively. A population of 293T cells transfected with rhLCVgH/gL stained with fluorescently-labeled AMMO1 indicated that the mAb is cross-reactive with the rhesus ortholog (Fig. 3, A and B). To assess whether the neutralizing activity of AMMO1 was conserved, the ability of AMMO1 to neutralize rhLCV infection of rhesus B cells was evaluated using viral expression of EBNA2 in rhesus B cells as a readout. In the absence of antibody or in the presence of the non-neutralizing mAb AMMO2, 6-7% of rhesus B cells stained positive for EBNA2 following challenge with rhLCV (Fig. 3D and F). In contrast, EBNA2 expression was absent when virus was pre-incubated with AMMO1 (Fig. 3E).

AMMO1 disrupts EBV gH/gL and gB-driven membrane fusion in a virus-free cell fusion assay[192]. Here we assessed whether AMMO1 could similarly disrupt rhLCV gH/gL and rhLCV gB-driven fusion using the same assay [197]. CHO-K1 cells were transfected with plasmids expressing rhLCV gH, rhLCV gL, rhLCV gB and with luciferase under the control of the T7 promoter. Transfected cells were overlaid on 293 cells stably expressing T7 polymerase. Expression of the entire rhLCV fusion machinery resulted in high levels of luciferase activity that was reduced to background levels in the presence of AMMO1 (Fig. 3G). CL40 and E1D1, which also bind rhLCV gH/gL [190] reduced fusion, but to a lesser degree, while the CL59 mAb

which does not bind rhLCV gH/gL [190] had no effect. Collectively, these data demonstrate AMMO1 cross-reacts with rhLCV gH/gL and that its neutralizing activity is conserved against rhLCV.

AMMO1 confers sterilizing immunity against rhLCV challenge in macaques

To establish whether AMMO1 could protect against oral rhLCV challenge, 6 infant rhesus macaques were obtained within 48 hours of birth and housed separately from other colony animals. Beginning at 2 months of age, the animals were tested for plasma antibodies to the rhLCV viral capsid antigen (VCA) [198] and for the presence rhLCV DNA in PBMC [108]. Maternal antibodies to VCA were detected in 4/6 study animals that waned by 6 months of age (Fig. S4A). All animals tested negative for rhLCV DNA during this time (Fig. S4B). When the animals were ~6 months old, VRC01 (n=2) or AMMO1 (n=4) human IgG was administered i.v. at a dose of 20 mg/kg. Three days after antibody transfer, all animals were challenged orally with 1.75 transforming units of rhLCV (Fig. S4C). During a 10 week period following challenge, none of the animals seroconverted (Fig. S4D) or became viremic (Fig. S4E), thus we performed a dose escalation.

At 11 weeks after the initial challenge, the study animals were re-infused with either VRC01 or AMMO1 then re-challenged orally, 48 hours later, with a higher dose of rhLCV (50 transforming units). Blood and oral swabs were collected weekly and assayed for the presence of anti-VCA antibodies in the plasma and for rhLCV DNA in PBMC and oral swabs. RhLCV DNA was detected in the blood and saliva of animals A18151 and A18152 from the VRC01 group beginning at 2-3 weeks following challenge (Fig. 4, A and B). These animals seroconverted at 10 and 5 weeks following the second challenge, respectively (Fig. 4C). AMMO1 recipient animal A18155 also tested positive for rhLCV DNA in the blood and saliva (Fig. 4, A and B). In contrast, however, this animal did not seroconvert (Fig. 4C). Most strikingly, 3 additional AMMO1 recipient animals (A18153, A18154, and A18156) lacked detectable rhLCV DNA or anti-VCA antibodies at all time points (Fig. 4, A to C).

We measured plasma levels of passively administered antibodies to determine whether differences in their levels could account for the absence of protection in A18155. AMMO1 was detectable at approximately 60 μg/ml in A18153, A18154, and A18156 at the time of challenge and the levels waned to nearly undetectable levels by 3 weeks (Fig. 4D). In A18155, AMMO1 was present at less than 20 μg/ml at the time of challenge and it waned to undetectable levels within a week. Plasma from A18153, A18154,

and A18156 were able to neutralize EBV infection of Raji cells *in vitro* with comparable potencies (ID_{50} ~100) while the potency of plasma animal A18155 was ~5-fold lower (ID_{50}~20, Fig. 4E). In summary, AMMO1 at plasma levels of ~60μg/ml provided sterilizing immunity against controlled oral LCV challenge.

IV. DISCUSSION

The correlate of protection for most effective vaccines is the elicitation of neutralizing antibodies [26]. Although previous subunit vaccines have shown partial efficacy against EBV infection in humans, it remains unclear whether neutralizing antibodies affected the outcome of these trials. Here we evaluated the effect of passively transferred neutralizing antibodies on EBV infection in two animal models of lymphocryptovirus infection, humanized mice and rhesus macaques. Passive delivery of AMMO1 prevented EBV-driven changes in lymphocyte populations and reduced viral loads to nearly undetectable levels in a humanized mouse model following a high-dose intravenous challenge of EBV, while other mAbs targeting distinct epitopes on gH/gL and a mAb that binds to gp350 and blocks viral attachment to complement receptors, failed to do so. We further demonstrated that AMMO1 conferred sterilizing immunity against controlled oral rhLCV challenge in macaques.

EBV subunit vaccine studies have focused on the gp350 protein and have shown partial efficacy in humans and rhesus macaques. A phase II study of a gp350 subunit vaccine reduced the incidence of IM but failed to protect against acquisition [99]. Although the vaccine elicited neutralizing antibodies [199] it is not clear whether these affected the outcome. In another study, a protein subunit vaccine based on the gp350 protein from rhLCV showed partial protection in a non-human primate rhLCV challenge study; however, similarly, the correlate(s) of protection was not identified [108]. Here, passive delivery of a recombinant version of the anti-gp350 mAb 72A1 failed to protect against i.v. challenge in humanized mice. This finding contrasts with a previous study demonstrating that repeated delivery of hybridoma-derived 72A1 suppressed tumor formation in a related humanized mouse model of EBV infection [187]. Experimental differences, including the human lymphocyte composition arising from engrafted PBMC vs. lymphocytes derived from PBSCs, the use of a hybridoma-derived murine mAb vs. a recombinant humanized mAb, and the dosing regimen, might account for these distinct observations.

In contrast to 72A1, passive delivery of AMMO1 provided a clear protective effect in humanized mice. This result indicates that vaccines based on gH/gL may complement or outperform vaccines based

on gp350 alone. Indeed gH/gL-derived vaccines have been shown to elicit higher B cell neutralizing titers than gp350 [200]. The finding that mAbs targeting other epitopes on gH/gL failed to prevent lymphoproliferation or viremia underscores the importance of the site of vulnerability on gH/gL defined by AMMO1, implying that AMMO1-like antibodies are a desirable vaccine target. In line with this, a gH/gL subunit vaccine presented on self-assembling ferritin nanoparticles elicited antibodies that competed binding of the 769B10 mAb to gH/gL which binds an epitope similar to AMMO1 [170].

Although AMMO1 limited i.v. infection in humanized mice, oral transmission is the normal route of lymphocryptovirus infection. The ability of AMMO1 to prevent rhLCV infection in the rhesus macaque model strongly supports the notion that neutralizing antibodies can prevent oral lymphocryptovirus transmission. In addition, our observation that one animal with lower plasma mAb levels became infected suggests that a protective vaccine will likely need to elicit neutralizing antibodies above a threshold titer. Here a fixed dose of antibody and a dose of virus that was sufficient to infect all control animals was administered. Future work will be required to define the relationship between viral inoculum and the neutralizing antibody titer that is sufficient for protection.

Collectively, our data demonstrate that AMMO1 is capable of blocking lymphocryptovirus transmission *in vivo* by limiting infection of both human B cells in humanized mice and preventing oral transmission in a non-human primate model. These findings strongly support the concept that gH/gL-based immunogens targeting this epitope may elicit neutralizing antibodies that will be important for an effective EBV vaccine. Moreover, these studies demonstrate that rhLCV infection of rhesus macaques is a suitable model to evaluate the efficacy of EBV vaccines based on the gH/gL glycoprotein.

V. Figures

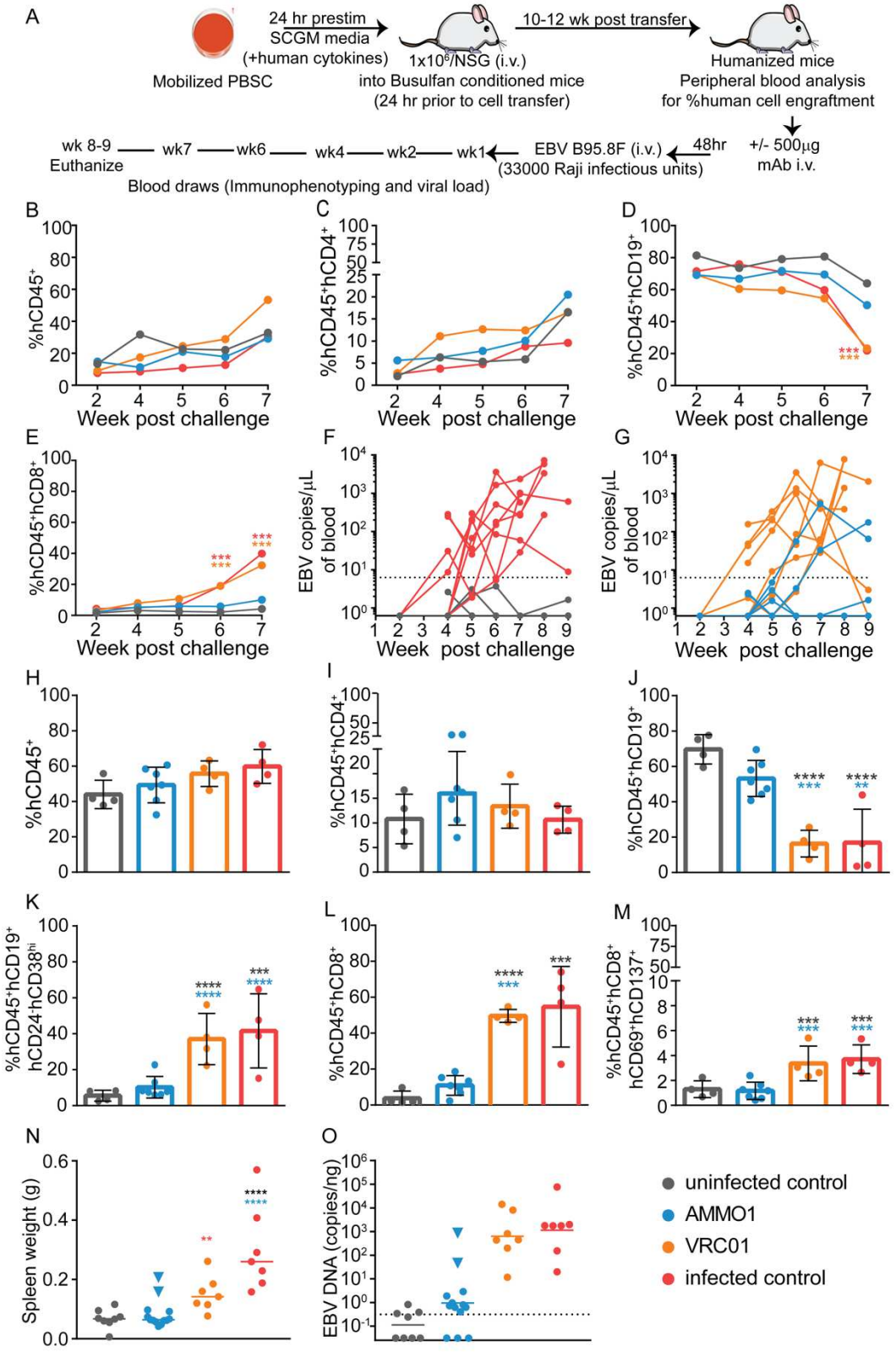
A
Mobilized PBSC
24 hr prestim
SCGM media
(+human cytokines)
1x10⁶/NSG (i.v.)
into Busulfan conditioned mice
(24 hr prior to cell transfer)
10-12 wk post transfer
Humanized mice
Peripheral blood analysis
for %human cell engraftment
+/- 500μg
mAb i.v.
48hr
EBV B95.8F (i.v.)
(33000 Raji infectious units)
wk 8-9
Euthanize
wk7
wk6
wk4
wk2
wk1
Blood draws (Immunophenotyping and viral load)
B
%hCD45+
Week post challenge
C
%hCD45+hCD4+
Week post challenge
D
%hCD45+hCD19+
Week post challenge
E
%hCD45+hCD8+
Week post challenge
F
EBV copies/μL of blood
Week post challenge
G
EBV copies/μL of blood
Week post challenge
H
%hCD45+
I
%hCD45+hCD4+
J
%hCD45+hCD19+
K
%hCD45+hCD19+ hCD24+hCD38hi
L
%hCD45+hCD8+
M
%hCD45+hCD8+ hCD69+hCD137+
N
Spleen weight (g)
O
EBV DNA (copies/ng)
uninfected control
AMMO1
VRC01
infected control

Figure 1. AMMO1 inhibits EBV infection in humanized mice. (**A**) Experimental timeline. Humanized mice received a dose of 0.5mg of AMMO1 or VRC01 via intravenous injection (i.v.) 48hr prior to an i.v. challenge of EBV B95.8/F equivalent to 33000 Raji infectious units. Infected control mice received virus but no antibody, and uninfected control mice received neither. The frequency of (**B**) $hCD45^+$, (**C**) $hCD45^+hCD4^+$, (**D**) $hCD45^+hCD19^+$ and (**E**) $hCD45^+hCD8^+$ cells in peripheral blood at the indicated time points post-challenge. Data points represent the mean of n=7 AMMO1, n=4 VRC01, n=4 infected control mice and n=4 uninfected control mice in **B**-**E**. A representative flow plot illustrating the gating strategy is shown in Figure S1. (**F**) Viral DNA was quantitated in the peripheral blood of infected control mice (n=8), uninfected control mice (n=8), and in (**G**) mice that received AMMO1 (n=13) or VRC01 (n=7) prior to challenge. Each dot represents an individual mouse and the dashed line indicates the limit of detection. 8-9 weeks after viral challenge, the animals were euthanized and the frequency of (**H**) $hCD45^+$, (**I**) $hCD45^+hCD4^+$, (**J**) $hCD45^+hCD19^+$, (**K**) $hCD45^+hCD19^+hCD24^-hCD38^{hi}$, (**L**) $hCD45^+hCD8^+$ and (**M**) $hCD45^+hCD8^+hCD69^+hCD137^+$ cells were measured in splenocytes. Data points represent individual mice, bar graphs indicate the mean and error bars represent the standard deviation in **H**-**M**. Representative flow plots illustrating the gating strategy used to analyze splenocytes are shown in Figures S2 and S3. (**N**) Spleen weight of study animals at necropsy. Each dot represents an individual mouse and the bar represents the mean. (**O**) qPCR was used to quantitate viral DNA in splenic extracts at necropsy. Each dot represents an individual mouse, the bar represents the mean and the dashed line indicates the limit of detection. Data shown in **B**-**E** and **H**-**M** is from one of two independent experiments. Combined data from 2 independent experiments is shown in **F**-**G** and **N**-**O**. Statistical analyses were performed using one-way ANOVA. The color of the asterisks, *p≤0.032, **p≤0.002, **p≤0.0003, ****p≤0.0002, denote groups that were significantly different from the control in **B**-**E,** or denote the groups with which there is a significant difference in **H**-**M** using the Sidak multiple comparisons test.

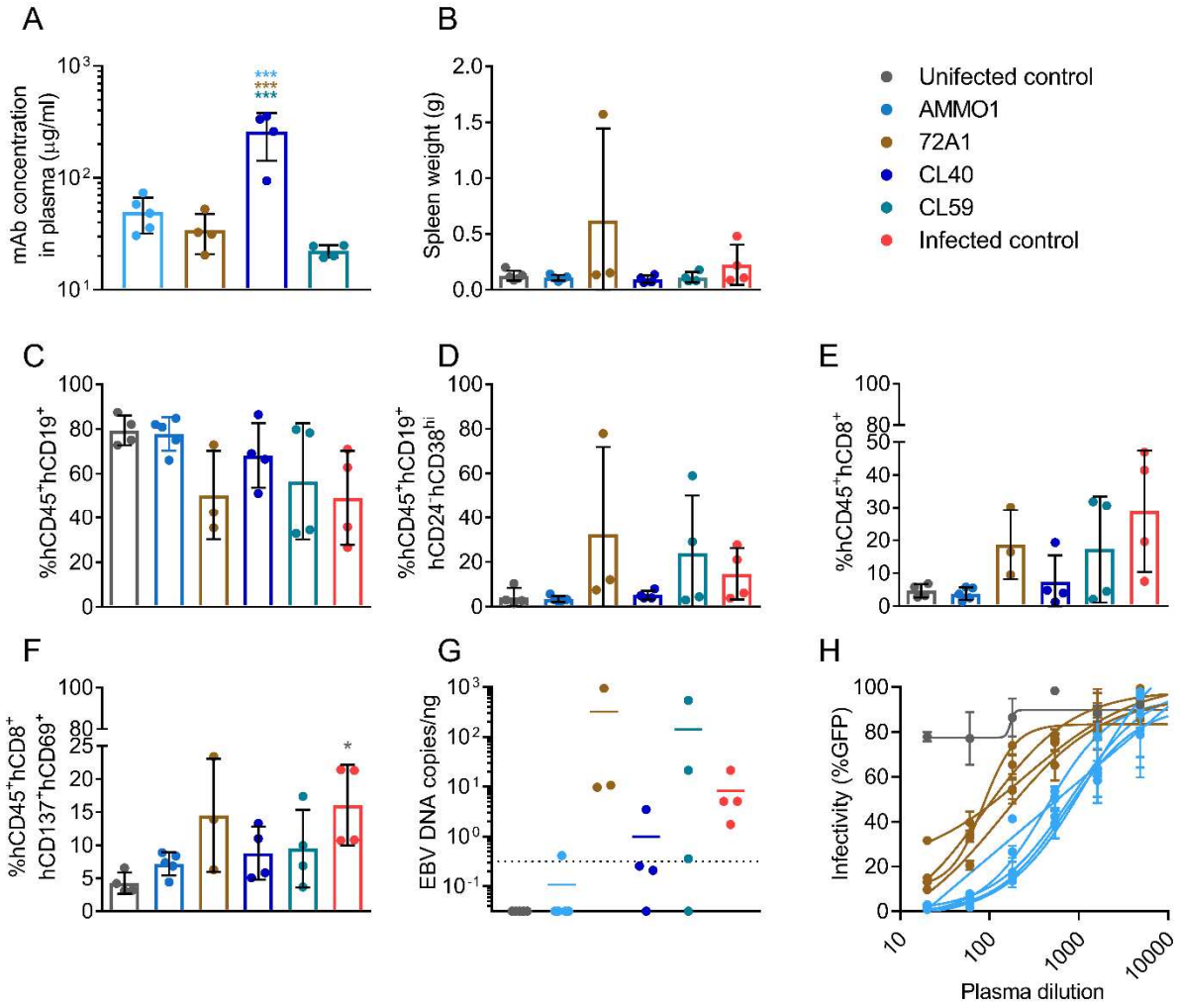

Figure 2. AMMO1 inhibits EBV infection more efficiently than other anti-EBV mAbs in humanized mice. Humanized mice received an intravenous injection containing 0.5mg of the mAbs AMMO1 (n=5), 72A1 (n=4), CL40 (n=4) or CL59 (n=4). Two days later the mice were challenged with 33000 Raji infectious units of EBV B95.8/F. (**A**) One week following challenge, the concentration of transferred mAbs in plasma was determined by antigen-specific ELISA against gH/gL for AMMO1, CL40 and CL59, and gp350 for 72A1. (**B**) Spleen weight of study animals 8 weeks after challenge. Uninfected control mice (n=4) which did not receive antibody or virus, and infected control mice (n=4) that were challenged with virus but did not receive antibody pre-treatment are included in **B**. At necropsy, the frequency of (**C**) $hCD45^+hCD19^+$, (**D**) $hCD45^+hCD19^+hCD24^-hCD38^{hi}$, (**E**) $hCD45^+hCD8^+$ and (**F**) $hCD8^+hCD69^+hCD137^+$ cells were measured in splenocytes. Bar graphs indicate the mean, error bars represent the standard

deviation, and each data point represents an individual mouse in **A**-**F**. (**G**) qPCR was used to quantitate viral DNA in splenic extracts at necropsy. Each data point represents an individual mouse, the bar indicates the mean, and the dashed line indicates the limit of detection. One of the animals in the 72A1 group died prior to necropsy, therefore only n=3 mice are shown in **B**-**G**. (**H**) The EBV-neutralizing titers in plasma from AMMO1 or 72A1 infused mice were measured one week following challenge. Statistical analyses were performed using one-way ANOVA. The color of the asterisks, *p≤0.0332 ***p≤0.0002, denote the group with which there is a significant difference determined by the Sidak multiple comparisons test.

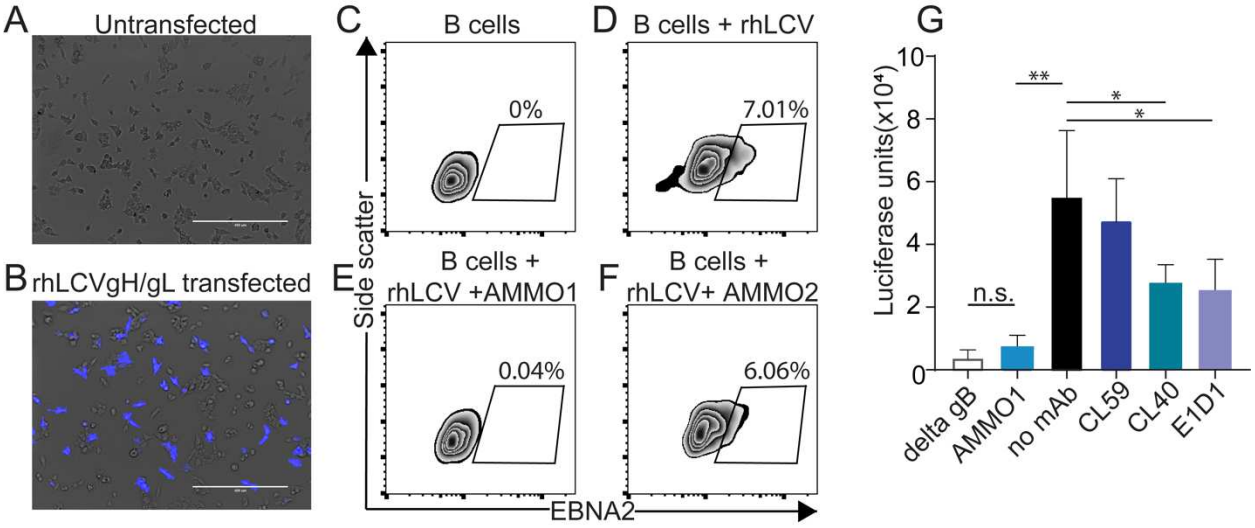

Figure 3. AMMO1 cross-reacts with rhesus lymphocryptovirus gH/gL. AMMO1 conjugated to Dylite-650 was used to stain (**A**) untransfected 293T cells or (**B**) 293T cells transfected with plasmids expressing rhLCV gH and rhLCV gL. The scale bar represents 400 μm. The fluorescence channel for Dylite-650 (shown in blue) is overlaid on the transmitted light channel (gray) in **A** and **B**. Images are representative of two independent experiments. Rhesus PBMC (**C**) or rhesus PBMC challenged with RhLCV alone (**D**) or rhLCV pre-incubated with AMMO1 (**E**) or AMMO2 (**F**) were cultured in media. 3 days later, B cells (live, $CD19^+$, $CD20^+$) were monitored for EBNA2 expression by flow cytometry. Values indicate the % $EBNA2^+$ B cells in **C**-**F**. (**G**) CHO-K1 cells were transfected with expression plasmids encoding rhLCV gH, rhLCV gL, rhLCV gB, and luciferase under the control of a T7 promoter. 24 hours later, the cells were trypsinized and then overlaid on HEK293 cells stably expressing T7 polymerase in wells containing AMMO1, CL59, CL40, E1D1 or no mAb as indicated. 24 hours later the cells were lysed and assayed for luciferase

activity. As a control for non-specific fusion, CHOK1 cells were transfected as above, except the plasmid rhLCV gB was replaced with an empty plasmid (delta gB). Significant differences *p≤0.05 and **p≤0.01 were determined using an unpaired 2-tailed t-test.

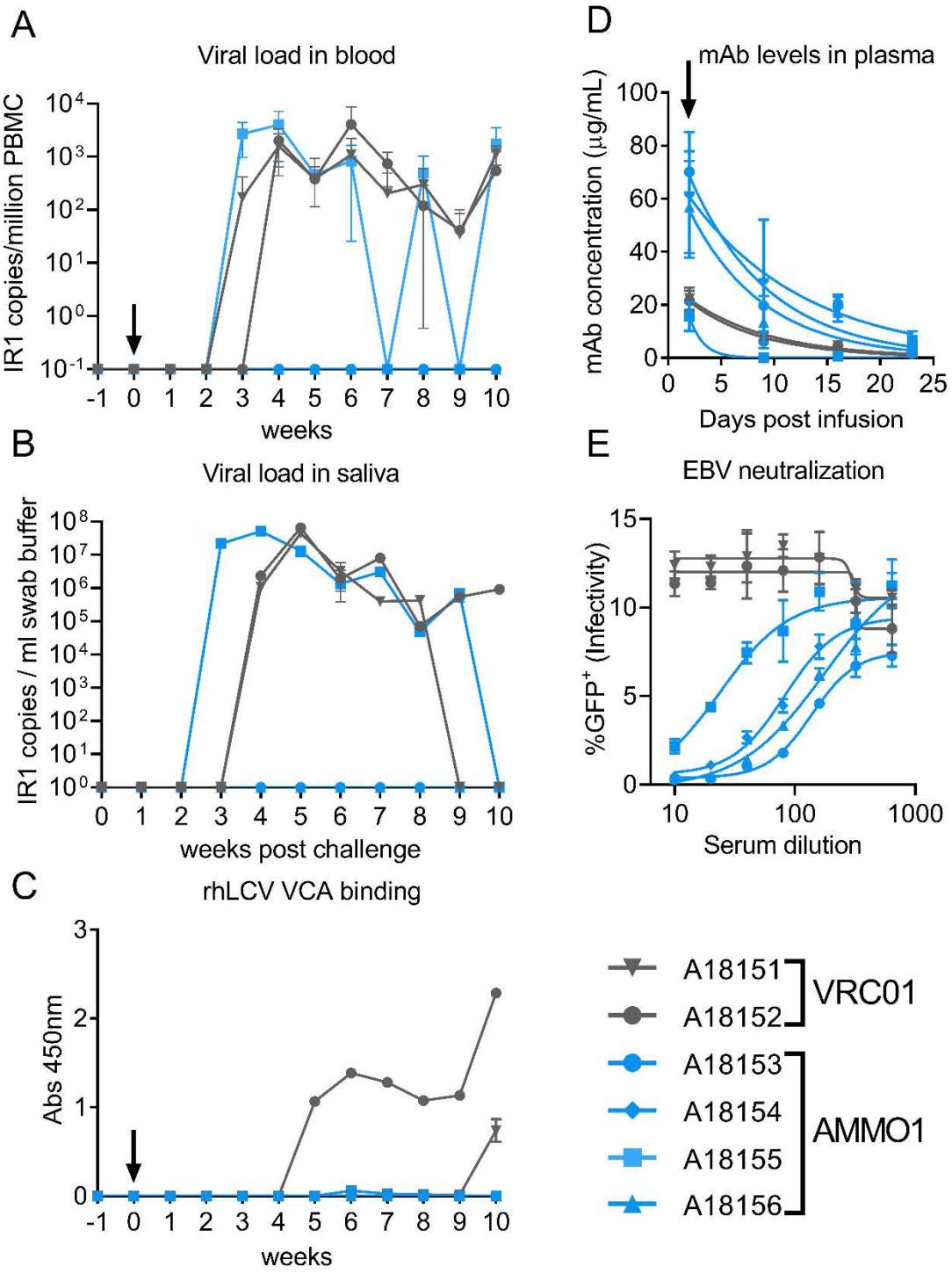

Figure 4. AMMO1 prevents rhesus lymphocryptovirus infection in macaques. 8 month-old rhLCV-negative rhesus macaques were infused i.v. with 20mg/kg of VRC01 (gray symbols) or AMMO1 (blue symbols). 2 days later the macaques were challenged orally with 50 transforming units of rhLCV. Viral DNA was quantitated in the blood (**A**) and oral swabs (**B**) using a digital droplet PCR assay with primers and probes specific for the internal repeat (IR1) of rhLCV at the indicated time points. Viral loads from blood were averaged from two aliquots of PBMC processed independently. Viral loads in swab buffer were determined from 3 independent measurements of the same DNA extract from swab buffer. (**C**) Plasma from the study macaques was diluted 1:10 and reactivity to pooled peptides corresponding to amino acids 117-146 and 147-170 of the rhesus small viral capsid antigen was measured by ELISA at the indicated time points. (**D**) ELISA was used to quantify the levels of AMMO1 and VRC01 in plasma at the indicated timepoints. The black arrow indicates the time of viral challenge in **A**, **C** and **D**. (**E**) Plasma collected from macaques at the time of challenge was evaluated for its ability of neutralize EBV B95.8F infection of Raji cells.

VI. Methods

Experimental Models:

Mice: NOD-*scid* Il2rg^{null} (NSG) mice were housed in a specific pathogen-free facility at SCRI. The facility is accredited by the Association for Assessment and Accreditation of Laboratory Animal Care. Mice were handled in accordance with the NIH Guide for the Care and Use of Laboratory Animals, and experiments were approved by the SCRI Institutional Animal Care and Use Committee and Institutional Review Board. All mice used in this study were female and were 8 weeks old when experiments were initiated.

Rhesus Macaques: All rhesus macaque work was approved by the University of Washington and Fred Hutchinson Cancer Research Center IACUCs. 4 male and 2 female infant rhesus macaques were obtained from the Oregon National Primate Research Center within 24-48 hours of birth and hand-reared in a nursery. 2-3 weeks later the animals were transported to the Washington National Primate Research Center and housed in pairs until they were 6 months of age. From 2 months of age to 6 months of age the animals we bled monthly and tested for serum responses to viral capsid antigen and assayed for viral DNA by qPCR. Prior to the start of the challenge study the animals were housed individually and remained so for the duration of the study.

Cell Lines:

All cell lines were incubated at 37°C in the presence of 5% CO_2 and were not tested for mycoplasma contamination. 293-F and 293E (human female) were maintained in Freestyle 293 media with gentle shaking. CHO-K1 (hamster female) cells were maintained in Ham's F-12 + 10% FBS, 2 mM L-glutamine, 100 U/ml penicillin, and 100 µg/ml streptomycin (cF-12). Raji cells (human male) and LCL 8664 (rhesus macaque male) were maintained in RMPI + 10% FBS, 2 mM L-glutamine, 100 U/ml penicillin, and 100 µg/ml streptomycin (cRPMI). 293T cells (human female) were maintained in DMEM + 10% FBS, 2 mM L-glutamine, 100 U/ml penicillin, and 100 µg/ml streptomycin (cDMEM). 293-T7 cells (human female) were maintained in cDMEM containing 100µg/ml Zeocin.

Human Subjects:

CD34-enriched PBSCs were obtained from granulocyte colony-stimulating factor mobilized healthy donors at the Fred Hutch Co-operative Center for Excellence in Hematology. All healthy donors

for mobilized peripheral blood products (PBSCs) provided written informed consent during a face-to-face meeting in compliance with the Declaration of Helsinki. The evaluation for donor eligibility, testing, mobilization, and collection were conducted under an approved protocol overseen by the Fred Hutch Institution Review Board. De-identified CD34 cryopreserved specimens were provided to user after transfer agreement and with the acknowledgement of user approval by the Seattle Children's Research Institute (SCRI). PBSCs used in this study were obtained from a 35 year old female and a 25 year old female.

EBV Infection in Humanized Mice:

Frozen human CD34-enriched PBSCs were thawed then cultured at a cell density of 1×10^6 cells/mL in a humidified 37˚C incubator with 5% CO_2. Culture media was SCGM (CellGenix) with 100ng/mL each of human recombinant Thrombopoietin, stem cell factor, and Flt3-ligand. After 24 hours in culture, cells were washed in normal saline and 1×10^6 $CD34^+$ cells delivered per busulfan-conditioned NSG mouse by retro-orbital injection. Busulfan conditioning was performed by intraperitoneal (i.p.) injection of 35 mg/kg clinical grade busulfan into 8 week-old NSG mice 24 hours prior to human PBSC transfer. 10-12 weeks post-cell transfer, successful human cell engraftment was confirmed by the presence of human $CD45^+$ cells in peripheral blood using flow cytometry.12-13 weeks post-human HSPC transfer, 500 µg of experimental or control antibodies were injected per humanized NSG mouse intravenously (i.v.). 48 hours later the mice received a dose of EBV B95.8/F [201] equivalent to 33,000 infectious units as determined by infection of Raji cells [202], via retro-orbital injection. Each group of mice receiving the same mAb and/or EBV were housed separately from unchallenged mice to avoid contamination. Beginning at one week post-infection, peripheral blood samples were collected to determine levels of transferred mAbs in plasma, the presence of EBV DNA in whole blood, or were used to assess immunophenotype of circulating lymphocytes using antibodies at a 1:100 dilution unless otherwise noted: hCD45-FITC, mCD45-APC (1:500 dilution), hCD33-PE, hCD19-PE-Cy7, hCD4-eFluor450 and hCD8-PerCP-Cy5.5.

Eight to nine weeks post-challenge, mice were euthanized and single cell suspensions of splenocytes were collected and immunophenotyping of B cells using hCD45-FITC, mCD45-APC, CD19-PE-Cy7, hCD38-PerCP-Cy5.5, and hCD24-BV605, or T cells using hCD45-FITC at a 1:100 dilution,

mCD45-APC at a 1:500 dilution, hCD4-Alexafluor647 at a 1:100 dilution, hCD8-PerCP-Cy5.5 at a 1:100 dilution, hCD137-BV421 at a 1:50 dilution and hCD69-BV605 at a 1:50 dilution, was performed by flow cytometry as described previously [203]. DNA was extracted from 5 million total splenocytes, utilizing the DNeasy Blood & Tissue Kit (Qiagen) and according to the manufacturer's instructions, for subsequent viral load analysis.

Antibody Expression Plasmids:

cDNA corresponding to the 72A1 VH (Accession number KT211017) (Accession number KT211018)[191], were codon optimized and cloned in-frame with the human IgG1 and human lambda constant regions in pTT3-based expression vectors [192]. Codon optimized cDNA corresponding to CL40 VH (Accession number MF104552) and CL59 VH (Accession number MF104554) was synthesized (Integrated DNA Technologies) and cloned in-frame with the human IgG1 constant region in pTT3-based expression vectors. Codon optimized cDNA corresponding to CL40 VL (Accession number MF104553) and CL59 VL (Accession number MF104555) were cloned in-frame with the human kappa constant regions in pTT3-based expression vectors.

Antibody Production:

The AMMO1 used in passive transfer studies in rhesus macaques was expressed from 293F cells using the Daedalus system [131] and purified at the Fred Hutchinson Cancer Research Center Molecular Therapeutics and Design Center. Recombinant AMMO1 (human IgG1) was purified using MabSelect SuRe resin according to the manufacturer's instructions. AMMO1 IgG1 was dialyzed into PBS, sterile filtered and stored at -80ºC until use. AMMO1 was verified to be endotoxin free (<0.5Eu/mg). GMP grade, recombinant VRC01 IgG was a kind gift from Dr. John Mascola (NIAID, Vaccine Research Center).

pTT3-derived antibody expression plasmids encoding antibody heavy and light chains [192] were co-transfected into 293E cells at a density of 10^6 cells/ml in Freestyle 293 media using the 293Free transfection reagent according to the manufacturer's instructions. Expression was carried out in Freestyle 293 media for 6 days, after which cells and cellular debris were removed by centrifugation at 4,000 × *g* followed by filtration through a 0.22 μm filter. Clarified cell supernatant containing recombinant antibodies was passed over Protein A Agarose, followed by extensive washing with PBS, and then eluted with 1 ml

of Pierce IgG Elution Buffer, pH 2.0, into 0.1 ml of Tris HCl, pH 8.0. Purified antibodies were then dialyzed overnight into PBS, passed through a 0.2μM filter under sterile conditions and stored at -80ºC until use.

Rhesus macaque PBMC Isolation:

Rhesus macaque blood was drawn by venipuncture and collected in vacutainers containing EDTA. Blood was centrifuged at 1000 × *g* for 30 min. Plasma was collected and stored at -20˚C until use. PBMC were further purified on a Ficoll cushion, subjected to DNA extraction using the Allprep DNA/RNA mini kit (Qiagen) according to the manufacturer's instructions, or aliquoted into FBS containing 10% DMSO and stored in liquid nitrogen.

Rhesus macaque Oral Swabs:

A sterile polyester swab was rubbed on the inside of the both cheeks (buccal mucosa), along the upper and lower gum-lines outside of the teeth. Swabs were placed in 1ml of 10mM Tris, 25mM EDTA, 50mM potassium chloride, 1% Igepal CA 630 pH 8.0. Swabs were stored at -20ºC until use. After thawing, DNA was extracted from 200μl of buffer was extracted using the QiaAmp blood DNA kit, and eluted in 100 μL of AE buffer (Qiagen).

Quantitative PCR Analysis of Human Cells in huCD34 Engrafted Mice:

A primer-probe mix specific for the EBV BALF5 gene [204] was used to quantify EBV in DNA extracted from blood or spleen in hCD34 engrafted NSG recipient mice at the timepoints described. Each 25μl qPCR reaction contained 12.5μl of 2 × QuantiTect Probe PCR Master Mix (Qiagen), 600nM of each primer, 300nM of FAM-labeled probe, 1.25μl of a TaqMan™ 20 × VIC-labeled RNase-P primer-probe mix. For analysis of splenocytes reactions contained 200ng DNA extracted from splenocytes as template. To analyze EBV in peripheral blood 70μl of blood collected via cardiac puncture or retro-orbital bleed was mixed with 3μg of sheared salmon sperm DNA using the DNeasy Blood and Tissue Kit (Qiagen) and eluted in 50μl of Buffer AE (Qiagen). 10μl of extracted DNA was used as template in qPCR. Reactions were heated to 95˚C for 15 minutes to activate DNA polymerase followed by 50 cycles of 95 ˚C for 15 seconds 60 ˚C for 60 seconds, on an Applied Biosystems QuantStudio 7 Flex Real Time PCR System. Synthetic DNA fragments containing the BALF5 target gene as well as flanking genomic regions were synthesized as double stranded DNA gBlocks, and were used to generate a standard curve with known gene copy numbers ranging from 10^7-10^0 copies/μl. The copy number in extracted DNA was

determined by interpolating from the standard curve. Serial dilutions of reference standard were used to experimentally determined a limit of detection of 6.25 copies, which corresponds to the amount of template that can be detected in >95% of reactions. For graphical purposes, samples with no amplification or those yielding values below the limit of detection were assigned a value of 0.625 copies.

Digital Droplet PCR:

Digital droplet PCR (ddPCR) was conducted on DNA extracted from rhesus macaque PBMC or saliva, utilizing Bio-Rad's QX200 ddPCR system in a 22µl total volume. To quantify rhLCV DNA, ddPCR reactions used primers and a FAM-labeled probe specific for the internal repeat 1 (IR1) region of rhLCV which is present at 5 copies per genome [108]. Viral loads in blood were normalized to the number of PBMC in a separate reaction using a primer/probe mix specific for the ribonuclease P/MRP subunit p30 (RPP30) which is present at 2 copies per cell. Each reaction contained 10µl ddPCR Supermix for Probes, no-dUTP, and 5 units of the AluI restriction-enzyme. Reactions which quantified IR1 contained 600nM of primer, 300nM of probe, and 1µg of extracted DNA, while those which quantified RPP30 contained 450nM of primer, 225nM of probe, and 0.05µl DNA extracted from PBMC. Each reaction was adjusted to a final volume of 22µl using dH2O. Each 22µl mixture was loaded into a Droplet Generator DG8 Cartridge (Bio-Rad) and placed in a QX200 Droplet Generator (Bio-Rad). After droplets were made, the droplets were transferred to a 96-well PCR plate, sealed and placed in a C1000 Touch Thermal Cycler (Bio-Rad) and subjected to one cycle of 95°C for 10 minutes for enzyme activation, 40 cycles of 94°C for 30 seconds for denaturation and 60°C for 1 minute for annealing/extension, one cycle of 98°C for 10 minutes for enzyme deactivation and a 4°C hold. Each step utilized a temperature rate increase or decrease of 2°C per second. After PCR, the droplet plate was placed in a QX200 Droplet Reader (Bio-Rad). The droplets whose fluorescence was measured higher than the threshold (4000 for FAM, 3000 for HEX) were counted as positive droplets. The data were analyzed using QuantaSoft™ Analysis Software (Bio-Rad) to determine the concentration of the rhLCV in copies per microliter of reaction.

The rhLCV copies per million copies macaque PBMC were determined using the following equation:

$$\left[\left(\frac{\left(\frac{2\ RPP30\ copies}{PBMC}\right) x(\mu l\ of\ input\ DNA)}{\left(\frac{Copies\ RPP30}{rxn}\right) x(DNA\ dil.\ factor)}\right) x\ (1{,}000{,}000\ PBMC)\right] x\ \left[\frac{\left(\frac{Copies\ rhLCV}{rxn}\right)}{(\mu l\ of\ input\ DNA)}\right]$$

rhLCV copies in saliva are expressed as copies/ml of swab buffer.

rhLCV Viral Capsid Antigen ELISA:

Peptides corresponding to rhLCV viral capsid antigen (VCA) amino acids 117-146, 147-170 [198] as well as scramble peptides of each were synthesized by Genscript. 50 ng/well of a 1:1 mixture of to rhLCV VCA 147-170 and rhLCV VCA117-146 or a 1:1 mixture of the respective scramble peptides were adsorbed onto 96 well half-area microplates at 37°C for 1 hour in a solution of 0.1 M $NaHCO_3$ pH 9.4-9.6. Plates were then washed 4 times with ELISA washing buffer (1× PBS, 0.02% Tween 20) prior to blocking at 37°C for 1 hour with 100 µl per well of PBS containing 3% BSA and 0.02% Tween 20 (blocking buffer). After blocking, plates were washed 4× with ELISA washing buffer. Serum was diluted 1:10 in 50µl of blocking buffer and added to triplicate wells of pooled rhLCV VCA and scramble peptides followed by a 1 hour incubation at 37°C. Following 4 additional washes with ELISA washing buffer, a 1:4000 dilution of goat anti-human IgG in blocking buffer was added to each well and incubated at 37°C for 1 hour followed by 4 washes with wash buffer. 50 µl/well of SureBlue Reserve TMB Microwell Peroxidase substrate was added. After 3 min, 50 µl/well of 1N sulfuric acid was added and the A_{450} of each well was read on a Molecular Devices SpectraMax M2 plate reader. Background signal of secondary antibody against peptide coated wells was averaged and subtracted from wells containing rhesus macaque sera. Absorbance values from triplicate wells from each animal's sera were averaged. The average absorbance of the wells coated with scramble peptides were subtracted from the corresponding pool of rhLCV VCA peptides. Negative values are reported as zero.

Detection of AMMO1 and VRC01 in Plasma:

200ng/well of EBV gH/gL [192] were adsorbed onto 96 well Immulon 2HB ELISA plates at 37°C for 1 hour in a solution of 0.1 M $NaHCO_3$ pH 9.4-9.6. Plates were then washed 4 times with ELISA washing buffer (1× PBS, 0.02% Tween 20) prior to blocking at 37°C for 1 hour with 250 µl per well of PBS containing 10% non-fat milk and 0.02% Tween 20 (blocking buffer). After blocking, plates were washed 4× with ELISA washing buffer. A known concentration of AMMO1 mAb, rhesus macaque serum collected just prior to mAb infusion, or rhesus macaque serum collected 2 days after mAb infusion was diluted 1:100 in blocking buffer and three-fold serial dilutions were performed in duplicate in 100µl volumes

followed by a 1 hour incubation at 37°C. Control wells were incubated with blocking buffer not containing mAb or sera. Following 4 additional washes with ELISA washing buffer, a 1:3000 dilution of goat anti-human IgG, cross-adsorbed with rhesus and cynomolgus macaque IgG in blocking buffer was added to each well and incubated at 37°C for 1 hour followed by 4 washes with wash buffer. 100 µl/well of SureBlue Reserve TMB Microwell Peroxidase substrate was added. After 3 min, 100 µl/well of 1N sulfuric acid was added and the A_{450} of each well was read on a Molecular Devices SpectraMax M2. The background A_{450} was averaged from control wells and subtracted from all other wells on the plate. To generate a standard curve, the corrected average A_{450} of duplicate wells were plotted against the known concentration of AMMO1 and the data was fit to a sigmoidal dose-response curve using Prism 7.03 software package (GraphPad Software).

To determine the concentration of AMMO1 in the plasma, the average A_{450} of wells containing pre-infusion plasma was subtracted from the absorbance of wells containing post-infusion plasma at each dilution. The background-subtracted absorbance values were averaged at each dilution and absorbance readings that fell on the linear (hill slope) part of the AMMO1 standard curve were used to interpolate the concentration of AMMO1 in plasma. The concentration of VRC01 in plasma was determined using the same method, except that the standard curve was generated with VRC01 binding to monomeric 426c.NLGS.TM4.ΔV1-3 [205].

EBV Neutralization Assay in B cells:

EBV neutralization assays were carried out in Raji cells essentially as described [82]. AMMO1 mAb, plasma from humanized mice, or plasma from rhesus macaques, was serially diluted in duplicate wells of 96-well round-bottom plates containing 25µl of cRPMI in duplicate. 12.5µl of B95-8/F virus (diluted to achieve an infection frequency of 1-5% at the final dilution) was added and incubated at 37°C for 1 hour. 12.5 µl of cRMPI containing 4×10^6 Raji cells/ml was added to each well and incubated for another hour at 37°C. The cells were then pelleted, washed once with cRPMI, and re-suspended in cRMPI. Antibody concentration or serum dilution is reported relative to the final infection volume (50µl). After 3 days at 37°C, cells were fixed in 2% paraformaldehyde. The percentage of GFP+ Raji cells as determined on a BD LSRII cytometer.

To account for any false positive cells due to auto-fluorescence in the GFP channel, the average %GFP$^+$ cells in negative control wells (n=5-10) was subtracted from each well. The infectivity (%GFP$^+$) for each well was plotted as a function of the $\log_{10}$ of the mAb concentration or serum dilution. The neutralization curve was fit using the log (inhibitor) vs response- variable slope (four parameters) analysis in Prism 7.03 (GraphPad Software).

rhLCV gH/gL Cell Surface Staining:

10ml of 293F cells at a density of 1×10^6 cells/ml were transfected with equal amounts of pCAGGS-rhLCVgH, pCAGGS-rhLCVgL[197], or mock transfected using 293 Free according to the manufacturer's instructions. 1 hour following transfection 500µl of cell culture was added to 500µl of DMEM in a 6-well dish. 24 hours later the cells were fixed in 10% formalin washed 3X with PBS containing 1% BSA and 0.1% Tween-20. The cells were then incubated with 1µg of AMMO1 conjugated to Dylite-650 in 1ml of PBS containing 1% BSA and 0.1% Tween-20 at room temperature for 30min. The cells were then washed 3 times with PBS and visualized on an EvosFL imaging system using a 20× objective lens and a Cy5 light cube (ThermoFisher).

Virus-free Fusion Assay:

CHO-K1 cells were seeded onto six-well plates at a density of 3×10^5 cells/well. 24 hours later, the cells were transfected with 0.5 µg each of pCAGGS-rhLCVgH, pCAGGS-rhLCVgL, pCAGGS-rhLCVgB [206] and 0.8 µg of pT7EMCLuc, which carries a luciferase-containing reporter plasmid under the control of the T7 promoter [207], using GeneJuice Transfection Reagent. As a control for background luciferase activity one well was transfected with the same mix as above, except the pCAGGS-$_{rhLCV}$gB plasmid was replaced by empty pTT3.

Meanwhile, 293-T7 cells were seeded into a 96 well plate at a density of 1×10^4 cells per well in a volume of 100 µl/well of cF-12 without Zeocin selection.

8 hours later, the transfected CHO cells were trypsinized, washed once with cF-12, and re-suspended at a density of 1×10^5 cells/ml in F-12 media. 100 µl/well of CHO-K1 suspension was added to the plate containing 293-T7[208] cells. Immediately after the addition of CHO-K1 cells, 2 µg of AMMO1, CL59, E1D1, CL40, or a no antibody control were added to 6 wells in parallel. 24 hours later, the media was aspirated

and the cells were lysed in 100 µl of Steady-Glo luciferase reagent. 75 µl of cell lysate was transferred to a white bottom assay plate and luciferase activity was read on a Fluroskan Ascent FL fluorimeter.

rhLCV Virus Production:

Rhesus LCV was isolated from LCL8664 cells using two methods.

TPA/Butyrate: LCL8664 cells were cultured in cRPMI at approximately 0.5-1×10^6 cells/ml. 1×10^9 cells were resuspended at a density of 3×10^6 cells/ml in cRMPI, to which 12-O-Tetradecanoylphorbol 13-acetate was added to a final concentration of 20ng/mL and sodium butyrate was added to a final concentration of 3mM. Cells were then incubated at 37ºC overnight. The next day, cells were pelleted by centrifugation at 300 × *g* for 10 minutes and resuspended at a density of 3×10^6 cells/ml in cRPMI and cultured at 37ºC for 6 days and then passed through a 0.45 µM filter. The supernatant was then centrifuged at 10,000 × *g* for 2 hours at 4ºC. The supernatant was aspirated and the pellet was resuspended in ~2ml of RPMI containing 10% FBS. Virus was dispensed into 250µl aliquots and stored at -80ºC.

Electroporation: 240 million LCL8664 cells were pelleted at 90 X *g* for 10 minutes. The cell pellet was resuspended in 2.4ml of Nucleofector Solution V containing supplement (Lonza). 0.1ml of cell suspension was added to 24 separate electroporation cuvettes each containing 2.5 µg of p509 an expression plasmid encoding EBV BZLF1. Electroporation was carried out using program X-001 on an Amaxa nucleofector (Lonza). Immediately following electroporation, cells were diluted with 500µl of cRPMI and then transferred to a T225 flask containing 120ml of cRPMI. Cells were cultured at 37ºC for 5 days and then passed through a 0.45 µM filter. The supernatant was then centrifuged at 10, 000 X *g* for 2 hours at 4ºC. The supernatant was aspirated and the pellet was resuspended in ~1.5ml of RPMI containing 10% FBS. Virus was dispensed into 250µl aliquots and stored at -80ºC.

rhLCV Titration:

Serial dilutions of rhLCV were added to 96 well plates containing 1×10^5 rhesus PBMC in RPMI containing 10% FBS, 2mM L-glutamine, 100U/ml penicillin, and 100µg/ml streptomycin and 0.5µg cyclosporin A. Each concentration of virus was tested against 20 PBMC-containing wells. Media was replenished weekly with 50-100µl and the cells were cultured for 7-10 weeks. Wells were visually inspected and scored as positive (clumping/growing cells, media turning to yellow) or negative (no cell growth, pink media). Virus

concentration was plotted against % transformed wells and fit with a sigmoidal dose-response (variable slope) curve using Prism 7.03 software. 1 Transforming unit is defined as the dilution that yields 62.5% positive wells [209]. The transforming units/ml of each stock were determined using PBMC drawn from 2 separate animals and averaged.

rhLCV Neutralization Assay:

2.5 transforming units of RhLCV were incubated with either no antibody or with 5μg of AMMO1 or AMMO2 in a 50μl volume of cRPMI containing 0.5μg cyclosporin A for 30 min at 37ºC. Next, 50μl of cRPMI containing 0.5μg cyclosporin A and 1.5×10^5 of fresh rhesus PBMC were added to each well and incubated for an additional hour at 37ºC. As a no-infection control 1.5×10^5 fresh rhesus PBMC were diluted into 100μl of cRPMI containing 0.5μg cyclosporin A. The contents of each well were then diluted to 500μl of cRPMI containing 0.5μg cyclosporin A in a 24 well plate. An additional 2μg of AMMO1 or AMMO2 were added to wells containing cells and virus that had been pre-incubated with these Abs. Following a 3 day incubation at 37ºC, the PBMC from each well were collected and resuspended in 100ul of PBS containing 3% bovine serum albumin and 1.5μl CD19 and 1μl CD20-AF700 and 0.75μl/sample eBioscience Fixable Viability Dye eFluor 506. The cells were then fixed and permeabilized using the eBioscience Foxp3 / Transcription Factor Staining Buffer Set according to the manufacturer's instructions and then and stained with a 1:50 dilution of EBNA 2 FITC conjugate derived from the PE2 mAb which reacts with EBNA2 from rhLCV [210]. The cells were then washed 2X and then analyzed on a BD-LSII cytometer. rhLCV infected B cells were defined as live, $CD19^+$, $CD20^+$, $EBNA2^+$.

Quantification and Statistical Analysis:

Statistical analyses were performed using GraphPad (version 7 and later). Statistical analyses for all humanized mouse studies were conducted using one way ANOVA, differences in the means of each group were determined using the Sidak multiple comparisons test, p values are indicated in the corresponding figure legends. Unless otherwise indicated, analyses were conducted on one representative experimental replicate; ie one group of mice engrafted with the same pool of HPSC on the same day, and also challenged with virus at the same time. No additional methods were used to determine whether the data met assumptions of the statistical approach. Differences in the cell-free fusion assay were determined using an unpaired 2-tailed T-test p values are shown in the corresponding figure

legend. Due to the relatively small number of animals, statistical analyses were not performed on rhesus macaque studies.

Chapter 4: Conclusions and Future Directions

EBV is a common virus which infects about 95% of the population and is associated with ~265,000 cases of cancer each year. An efficacious EBV vaccine could help to alleviate the significant global disease burden resulting from EBV infection. In Chapters 2 and 3, I describe our lab's recent efforts towards the development of EBV therapeutics. Chapter 3 highlights experimental work showing that AMMO1, an anti-gH/gL antibody previously isolated by our group, protects humanized mice and rhesus macaques from challenge with EBV and RhLCV, respectively. For this study, I generated *in vitro* data measuring the neutralizing activity of plasma from mice receiving passive transfer of AMMO1 and 72A1 monoclonal antibody using B cell neutralizing assays which I helped to optimize for the lab.

Spurred by the findings described in Chapter 3, our lab set out to develop a vaccine targeting gH/gL by utilizing recent advances in vaccinology, specifically antigen multimerization. Multimerization has been shown to improve immunogenicity for a variety of antigens, including those from HIV, RSV, SARS-CoV-2, and influenza. In Chapter 2, I outline how our lab, alongside our collaborators, developed several multimeric and one monomeric vaccine displaying the gH/gL ectodomain. I then immunized mice with each of these constructs and evaluated the antibody response by assaying gH/gL binding titers and EBV infection neutralizing titers in plasma from the immunized mice. I demonstrated that multimeric gH/gL elicited superior immunogenicity, both in terms of gH/gL binding titers and EBV neutralizing titers, when compared to monomeric gH/gL *in vitro*. The 60-mer gH/gL and the monomer gH/gL vaccine candidates were then evaluated for their ability to protect humanized mice against lethal challenge by EBV using a passive transfer approach. In this experiment, vaccine IgG elicited by a 60-mer gH/gL conferred superior protection against lethal challenge by EBV *in vivo* when compared to vaccine IgG elicited by a monomer gH/gL vaccine. In general, multimerization also increased the antigenicity of each multimeric construct, as measured by mAb binding to each construct by ELISA. Interestingly, there did not appear to be any correlation between the valency of these constructs and their immunogenicity, contrary to a valency dependent increase in immunogenicity which was observed in a recent study comparing multimeric RSV vaccines.[118] A notably difference between our study and this RSV study is that the RSV study used the same multimerization scaffold for each valency tested whereas we used a different scaffold for each

construct. This suggests that scaffold-specific differences may play a role in the immune response, perhaps due to differences in T cell epitope recognition.

In addition to observing strong immunogenicity *in vitro* with multimeric constructs as compared to monomeric gH/gL, vaccine IgG elicited by the 60-mer gH/gL construct conferred superior protection, protecting 5 of 5 mice, in an *in vivo* humanized mouse animal model than IgG from the monomer gH/gL construct, which only protected 1 of 4 mice. In another study, passive transfer of sera from rabbits immunized with monomeric gH/gL to humanized mice also only partially protected the mice from lethal EBV challenge. Because EBV infection in humanized mice is restricted to human B cells, the lack of monomeric gH/gL vaccine IgG to completely protect the humanized mice in our study and other studies may be due to its inability to elicit sufficient neutralizing titers against EBV infection of B cells following two immunizations, whereas gH/gL 60-mer vaccine IgG can do so sufficiently. It is worth nothing that sterilizing immunity was not achieved by 60-mer vaccine IgG in all animals in this model, and it is possible that more of the 60-mer IgG animals may have succumbed to infection if observed for a longer period.

There may be several reasons for why we observed differences in immunogenicity between each of our vaccine constructs, including potential differences in the stability of the constructs and/or in the display of T cell epitopes resulting from the different multimer geometries. To explore potential mechanisms for why we observed differences in neutralization and binding, I first performed antibody competition studies to compare the epitopes targeted by vaccine-elicited antibody from mice immunized with each vaccine. Our hypothesis was that multimers may elicit greater levels of antibody against epitopes which have known, neutralizing antibodies targeting them, such as the AMMO1, CL40, CL59, and E1D1 epitopes. Surprisingly, for each construct tested, relatively minor differences were observed between which epitopes were targeted. Notably, antibodies against the AMMO1 epitope were rare in each group. In terms of vaccine design, this suggests that it may be worthwhile developing a vaccine which focuses the immune response against AMMO1. Further work to identify additional gH/gL epitopes targeted by potently neutralizing antibodies in natural infection and immunized animals would help to better inform such immune-focusing strategies.

In summary, our lab showed in Chapter 3 how AMMO1, a monoclonal antibody targeting gH/gL, was able to confer protection in animal models against challenge with EBV and RhLCV. This study serves

as a proof of concept for the hypothesis that vaccine-elicited antibodies targeting gH/gL may be protective against EBV infection. To explore this idea, our lab generated a series of multimeric gH/gL vaccine constructs, both in-house and alongside collaborators. In Chapter 2, I demonstrate that multivalent display of EBV gH/gL glycoprotein enhances the immunogenicity of each of these constructs compared to monomer gH/gL, and that the gH/gL 60-mer elicits antibodies that completely protect and lethal EBV challenge in humanized mice, whereas gH/gL monomer only confers partial protection. Taken together, these results provide evidence that gH/gL is an important antigen and that both monoclonal as well as vaccine-elicited antibodies which target gH/gL protect against lethal EBV challenge in a humanized mouse model. Given this observed protection, further studies in non-human primate models are warranted.

Appendix A - Bibliography

1. Mentzer, A.J., Brenner, N., Allen, N., Littlejohns, T.J., Chong, A.Y., Cortes, A., Almond, R., Hill, M., Sheard, S., Mcvean, G., et al. (2022). Identification of host–pathogen-disease relationships using a scalable multiplex serology platform in UK Biobank. Nature Communications *13*. 10.1038/s41467-022-29307-3.
2. Shannon-Lowe, C., and Rickinson, A. (2019). The Global Landscape of EBV-Associated Tumors. Frontiers in oncology *9*, 713. 10.3389/fonc.2019.00713.
3. Taylor, G.S., Long, H.M., Brooks, J.M., Rickinson, A.B., and Hislop, A.D. (2015). The immunology of Epstein-Barr virus-induced disease. Annual review of immunology *33*, 787-821. 10.1146/annurev-immunol-032414-112326.
4. Cohen, J.I. (2018). Vaccine Development for Epstein-Barr Virus. Advances in experimental medicine and biology *1045*, 477-493. 10.1007/978-981-10-7230-7_22.
5. Kutok, J.L., and Wang, F. (2006). Spectrum of Epstein-Barr virus-associated diseases. Annual review of pathology *1*, 375-404. 10.1146/annurev.pathol.1.110304.100209.
6. Cohen, J.I., Fauci, A.S., Varmus, H., and Nabel, G.J. (2011). Epstein-Barr virus: an important vaccine target for cancer prevention. Science translational medicine *3*, 107fs107. 10.1126/scitranslmed.3002878.
7. Khan, G., Fitzmaurice, C., Naghavi, M., and Ahmed, L.A. (2020). Global and regional incidence, mortality and disability-adjusted life-years for Epstein-Barr virus-attributable malignancies, 1990-2017. BMJ Open *10*, e037505. 10.1136/bmjopen-2020-037505.
8. Levin, L.I., Munger, K.L., O'Reilly, E.J., Falk, K.I., and Ascherio, A. (2010). Primary infection with the Epstein-Barr virus and risk of multiple sclerosis. Annals of neurology *67*, 824-830. 10.1002/ana.21978.
9. Handel, A.E., Williamson, A.J., Disanto, G., Handunnetthi, L., Giovannoni, G., and Ramagopalan, S.V. (2010). An updated meta-analysis of risk of multiple sclerosis following infectious mononucleosis. PloS one *5*. 10.1371/journal.pone.0012496.
10. Thacker, E.L., Mirzaei, F., and Ascherio, A. (2006). Infectious mononucleosis and risk for multiple sclerosis: a meta-analysis. Annals of neurology *59*, 499-503. 10.1002/ana.20820.
11. Munger, K.L., Levin, L.I., O'Reilly, E.J., Falk, K.I., and Ascherio, A. (2011). Anti-Epstein-Barr virus antibodies as serological markers of multiple sclerosis: a prospective study among United States military personnel. Mult Scler *17*, 1185-1193. 10.1177/1352458511408991.
12. Balandraud, N., and Roudier, J. (2018). Epstein-Barr virus and rheumatoid arthritis. Joint, bone, spine : revue du rhumatisme *85*, 165-170. 10.1016/j.jbspin.2017.04.011.
13. Angelini, D.F., Serafini, B., Piras, E., Severa, M., Coccia, E.M., Rosicarelli, B., Ruggieri, S., Gasperini, C., Buttari, F., Centonze, D., et al. (2013). Increased CD8+ T cell response to Epstein-Barr virus lytic antigens in the active phase of multiple sclerosis. PLoS Pathog *9*, e1003220. 10.1371/journal.ppat.1003220.
14. Bjornevik, K., Cortese, M., Healy, B.C., Kuhle, J., Mina, M.J., Leng, Y., Elledge, S.J., Niebuhr, D.W., Scher, A.I., Munger, K.L., and Ascherio, A. (2022). Longitudinal analysis reveals high prevalence of Epstein-Barr virus associated with multiple sclerosis. Science. 10.1126/science.abj8222.
15. Balfour, H.H., Jr., Odumade, O.A., Schmeling, D.O., Mullan, B.D., Ed, J.A., Knight, J.A., Vezina, H.E., Thomas, W., and Hogquist, K.A. (2013). Behavioral, virologic, and immunologic factors associated with acquisition and severity of primary Epstein-Barr virus infection in university students. J Infect Dis *207*, 80-88. 10.1093/infdis/jis646.
16. Jayasooriya, S., de Silva, T.I., Njie-jobe, J., Sanyang, C., Leese, A.M., Bell, A.I., McAulay, K.A., Yanchun, P., Long, H.M., Dong, T., et al. (2015). Early virological and immunological events in

asymptomatic Epstein-Barr virus infection in African children. PLoS Pathog *11*, e1004746. 10.1371/journal.ppat.1004746.

17. Williams, H., Macsween, K., McAulay, K., Higgins, C., Harrison, N., Swerdlow, A., Britton, K., and Crawford, D. (2004). Analysis of immune activation and clinical events in acute infectious mononucleosis. J Infect Dis *190*, 63-71. 10.1086/421276.
18. Rickinson, A.B., Long, H.M., Palendira, U., Münz, C., and Hislop, A.D. (2014). Cellular immune controls over Epstein-Barr virus infection: new lessons from the clinic and the laboratory. Trends Immunol *35*, 159-169. 10.1016/j.it.2014.01.003.
19. Dunmire, S.K., Hogquist, K.A., and Balfour, H.H. (2015). Infectious Mononucleosis. In Current Topics in Microbiology and Immunology, (Springer International Publishing), pp. 211-240. 10.1007/978-3-319-22822-8_9.
20. Niederman, J.C. (1968). Infectious Mononucleosis. JAMA *203*, 205. 10.1001/jama.1968.03140030037009.
21. Thorley-Lawson, D.A., Duca, K.A., and Shapiro, M. (2008). Epstein-Barr virus: a paradigm for persistent infection - for real and in virtual reality. Trends Immunol *29*, 195-201. 10.1016/j.it.2008.01.006.
22. Farrell, P.J. (2019). Epstein-Barr Virus and Cancer. Annu Rev Pathol *14*, 29-53. 10.1146/annurev-pathmechdis-012418-013023.
23. da Silva, S.R., and de Oliveira, D.E. (2011). HIV, EBV and KSHV: viral cooperation in the pathogenesis of human malignancies. Cancer Lett *305*, 175-185. 10.1016/j.canlet.2011.02.007.
24. Lanz, T.V., Brewer, R.C., Ho, P.P., Moon, J.S., Jude, K.M., Fernandez, D., Fernandes, R.A., Gomez, A.M., Nadj, G.S., Bartley, C.M., et al. (2022). Clonally expanded B cells in multiple sclerosis bind EBV EBNA1 and GlialCAM. Nature *603*, 321-327. 10.1038/s41586-022-04432-7.
25. Ainsworth, C. (2018). Building a better lymphoma vaccine. Nature *563*, S52-s54. 10.1038/d41586-018-07366-1.
26. Plotkin, S.A. (2010). Correlates of protection induced by vaccination. Clinical and vaccine immunology : CVI *17*, 1055-1065. 10.1128/cvi.00131-10.
27. Gilbert, P.B., Montefiori, D.C., McDermott, A.B., Fong, Y., Benkeser, D., Deng, W., Zhou, H., Houchens, C.R., Martins, K., Jayashankar, L., et al. (2022). Immune correlates analysis of the mRNA-1273 COVID-19 vaccine efficacy clinical trial. Science *375*, 43-50. 10.1126/science.abm3425.
28. Connolly, S.A., Jardetzky, T.S., and Longnecker, R. (2021). The structural basis of herpesvirus entry. Nat Rev Microbiol *19*, 110-121. 10.1038/s41579-020-00448-w.
29. Backovic, M., Longnecker, R., and Jardetzky, T.S. (2009). Structure of a trimeric variant of the Epstein-Barr virus glycoprotein B. Proceedings of the National Academy of Sciences of the United States of America *106*, 2880-2885. 10.1073/pnas.0810530106.
30. Oda, T., Imai, S., Chiba, S., and Takada, K. (2000). Epstein-Barr virus lacking glycoprotein gp85 cannot infect B cells and epithelial cells. Virology *276*, 52-58. 10.1006/viro.2000.0531.
31. Stampfer, S.D., and Heldwein, E.E. (2013). Stuck in the middle: structural insights into the role of the gH/gL heterodimer in herpesvirus entry. Current opinion in virology *3*, 13-19. 10.1016/j.coviro.2012.10.005.
32. Haddad, R.S., and Hutt-Fletcher, L.M. (1989). Depletion of glycoprotein gp85 from virosomes made with Epstein-Barr virus proteins abolishes their ability to fuse with virus receptor-bearing cells. J Virol *63*, 4998-5005. 10.1128/JVI.63.12.4998-5005.1989.
33. Mohl, B.S., Chen, J., Sathiyamoorthy, K., Jardetzky, T.S., and Longnecker, R. (2016). Structural and Mechanistic Insights into the Tropism of Epstein-Barr Virus. Molecules and cells *39*, 286-291. 10.14348/molcells.2016.0066.

34. Tugizov, S.M., Berline, J.W., and Palefsky, J.M. (2003). Epstein-Barr virus infection of polarized tongue and nasopharyngeal epithelial cells. Nature medicine *9*, 307-314. 10.1038/nm830.
35. Chesnokova, L.S., Nishimura, S.L., and Hutt-Fletcher, L.M. (2009). Fusion of epithelial cells by Epstein-Barr virus proteins is triggered by binding of viral glycoproteins gHgL to integrins alphavbeta6 or alphavbeta8. Proceedings of the National Academy of Sciences of the United States of America *106*, 20464-20469. 10.1073/pnas.0907508106.
36. Chen, J., Sathiyamoorthy, K., Zhang, X., Schaller, S., Perez White, B.E., Jardetzky, T.S., and Longnecker, R. (2018). Ephrin receptor A2 is a functional entry receptor for Epstein-Barr virus. Nat Microbiol *3*, 172-180. 10.1038/s41564-017-0081-7.
37. Zhang, H., Li, Y., Wang, H.B., Zhang, A., Chen, M.L., Fang, Z.X., Dong, X.D., Li, S.B., Du, Y., Xiong, D., et al. (2018). Ephrin receptor A2 is an epithelial cell receptor for Epstein-Barr virus entry. Nat Microbiol *3*, 1-8. 10.1038/s41564-017-0080-8.
38. Wang, H.B., Zhang, H., Zhang, J.P., Li, Y., Zhao, B., Feng, G.K., Du, Y., Xiong, D., Zhong, Q., Liu, W.L., et al. (2015). Neuropilin 1 is an entry factor that promotes EBV infection of nasopharyngeal epithelial cells. Nat Commun *6*, 6240. 10.1038/ncomms7240.
39. Xiong, D., Du, Y., Wang, H.B., Zhao, B., Zhang, H., Li, Y., Hu, L.J., Cao, J.Y., Zhong, Q., Liu, W.L., et al. (2015). Nonmuscle myosin heavy chain IIA mediates Epstein-Barr virus infection of nasopharyngeal epithelial cells. Proc Natl Acad Sci U S A *112*, 11036-11041. 10.1073/pnas.1513359112.
40. Su, C., Wu, L., Chai, Y., Qi, J., Tan, S., Gao, G.F., Song, H., and Yan, J. (2020). Molecular basis of EphA2 recognition by gHgL from gammaherpesviruses. Nature communications *11*, 5964. 10.1038/s41467-020-19617-9.
41. Tanner, J., Weis, J., Fearon, D., Whang, Y., and Kieff, E. (1987). Epstein-Barr virus gp350/220 binding to the B lymphocyte C3d receptor mediates adsorption, capping, and endocytosis. Cell *50*, 203-213.
42. Ogembo, J.G., Kannan, L., Ghiran, I., Nicholson-Weller, A., Finberg, R.W., Tsokos, G.C., and Fingeroth, J.D. (2013). Human complement receptor type 1/CD35 is an Epstein-Barr Virus receptor. Cell reports *3*, 371-385. 10.1016/j.celrep.2013.01.023.
43. Nemerow, G.R., Mold, C., Schwend, V.K., Tollefson, V., and Cooper, N.R. (1987). Identification of gp350 as the viral glycoprotein mediating attachment of Epstein-Barr virus (EBV) to the EBV/C3d receptor of B cells: sequence homology of gp350 and C3 complement fragment C3d. J Virol *61*, 1416-1420. 10.1128/JVI.61.5.1416-1420.1987.
44. Spriggs, M.K., Armitage, R.J., Comeau, M.R., Strockbine, L., Farrah, T., Macduff, B., Ulrich, D., Alderson, M.R., Mullberg, J., and Cohen, J.I. (1996). The extracellular domain of the Epstein-Barr virus BZLF2 protein binds the HLA-DR beta chain and inhibits antigen presentation. Journal of virology *70*, 5557-5563.
45. Sathiyamoorthy, K., Jiang, J., Hu, Y.X., Rowe, C.L., Mohl, B.S., Chen, J., Jiang, W., Mellins, E.D., Longnecker, R., Zhou, Z.H., and Jardetzky, T.S. (2014). Assembly and architecture of the EBV B cell entry triggering complex. PLoS pathogens *10*, e1004309. 10.1371/journal.ppat.1004309.
46. Haan, K.M., Kwok, W.W., Longnecker, R., and Speck, P. (2000). Epstein-Barr virus entry utilizing HLA-DP or HLA-DQ as a coreceptor. J Virol *74*, 2451-2454. 10.1128/jvi.74.5.2451-2454.2000.
47. Berggren, K.A., Suzuki, S., and Ploss, A. (2020). Animal Models Used in Hepatitis C Virus Research. Int J Mol Sci *21*. 10.3390/ijms21113869.
48. Chu, Y.K., Ali, G.D., Jia, F., Li, Q., Kelvin, D., Couch, R.C., Harrod, K.S., Hutt, J.A., Cameron, C., Weiss, S.R., and Jonsson, C.B. (2008). The SARS-CoV ferret model in an infection-challenge study. Virology *374*, 151-163. 10.1016/j.virol.2007.12.032.
49. Geisbert, T.W., Feldmann, H., and Broder, C.C. (2012). Animal challenge models of henipavirus infection and pathogenesis. Curr Top Microbiol Immunol *359*, 153-177. 10.1007/82_2012_208.

50. Gurumurthy, C.B., Quadros, R.M., Richardson, G.P., Poluektova, L.Y., Mansour, S.L., and Ohtsuka, M. (2020). Genetically modified mouse models to help fight COVID-19. Nat Protoc *15*, 3777-3787. 10.1038/s41596-020-00403-2.
51. Hatziioannou, T., and Evans, D.T. (2012). Animal models for HIV/AIDS research. Nat Rev Microbiol *10*, 852-867. 10.1038/nrmicro2911.
52. Munz, C. (2020). Probing Reconstituted Human Immune Systems in Mice With Oncogenic gamma-Herpesvirus Infections. Front Immunol *11*, 581419. 10.3389/fimmu.2020.581419.
53. Gujer, C., Chatterjee, B., Landtwing, V., Raykova, A., McHugh, D., and Munz, C. (2015). Animal models of Epstein Barr virus infection. Curr Opin Virol *13*, 6-10. 10.1016/j.coviro.2015.03.014.
54. Chatterjee, B., Leung, C.S., and Munz, C. (2014). Animal models of Epstein Barr virus infection. J Immunol Methods *410*, 80-87. 10.1016/j.jim.2014.04.009.
55. Sun, C., Chen, X.C., Kang, Y.F., and Zeng, M.S. (2021). The Status and Prospects of Epstein-Barr Virus Prophylactic Vaccine Development. Front Immunol *12*, 677027. 10.3389/fimmu.2021.677027.
56. Wang, F. (2013). Nonhuman primate models for Epstein-Barr virus infection. Curr Opin Virol *3*, 233-237. 10.1016/j.coviro.2013.03.003.
57. International Union for Conservation of Nature and Natural Resources. Species Survival Commission., and IUCN--The World Conservation Union. Species Survival Commission. The IUCN red list of threatened species. International Union for Conservation of Nature and Natural Resources.
58. Moghaddam, A., Koch, J., Annis, B., and Wang, F. (1998). Infection of human B lymphocytes with lymphocryptoviruses related to Epstein-Barr virus. J Virol *72*, 3205-3212. 10.1128/JVI.72.4.3205-3212.1998.
59. Estes, J.D., Wong, S.W., and Brenchley, J.M. (2018). Nonhuman primate models of human viral infections. Nat Rev Immunol *18*, 390-404. 10.1038/s41577-018-0005-7.
60. Singh, S., Homad, L.J., Akins, N.R., Stoffers, C.M., Lackhar, S., Malhi, H., Wan, Y.H., Rawlings, D.J., and McGuire, A.T. (2020). Neutralizing Antibodies Protect against Oral Transmission of Lymphocryptovirus. Cell reports. Medicine *1*. 10.1016/j.xcrm.2020.100033.
61. Fujiwara, S., and Nakamura, H. (2020). Animal Models for Gammaherpesvirus Infections: Recent Development in the Analysis of Virus-Induced Pathogenesis. Pathogens *9*. 10.3390/pathogens9020116.
62. Münz, C. (2017). Humanized mouse models for Epstein Barr virus infection. Current Opinion in Virology *25*, 113-118. 10.1016/j.coviro.2017.07.026.
63. Zhu, Q.Y., Shan, S., Yu, J., Peng, S.Y., Sun, C., Zuo, Y., Zhong, L.Y., Yan, S.M., Zhang, X., Yang, Z., et al. (2021). A potent and protective human neutralizing antibody targeting a novel vulnerable site of Epstein-Barr virus. Nat Commun *12*, 6624. 10.1038/s41467-021-26912-6.
64. Cui, X., Cao, Z., Ishikawa, Y., Cui, S., Imadome, K.-I., and Snapper, C.M. (2021). Immunization with Epstein–Barr Virus Core Fusion Machinery Envelope Proteins Elicit High Titers of Neutralizing Activities and Protect Humanized Mice from Lethal Dose EBV Challenge. Vaccines *9*, 285. 10.3390/vaccines9030285.
65. Kim, J., Bu, W., Mine, S., Tariq, Z., Nguyen, H., Wang, Y., Tolman, C., Mond, J., and Cohen, J.I. (2021). Epstein-Barr virus (EBV) hyperimmune globulin isolated from donors with high gp350 antibody titers protect humanized mice from challenge with EBV. Virology *561*, 80-86. 10.1016/j.virol.2021.06.006.
66. Yu, H., Borsotti, C., Schickel, J.N., Zhu, S., Strowig, T., Eynon, E.E., Frleta, D., Gurer, C., Murphy, A.J., Yancopoulos, G.D., et al. (2017). A novel humanized mouse model with significant improvement of class-switched, antigen-specific antibody production. Blood *129*, 959-969. 10.1182/blood-2016-04-709584.

67. Munz, C. (2017). Humanized mouse models for Epstein Barr virus infection. Current opinion in virology *25*, 113-118. 10.1016/j.coviro.2017.07.026.
68. Malhi, H., Homad, L.J., Wan, Y.-H., Poudel, B., Fiala, B., Borst, A.J., Wang, J.Y., Walkey, C., Price, J., Wall, A., et al. (2022). Immunization with a self-assembling nanoparticle vaccine displaying EBV gH/gL protects humanized mice against lethal viral challenge. Cell Reports Medicine *3*, 100658. 10.1016/j.xcrm.2022.100658.
69. Cui, X., Cao, Z., Chen, Q., Arjunaraja, S., Snow, A.L., and Snapper, C.M. (2016). Rabbits immunized with Epstein-Barr virus gH/gL or gB recombinant proteins elicit higher serum virus neutralizing activity than gp350. Vaccine *34*, 4050-4055. https://doi.org/10.1016/j.vaccine.2016.06.021.
70. Escalante, G.M., Foley, J., Mutsvunguma, L.Z., Rodriguez, E., Mulama, D.H., Muniraju, M., Ye, P., Barasa, A.K., and Ogembo, J.G. (2020). A Pentavalent Epstein-Barr Virus-Like Particle Vaccine Elicits High Titers of Neutralizing Antibodies against Epstein-Barr Virus Infection in Immunized Rabbits. Vaccines *8*. 10.3390/vaccines8020169.
71. Servat, E., Ro, B.W., Cayatte, C., Gemmell, L., Barton, C., Rao, E., Lin, R., Zuo, F., Woo, J.C., and Hayes, G.M. (2015). Identification of the critical attribute(s) of EBV gp350 antigen required for elicitation of a neutralizing antibody response in vivo. Vaccine *33*, 6771-6777. 10.1016/j.vaccine.2015.10.024.
72. Mackett, M., and Arrand, J.R. (1985). Recombinant vaccinia virus induces neutralising antibodies in rabbits against Epstein-Barr virus membrane antigen gp340. The EMBO Journal *4*, 3229-3234. 10.1002/j.1460-2075.1985.tb04070.x.
73. Winthrop, T.J.a.K.A.M.a.H.J.H.a.R.R.S. (1999). Expression of Epstein–Barr virus gp350 as a single chain glycoprotein for an EBV subunit vaccine. Vaccine *17*, 660-668. https://doi.org/10.1016/S0264-410X(98)00248-5.
74. Kanai, K., Kato, K., Sano, H., Nagata, K., Okuno, K., Kuwamoto, S., Higaki, H., Sugihara, H., Kato, M., Murakami, I., and Hayashi, K. (2011). In vitro Epstein-Barr Virus Infection Model of Rabbit Lymphocytes from Peripheral Blood or Spleen. Intervirology *54*, 17-24. 10.1159/000318882.
75. Okuno, K., Takashima, K., Kanai, K., Ohashi, M., Hyuga, R., Sugihara, H., Kuwamoto, S., Kato, M., Sano, H., Sairenji, T., et al. (2010). Epstein-Barr virus can infect rabbits by the intranasal or peroral route: an animal model for natural primary EBV infection in humans. Journal of medical virology *82*, 977-986. 10.1002/jmv.21597.
76. Takashima, K., Ohashi, M., Kitamura, Y., Ando, K., Nagashima, K., Sugihara, H., Okuno, K., Sairenji, T., and Hayashi, K. (2008). A new animal model for primary and persistent Epstein-Barr virus infection: human EBV-infected rabbit characteristics determined using sequential imaging and pathological analysis. Journal of medical virology *80*, 455-466. 10.1002/jmv.21102.
77. Wang, Z., Yi, X., Du, L., Wang, H., Tang, J., Wang, M., Qi, C., Li, H., Lai, Y., Xia, W., and Tang, A. (2017). A study of Epstein-Barr virus infection in the Chinese tree shrew(Tupaia belangeri chinensis). Virol J *14*, 193. 10.1186/s12985-017-0859-5.
78. Xiao, J., Liu, R., and Chen, C.S. (2017). Tree shrew (Tupaia belangeri) as a novel laboratory disease animal model. Zool Res *38*, 127-137. 10.24272/j.issn.2095-8137.2017.033.
79. Thorley-Lawson, D.A., and Poodry, C.A. (1982). Identification and isolation of the main component (gp350-gp220) of Epstein-Barr virus responsible for generating neutralizing antibodies in vivo. Journal of virology *43*, 730-736.
80. Xiao, J., Palefsky, J.M., Herrera, R., Sunshine, C., and Tugizov, S.M. (2009). EBV-positive human sera contain antibodies against the EBV BMRF-2 protein. Virology *393*, 151-159. 10.1016/j.virol.2009.07.025.
81. Bu, W., Joyce, M.G., Nguyen, H., Banh, D.V., Aguilar, F., Tariq, Z., Yap, M.L., Tsujimura, Y., Gillespie, R.A., Tsybovsky, Y., et al. (2019). Immunization with Components of the Viral Fusion

Apparatus Elicits Antibodies That Neutralize Epstein-Barr Virus in B Cells and Epithelial Cells. Immunity *50*, 1305-1316.e1306. 10.1016/j.immuni.2019.03.010.

82. Sashihara, J., Burbelo, P.D., Savoldo, B., Pierson, T.C., and Cohen, J.I. (2009). Human antibody titers to Epstein-Barr Virus (EBV) gp350 correlate with neutralization of infectivity better than antibody titers to EBV gp42 using a rapid flow cytometry-based EBV neutralization assay. Virology *391*, 249-256. 10.1016/j.virol.2009.06.013.
83. Miller, G., Niederman, J.C., and Stitt, D.A. (1972). Infectious mononucleosis: appearance of neutralizing antibody to Epstein-Barr virus measured by inhibition of formation of lymphoblastoid cell lines. The Journal of infectious diseases *125*, 403-406.
84. Moss, D.J., and Pope, J.H. (1972). Assay of the infectivity of Epstein-Barr virus by transformation of human leucocytes in vitro. The Journal of general virology *17*, 233-236. 10.1099/0022-1317-17-2-233.
85. Sitki-Green, D., Covington, M., and Raab-Traub, N. (2003). Compartmentalization and Transmission of Multiple Epstein-Barr Virus Strains in Asymptomatic Carriers. Journal of Virology *77*, 1840-1847. 10.1128/jvi.77.3.1840-1847.2003.
86. Brooks, J.M., Croom-Carter, D.S.G., Leese, A.M., Tierney, R.J., Habeshaw, G., and Rickinson, A.B. (2000). Cytotoxic T-Lymphocyte Responses to a Polymorphic Epstein-Barr Virus Epitope Identify Healthy Carriers with Coresident Viral Strains. Journal of Virology *74*, 1801-1809. 10.1128/jvi.74.4.1801-1809.2000.
87. Kwok, H., Chan, K.W., Chan, K.H., and Chiang, A.K.S. (2015). Distribution, Persistence and Interchange of Epstein-Barr Virus Strains among PBMC, Plasma and Saliva of Primary Infection Subjects. PloS one *10*, e0120710. 10.1371/journal.pone.0120710.
88. Weiss, E.R., Lamers, S.L., Henderson, J.L., Melnikov, A., Somasundaran, M., Garber, M., Selin, L., Nusbaum, C., and Luzuriaga, K. (2018). Early Epstein-Barr Virus Genomic Diversity and Convergence toward the B95.8 Genome in Primary Infection. Journal of Virology *92*. 10.1128/jvi.01466-17.
89. Renzette, N., Somasundaran, M., Brewster, F., Coderre, J., Weiss, E.R., McManus, M., Greenough, T., Tabak, B., Garber, M., Kowalik, T.F., and Luzuriaga, K. (2014). Epstein-Barr Virus Latent Membrane Protein 1 Genetic Variability in Peripheral Blood B Cells and Oropharyngeal Fluids. Journal of Virology *88*, 3744-3755. 10.1128/jvi.03378-13.
90. Bu, W., Hayes, G.M., Liu, H., Gemmell, L., Schmeling, D.O., Radecki, P., Aguilar, F., Burbelo, P.D., Woo, J., Balfour, H.H., and Cohen, J.I. (2016). Kinetics of Epstein-Barr Virus (EBV) Neutralizing and Virus-Specific Antibodies after Primary Infection with EBV. Clinical and Vaccine Immunology *23*, 363-369. 10.1128/cvi.00674-15.
91. Biggar, R.J., Henle, W., Fleisher, G., Böcker, J., Lennette, E.T., and Henle, G. (1978). Primary epstein-barr virus infections in african infants. I. Decline of maternal antibodies and time of infection. International Journal of Cancer *22*, 239-243. 10.1002/ijc.2910220304.
92. Piriou, E., Asito, A.S., Sumba, P.O., Fiore, N., Middeldorp, J.M., Moormann, A.M., Ploutz-Snyder, R., and Rochford, R. (2012). Early Age at Time of Primary Epstein–Barr Virus Infection Results in Poorly Controlled Viral Infection in Infants From Western Kenya: Clues to the Etiology of Endemic Burkitt Lymphoma. The Journal of Infectious Diseases *205*, 906-913. 10.1093/infdis/jir872.
93. Rickinson, A.B., and Fox, C.P. (2012). Epstein–Barr Virus and Infectious Mononucleosis: What Students Can Teach Us. The Journal of Infectious Diseases *207*, 6-8. 10.1093/infdis/jis647.
94. Chan, K.H., Tam, J.S.L., Peiris, J.S.M., Seto, W.H., and Ng, M.H. (2001). Epstein–Barr virus (EBV) infection in infancy. Journal of Clinical Virology *21*, 57-62. 10.1016/s1386-6532(01)00149-4.
95. Slyker, J.A., Casper, C., Tapia, K., Richardson, B., Bunts, L., Huang, M.-L., Maleche-Obimbo, E., Nduati, R., and John-Stewart, G. (2013). Clinical and Virologic Manifestations of Primary Epstein-

Barr Virus (EBV) Infection in Kenyan Infants Born to HIV-Infected Women. The Journal of Infectious Diseases *207*, 1798-1806. 10.1093/infdis/jit093.

96. Thorley-Lawson, D.A., and Geilinger, K. (1980). Monoclonal antibodies against the major glycoprotein (gp350/220) of Epstein-Barr virus neutralize infectivity. Proceedings of the National Academy of Sciences of the United States of America *77*, 5307-5311.
97. Pearson, G., Dewey, F., Klein, G., Henle, G., and Henle, W. (1970). Relation between neutralization of Epstein-Barr virus and antibodies to cell-membrane antigens-induced by the virus. Journal of the National Cancer Institute *45*, 989-995.
98. North, J.R., Morgan, A.J., and Epstein, M.A. (1980). Observations on the EB virus envelope and virus-determined membrane antigen (MA) polypeptides. International journal of cancer. Journal international du cancer *26*, 231-240.
99. Sokal, E.M., Hoppenbrouwers, K., Vandermeulen, C., Moutschen, M., Leonard, P., Moreels, A., Haumont, M., Bollen, A., Smets, F., and Denis, M. (2007). Recombinant gp350 vaccine for infectious mononucleosis: a phase 2, randomized, double-blind, placebo-controlled trial to evaluate the safety, immunogenicity, and efficacy of an Epstein-Barr virus vaccine in healthy young adults. The Journal of infectious diseases *196*, 1749-1753. 10.1086/523813.
100. Molesworth, S.J., Lake, C.M., Borza, C.M., Turk, S.M., and Hutt-Fletcher, L.M. (2000). Epstein-Barr virus gH is essential for penetration of B cells but also plays a role in attachment of virus to epithelial cells. Journal of virology *74*, 6324-6332.
101. Turk, S.M., Jiang, R., Chesnokova, L.S., and Hutt-Fletcher, L.M. (2006). Antibodies to gp350/220 enhance the ability of Epstein-Barr virus to infect epithelial cells. Journal of virology *80*, 9628-9633. 10.1128/JVI.00622-06.
102. Hoffman, G.J., Lazarowitz, S.G., and Hayward, S.D. (1980). Monoclonal antibody against a 250,000-dalton glycoprotein of Epstein-Barr virus identifies a membrane antigen and a neutralizing antigen. Proceedings of the National Academy of Sciences of the United States of America *77*, 2979-2983.
103. Tanner, J., Whang, Y., Sample, J., Sears, A., and Kieff, E. (1988). Soluble gp350/220 and deletion mutant glycoproteins block Epstein-Barr virus adsorption to lymphocytes. J Virol *62*, 4452-4464. 10.1128/JVI.62.12.4452-4464.1988.
104. Mutsvunguma, L.Z., Rodriguez, E., Escalante, G.M., Muniraju, M., Williams, J.C., Warden, C., Qin, H., Wang, J., Wu, X., Barasa, A., et al. (2019). Identification of multiple potent neutralizing and non-neutralizing antibodies against Epstein-Barr virus gp350 protein with potential for clinical application and as reagents for mapping immunodominant epitopes. Virology *536*, 1-15. 10.1016/j.virol.2019.07.026.
105. Szakonyi, G., Klein, M.G., Hannan, J.P., Young, K.A., Ma, R.Z., Asokan, R., Holers, V.M., and Chen, X.S. (2006). Structure of the Epstein-Barr virus major envelope glycoprotein. Nat Struct Mol Biol *13*, 996-1001. 10.1038/nsmb1161.
106. Busse, C., Feederle, R., Schnölzer, M., Behrends, U., Mautner, J., and Delecluse, H.J. (2010). Epstein-Barr viruses that express a CD21 antibody provide evidence that gp350's functions extend beyond B-cell surface binding. J Virol *84*, 1139-1147. 10.1128/JVI.01953-09.
107. Mühe, J., Aye, P.P., Quink, C., Eng, J.Y., Engelman, K., Reimann, K.A., and Wang, F. (2021). Neutralizing antibodies against Epstein-Barr virus infection of B cells can protect from oral viral challenge in the rhesus macaque animal model. Cell reports. Medicine *2*, 100352. 10.1016/j.xcrm.2021.100352.
108. Sashihara, J., Hoshino, Y., Bowman, J.J., Krogmann, T., Burbelo, P.D., Coffield, V.M., Kamrud, K., and Cohen, J.I. (2011). Soluble rhesus lymphocryptovirus gp350 protects against infection and reduces viral loads in animals that become infected with virus after challenge. PLoS pathogens *7*, e1002308. 10.1371/journal.ppat.1002308.

109. Cohen, J.I., Mocarski, E.S., Raab-Traub, N., Corey, L., and Nabel, G.J. (2013). The need and challenges for development of an Epstein-Barr virus vaccine. Vaccine *31 Suppl 2*, B194-196. 10.1016/j.vaccine.2012.09.041.
110. Chesnokova, L.S., and Hutt-Fletcher, L.M. (2011). Fusion of Epstein-Barr virus with epithelial cells can be triggered by αvβ5 in addition to αvβ6 and αvβ8, and integrin binding triggers a conformational change in glycoproteins gHgL. J Virol *85*, 13214-13223. 10.1128/JVI.05580-11.
111. Sathiyamoorthy, K., Jiang, J., Möhl, B.S., Chen, J., Zhou, Z.H., Longnecker, R., and Jardetzky, T.S. (2017). Inhibition of EBV-mediated membrane fusion by anti-gHgL antibodies. Proceedings of the National Academy of Sciences *114*, E8703-E8710. 10.1073/pnas.1704661114.
112. Snijder, J., Ortego, M.S., Weidle, C., Stuart, A.B., Gray, M.D., McElrath, M.J., Pancera, M., Veesler, D., and McGuire, A.T. (2018). An Antibody Targeting the Fusion Machinery Neutralizes Dual-Tropic Infection and Defines a Site of Vulnerability on Epstein-Barr Virus. Immunity *48*, 799-811.e799. 10.1016/j.immuni.2018.03.026.
113. Sathiyamoorthy, K., Hu, Y.X., Mohl, B.S., Chen, J., Longnecker, R., and Jardetzky, T.S. (2016). Structural basis for Epstein-Barr virus host cell tropism mediated by gp42 and gHgL entry glycoproteins. Nature communications *7*, 13557. 10.1038/ncomms13557.
114. Li, Q., Turk, S.M., and Hutt-Fletcher, L.M. (1995). The Epstein-Barr virus (EBV) BZLF2 gene product associates with the gH and gL homologs of EBV and carries an epitope critical to infection of B cells but not of epithelial cells. J Virol *69*, 3987-3994. 10.1128/JVI.69.7.3987-3994.1995.
115. Kanekiyo, M., Joyce, M.G., Gillespie, R.A., Gallagher, J.R., Andrews, S.F., Yassine, H.M., Wheatley, A.K., Fisher, B.E., Ambrozak, D.R., Creanga, A., et al. (2019). Mosaic nanoparticle display of diverse influenza virus hemagglutinins elicits broad B cell responses. Nature immunology *20*, 362-372. 10.1038/s41590-018-0305-x.
116. Walls, A.C., Miranda, M.C., Schäfer, A., Pham, M.N., Greaney, A., Arunachalam, P.S., Navarro, M.J., Tortorici, M.A., Rogers, K., O'Connor, M.A., et al. (2021). Elicitation of broadly protective sarbecovirus immunity by receptor-binding domain nanoparticle vaccines. Cell *184*, 5432-5447.e5416. 10.1016/j.cell.2021.09.015.
117. Boyoglu-Barnum, S., Ellis, D., Gillespie, R.A., Hutchinson, G.B., Park, Y.J., Moin, S.M., Acton, O.J., Ravichandran, R., Murphy, M., Pettie, D., et al. (2021). Quadrivalent influenza nanoparticle vaccines induce broad protection. Nature *592*, 623-628. 10.1038/s41586-021-03365-x.
118. Marcandalli, J., Fiala, B., Ols, S., Perotti, M., de van der Schueren, W., Snijder, J., Hodge, E., Benhaim, M., Ravichandran, R., Carter, L., et al. (2019). Induction of Potent Neutralizing Antibody Responses by a Designed Protein Nanoparticle Vaccine for Respiratory Syncytial Virus. Cell *176*, 1420-1431.e1417. 10.1016/j.cell.2019.01.046.
119. Brouwer, P.J.M., Antanasijevic, A., Berndsen, Z., Yasmeen, A., Fiala, B., Bijl, T.P.L., Bontjer, I., Bale, J.B., Sheffler, W., Allen, J.D., et al. (2019). Enhancing and shaping the immunogenicity of native-like HIV-1 envelope trimers with a two-component protein nanoparticle. Nat Commun *10*, 4272. 10.1038/s41467-019-12080-1.
120. Jardine, J., Julien, J.P., Menis, S., Ota, T., Kalyuzhniy, O., McGuire, A., Sok, D., Huang, P.S., MacPherson, S., Jones, M., et al. (2013). Rational HIV immunogen design to target specific germline B cell receptors. Science *340*, 711-716. 10.1126/science.1234150.
121. Jelínková, L., Jhun, H., Eaton, A., Petrovsky, N., Zavala, F., and Chackerian, B. (2021). An epitope-based malaria vaccine targeting the junctional region of circumsporozoite protein. NPJ Vaccines *6*, 13. 10.1038/s41541-020-00274-4.
122. Moon, J.J., Suh, H., Li, A.V., Ockenhouse, C.F., Yadava, A., and Irvine, D.J. (2012). Enhancing humoral responses to a malaria antigen with nanoparticle vaccines that expand Tfh cells and

promote germinal center induction. Proc Natl Acad Sci U S A *109*, 1080-1085. 10.1073/pnas.1112648109.

123. Bachmann, M.F., and Jennings, G.T. (2010). Vaccine delivery: a matter of size, geometry, kinetics and molecular patterns. Nat Rev Immunol *10*, 787-796. 10.1038/nri2868.
124. Irvine, D.J., Swartz, M.A., and Szeto, G.L. (2013). Engineering synthetic vaccines using cues from natural immunity. Nat Mater *12*, 978-990. 10.1038/nmat3775.
125. Irvine, D.J., and Read, B.J. (2020). Shaping humoral immunity to vaccines through antigen-displaying nanoparticles. Curr Opin Immunol *65*, 1-6. 10.1016/j.coi.2020.01.007.
126. Khan, G., and Hashim, M.J. (2014). Global burden of deaths from Epstein-Barr virus attributable malignancies 1990-2010. Infectious agents and cancer *9*, 38. 10.1186/1750-9378-9-38.
127. Correnti, C.E., Hallinan, J.P., Doyle, L.A., Ruff, R.O., Jaeger-Ruckstuhl, C.A., Xu, Y., Shen, B.W., Qu, A., Polkinghorn, C., Friend, D.J., et al. (2020). Engineering and functionalization of large circular tandem repeat protein nanoparticles. Nat Struct Mol Biol *27*, 342-350. 10.1038/s41594-020-0397-5.
128. Ogun, S.A., Dumon-Seignovert, L., Marchand, J.B., Holder, A.A., and Hill, F. (2008). The oligomerization domain of C4-binding protein (C4bp) acts as an adjuvant, and the fusion protein comprised of the 19-kilodalton merozoite surface protein 1 fused with the murine C4bp domain protects mice against malaria. Infection and immunity *76*, 3817-3823. 10.1128/IAI.01369-07.
129. Kanekiyo, M., Bu, W., Joyce, M.G., Meng, G., Whittle, J.R., Baxa, U., Yamamoto, T., Narpala, S., Todd, J.P., Rao, S.S., et al. (2015). Rational Design of an Epstein-Barr Virus Vaccine Targeting the Receptor-Binding Site. Cell *162*, 1090-1100. 10.1016/j.cell.2015.07.043.
130. Hsia, Y., Bale, J.B., Gonen, S., Shi, D., Sheffler, W., Fong, K.K., Nattermann, U., Xu, C., Huang, P.S., Ravichandran, R., et al. (2016). Design of a hyperstable 60-subunit protein dodecahedron. [corrected]. Nature *535*, 136-139. 10.1038/nature18010.
131. Bandaranayake, A.D., Correnti, C., Ryu, B.Y., Brault, M., Strong, R.K., and Rawlings, D.J. (2011). Daedalus: a robust, turnkey platform for rapid production of decigram quantities of active recombinant proteins in human cell lines using novel lentiviral vectors. Nucleic acids research *39*, e143. 10.1093/nar/gkr706.
132. Li, Q.X., Young, L.S., Niedobitek, G., Dawson, C.W., Birkenbach, M., Wang, F., and Rickinson, A.B. (1992). Epstein–Barr virus infection and replication in a human epithelial cell system. Nature *356*, 347-350. 10.1038/356347a0.
133. Yajima, M., Imadome, K.I., Nakagawa, A., Watanabe, S., Terashima, K., Nakamura, H., Ito, M., Shimizu, N., Honda, M., Yamamoto, N., and Fujiwara, S. (2008). A New Humanized Mouse Model of Epstein-Barr Virus Infection That Reproduces Persistent Infection, Lymphoproliferative Disorder, and Cell-Mediated and Humoral Immune Responses. The Journal of Infectious Diseases *198*, 673-682. 10.1086/590502.
134. Yajima, M., Imadome, K., Nakagawa, A., Watanabe, S., Terashima, K., Nakamura, H., Ito, M., Shimizu, N., Yamamoto, N., and Fujiwara, S. (2009). T cell-mediated control of Epstein-Barr virus infection in humanized mice. The Journal of infectious diseases *200*, 1611-1615. 10.1086/644644.
135. Veneziano, R., Moyer, T.J., Stone, M.B., Wamhoff, E.C., Read, B.J., Mukherjee, S., Shepherd, T.R., Das, J., Schief, W.R., Irvine, D.J., and Bathe, M. (2020). Role of nanoscale antigen organization on B-cell activation probed using DNA origami. Nat Nanotechnol *15*, 716-723. 10.1038/s41565-020-0719-0.
136. Kato, Y., Abbott, R.K., Freeman, B.L., Haupt, S., Groschel, B., Silva, M., Menis, S., Irvine, D.J., Schief, W.R., and Crotty, S. (2020). Multifaceted Effects of Antigen Valency on B Cell Response Composition and Differentiation In Vivo. Immunity *53*, 548-563.e548. 10.1016/j.immuni.2020.08.001.

137. Arunachalam, P.S., Walls, A.C., Golden, N., Atyeo, C., Fischinger, S., Li, C., Aye, P., Navarro, M.J., Lai, L., Edara, V.V., et al. (2021). Adjuvanting a subunit COVID-19 vaccine to induce protective immunity. Nature *594*, 253-258. 10.1038/s41586-021-03530-2.
138. van Zyl, D.G., Mautner, J., and Delecluse, H.J. (2019). Progress in EBV Vaccines. Frontiers in oncology *9*, 104. 10.3389/fonc.2019.00104.
139. Fujiwara, S., Imadome, K.-I., and Takei, M. (2015). Modeling EBV infection and pathogenesis in new-generation humanized mice. Experimental & Molecular Medicine *47*, e135-e135. 10.1038/emm.2014.88.
140. Moghaddam, A., Rosenzweig, M., Lee-Parritz, D., Annis, B., Johnson, R.P., and Wang, F. (1997). An animal model for acute and persistent Epstein-Barr virus infection. Science *276*, 2030-2033.
141. Delecluse, H.-J., Hilsendegen, T., Pich, D., Zeidler, R., and Hammerschmidt, W. (1998). Propagation and recovery of intact, infectious Epstein-Barr virus from prokaryotic to human cells. Proceedings of the National Academy of Sciences *95*, 8245-8250. 10.1073/pnas.95.14.8245.
142. Mcguire, A.T., Gray, M.D., Dosenovic, P., Gitlin, A.D., Freund, N.T., Petersen, J., Correnti, C., Johnsen, W., Kegel, R., Stuart, A.B., et al. (2016). Specifically modified Env immunogens activate B-cell precursors of broadly neutralizing HIV-1 antibodies in transgenic mice. Nature Communications *7*, 10618. 10.1038/ncomms10618.
143. Veesler, D., Cupelli, K., Burger, M., Graber, P., Stehle, T., and Johnson, J.E. (2014). Single-particle EM reveals plasticity of interactions between the adenovirus penton base and integrin V 3. Proceedings of the National Academy of Sciences *111*, 8815-8819. 10.1073/pnas.1404575111.
144. Suloway, C., Pulokas, J., Fellmann, D., Cheng, A., Guerra, F., Quispe, J., Stagg, S., Potter, C.S., and Carragher, B. (2005). Automated molecular microscopy: The new Leginon system. Journal of Structural Biology *151*, 41-60. 10.1016/j.jsb.2005.03.010.
145. Punjani, A., Rubinstein, J.L., Fleet, D.J., and Brubaker, M.A. (2017). cryoSPARC: algorithms for rapid unsupervised cryo-EM structure determination. Nature Methods *14*, 290-296. 10.1038/nmeth.4169.
146. Lander, G.C., Stagg, S.M., Voss, N.R., Cheng, A., Fellmann, D., Pulokas, J., Yoshioka, C., Irving, C., Mulder, A., Lau, P.-W., et al. (2009). Appion: An integrated, database-driven pipeline to facilitate EM image processing. Journal of Structural Biology *166*, 95-102. 10.1016/j.jsb.2009.01.002.
147. Mindell, J.A., and Grigorieff, N. (2003). Accurate determination of local defocus and specimen tilt in electron microscopy. Journal of Structural Biology *142*, 334-347. 10.1016/s1047-8477(03)00069-8.
148. Voss, N.R., Yoshioka, C.K., Radermacher, M., Potter, C.S., and Carragher, B. (2009). DoG Picker and TiltPicker: Software tools to facilitate particle selection in single particle electron microscopy. Journal of Structural Biology *166*, 205-213. 10.1016/j.jsb.2009.01.004.
149. Ludtke, S.J., Baldwin, P.R., and Chiu, W. (1999). EMAN: Semiautomated Software for High-Resolution Single-Particle Reconstructions. Journal of Structural Biology *128*, 82-97. 10.1006/jsbi.1999.4174.
150. Kimanius, D., Forsberg, B.O., Scheres, S.H., and Lindahl, E. (2016). Accelerated cryo-EM structure determination with parallelisation using GPUs in RELION-2. eLife *5*. 10.7554/elife.18722.
151. Scheres, S.H.W. (2012). A Bayesian View on Cryo-EM Structure Determination. Journal of Molecular Biology *415*, 406-418. 10.1016/j.jmb.2011.11.010.
152. Scheres, S.H.W. (2012). RELION: Implementation of a Bayesian approach to cryo-EM structure determination. Journal of Structural Biology *180*, 519-530. 10.1016/j.jsb.2012.09.006.
153. Pettersen, E.F., Goddard, T.D., Huang, C.C., Meng, E.C., Couch, G.S., Croll, T.I., Morris, J.H., and Ferrin, T.E. (2021). UCSF ChimeraX: Structure visualization for researchers, educators, and developers. Protein Science *30*, 70-82. 10.1002/pro.3943.

154. Carter, D., Fox, C.B., Day, T.A., Guderian, J.A., Liang, H., Rolf, T., Vergara, J., Sagawa, Z.K., Ireton, G., Orr, M.T., et al. (2016). A structure-function approach to optimizing TLR4 ligands for human vaccines. Clin Transl Immunology *5*, e108. 10.1038/cti.2016.63.
155. Neuhierl, B., Feederle, R., Hammerschmidt, W., and Delecluse, H.J. (2002). Glycoprotein gp110 of Epstein-Barr virus determines viral tropism and efficiency of infection. Proceedings of the National Academy of Sciences *99*, 15036-15041. 10.1073/pnas.232381299.
156. Kimura, H., Morita, M., Yabuta, Y., Kuzushima, K., Kato, K., Kojima, S., Matsuyama, T., and Morishima, T. (1999). Quantitative Analysis of Epstein-Barr Virus Load by Using a Real-Time PCR Assay. Journal of Clinical Microbiology *37*, 132-136. 10.1128/jcm.37.1.132-136.1999.
157. Balfour, H.H., Jr., Schmeling, D.O., and Grimm-Geris, J.M. (2020). The promise of a prophylactic Epstein-Barr virus vaccine. Pediatric research *87*, 345-352. 10.1038/s41390-019-0591-5.
158. Biggar, R.J., Henle, W., Fleisher, G., Bocker, J., Lennette, E.T., and Henle, G. (1978). Primary Epstein-Barr virus infections in African infants. I. Decline of maternal antibodies and time of infection. Int J Cancer *22*, 239-243.
159. Piriou, E., Asito, A.S., Sumba, P.O., Fiore, N., Middeldorp, J.M., Moormann, A.M., Ploutz-Snyder, R., and Rochford, R. (2012). Early age at time of primary Epstein-Barr virus infection results in poorly controlled viral infection in infants from Western Kenya: clues to the etiology of endemic Burkitt lymphoma. J Infect Dis *205*, 906-913. 10.1093/infdis/jir872.
160. Rickinson, A.B., and Fox, C.P. (2013). Epstein-Barr virus and infectious mononucleosis: what students can teach us. J Infect Dis *207*, 6-8. 10.1093/infdis/jis647.
161. Chan, K.H., Tam, J.S., Peiris, J.S., Seto, W.H., and Ng, M.H. (2001). Epstein-Barr virus (EBV) infection in infancy. J Clin Virol *21*, 57-62.
162. Slyker, J.A., Casper, C., Tapia, K., Richardson, B., Bunts, L., Huang, M.L., Maleche-Obimbo, E., Nduati, R., and John-Stewart, G. (2013). Clinical and virologic manifestations of primary Epstein-Barr virus (EBV) infection in Kenyan infants born to HIV-infected women. J Infect Dis *207*, 1798-1806. 10.1093/infdis/jit093.
163. Sitki-Green, D., Covington, M., and Raab-Traub, N. (2003). Compartmentalization and transmission of multiple epstein-barr virus strains in asymptomatic carriers. Journal of virology *77*, 1840-1847.
164. Brooks, J.M., Croom-Carter, D.S., Leese, A.M., Tierney, R.J., Habeshaw, G., and Rickinson, A.B. (2000). Cytotoxic T-lymphocyte responses to a polymorphic Epstein-Barr virus epitope identify healthy carriers with coresident viral strains. Journal of virology *74*, 1801-1809.
165. Kwok, H., Chan, K.W., Chan, K.H., and Chiang, A.K. (2015). Distribution, persistence and interchange of Epstein-Barr virus strains among PBMC, plasma and saliva of primary infection subjects. PloS one *10*, e0120710. 10.1371/journal.pone.0120710.
166. Tierney, R.J., Edwards, R.H., Sitki-Green, D., Croom-Carter, D., Roy, S., Yao, Q.Y., Raab-Traub, N., and Rickinson, A.B. (2006). Multiple Epstein-Barr virus strains in patients with infectious mononucleosis: comparison of ex vivo samples with in vitro isolates by use of heteroduplex tracking assays. The Journal of infectious diseases *193*, 287-297. 10.1086/498913.
167. Weiss, E.R., Lamers, S.L., Henderson, J.L., Melnikov, A., Somasundaran, M., Garber, M., Selin, L., Nusbaum, C., and Luzuriaga, K. (2018). Early Epstein-Barr Virus Genomic Diversity and Convergence toward the B95.8 Genome in Primary Infection. Journal of virology *92*. 10.1128/jvi.01466-17.
168. Smith, N.A., Baresel, P.C., Jackson, C.L., Ogolla, S., Toko, E.N., Heit, S., Piriou, E., Sumba, O.P., Middeldorp, J.M., Colborn, K.L., and Rochford, R. (2018). Differences in the Epstein-Barr Virus gp350 IgA Antibody Response Are Associated With Increased Risk for Coinfection With a Second Strain of Epstein-Barr Virus. The Journal of infectious diseases *219*, 955-963. 10.1093/infdis/jiy601.

169. Sathiyamoorthy, K., Chen, J., Longnecker, R., and Jardetzky, T.S. (2017). The COMPLEXity in herpesvirus entry. Current opinion in virology *24*, 97-104. 10.1016/j.coviro.2017.04.006.
170. Bu, W., Joyce, M.G., Nguyen, H., Banh, D.V., Aguilar, F., Tariq, Z., Yap, M.L., Tsujimura, Y., Gillespie, R.A., Tsybovsky, Y., et al. (2019). Immunization with Components of the Viral Fusion Apparatus Elicits Antibodies That Neutralize Epstein-Barr Virus in B Cells and Epithelial Cells. Immunity. 10.1016/j.immuni.2019.03.010.
171. Mascola, J.R., Stiegler, G., VanCott, T.C., Katinger, H., Carpenter, C.B., Hanson, C.E., Beary, H., Hayes, D., Frankel, S.S., Birx, D.L., and Lewis, M.G. (2000). Protection of macaques against vaginal transmission of a pathogenic HIV-1/SIV chimeric virus by passive infusion of neutralizing antibodies. Nature medicine *6*, 207-210.
172. Hessell, A.J., Hangartner, L., Hunter, M., Havenith, C.E., Beurskens, F.J., Bakker, J.M., Lanigan, C.M., Landucci, G., Forthal, D.N., Parren, P.W., et al. (2007). Fc receptor but not complement binding is important in antibody protection against HIV. Nature *449*, 101-104. 10.1038/nature06106.
173. Hessell, A.J., Poignard, P., Hunter, M., Hangartner, L., Tehrani, D.M., Bleeker, W.K., Parren, P.W., Marx, P.A., and Burton, D.R. (2009). Effective, low-titer antibody protection against low-dose repeated mucosal SHIV challenge in macaques. Nature medicine *15*, 951-954. nm.1974 [pii]

10.1038/nm.1974.
174. Parren, P.W., Marx, P.A., Hessell, A.J., Luckay, A., Harouse, J., Cheng-Mayer, C., Moore, J.P., and Burton, D.R. (2001). Antibody protects macaques against vaginal challenge with a pathogenic R5 simian/human immunodeficiency virus at serum levels giving complete neutralization in vitro. Journal of virology *75*, 8340-8347.
175. Wang, L., Shi, W., Chappell, J.D., Joyce, M.G., Zhang, Y., Kanekiyo, M., Becker, M.M., van Doremalen, N., Fischer, R., Wang, N., et al. (2018). Importance of neutralizing monoclonal antibodies targeting multiple antigenic sites on MERS-CoV Spike to avoid neutralization escape. Journal of virology. 10.1128/jvi.02002-17.
176. Shingai, M., Donau, O.K., Plishka, R.J., Buckler-White, A., Mascola, J.R., Nabel, G.J., Nason, M.C., Montefiori, D., Moldt, B., Poignard, P., et al. (2014). Passive transfer of modest titers of potent and broadly neutralizing anti-HIV monoclonal antibodies block SHIV infection in macaques. The Journal of experimental medicine *211*, 2061-2074. 10.1084/jem.20132494.
177. Magnani, D.M., Rogers, T.F., Beutler, N., Ricciardi, M.J., Bailey, V.K., Gonzalez-Nieto, L., Briney, B., Sok, D., Le, K., Strubel, A., et al. (2017). Neutralizing human monoclonal antibodies prevent Zika virus infection in macaques. Science translational medicine *9*. 10.1126/scitranslmed.aan8184.
178. Wang, K., Tomaras, G.D., Jegaskanda, S., Moody, M.A., Liao, H.X., Goodman, K.N., Berman, P.W., Rerks-Ngarm, S., Pitisuttithum, P., Nitayapan, S., et al. (2017). Monoclonal Antibodies, Derived from Humans Vaccinated with the RV144 HIV Vaccine Containing the HVEM Binding Domain of Herpes Simplex Virus (HSV) Glycoprotein D, Neutralize HSV Infection, Mediate Antibody-Dependent Cellular Cytotoxicity, and Protect Mice from Ocular Challenge with HSV-1. Journal of virology *91*. 10.1128/jvi.00411-17.
179. Renegar, K.B., and Small, P.A., Jr. (1991). Passive transfer of local immunity to influenza virus infection by IgA antibody. J Immunol *146*, 1972-1978.
180. Hessell, A.J., Rakasz, E.G., Poignard, P., Hangartner, L., Landucci, G., Forthal, D.N., Koff, W.C., Watkins, D.I., and Burton, D.R. (2009). Broadly neutralizing human anti-HIV antibody 2G12 is effective in protection against mucosal SHIV challenge even at low serum neutralizing titers. PLoS pathogens *5*, e1000433. 10.1371/journal.ppat.1000433 [doi].

181. Traggiai, E., Chicha, L., Mazzucchelli, L., Bronz, L., Piffaretti, J.C., Lanzavecchia, A., and Manz, M.G. (2004). Development of a human adaptive immune system in cord blood cell-transplanted mice. Science *304*, 104-107. 10.1126/science.1093933.
182. Yajima, M., Imadome, K., Nakagawa, A., Watanabe, S., Terashima, K., Nakamura, H., Ito, M., Shimizu, N., Honda, M., Yamamoto, N., and Fujiwara, S. (2008). A new humanized mouse model of Epstein-Barr virus infection that reproduces persistent infection, lymphoproliferative disorder, and cell-mediated and humoral immune responses. The Journal of infectious diseases *198*, 673-682. 10.1086/590502.
183. Fujiwara, S., Imadome, K., and Takei, M. (2015). Modeling EBV infection and pathogenesis in new-generation humanized mice. Experimental & molecular medicine *47*, e135. 10.1038/emm.2014.88.
184. Fujiwara, S., Matsuda, G., and Imadome, K. (2013). Humanized mouse models of epstein-barr virus infection and associated diseases. Pathogens (Basel, Switzerland) *2*, 153-176. 10.3390/pathogens2010153.
185. van Zyl, D.G., Tsai, M.-H., Shumilov, A., Schneidt, V., Poirey, R., Schlehe, B., Fluhr, H., Mautner, J., and Delecluse, H.-J. (2018). Immunogenic particles with a broad antigenic spectrum stimulate cytolytic T cells and offer increased protection against EBV infection ex vivo and in mice. PLoS pathogens *14*, e1007464-e1007464. 10.1371/journal.ppat.1007464.
186. Strowig, T., Gurer, C., Ploss, A., Liu, Y.F., Arrey, F., Sashihara, J., Koo, G., Rice, C.M., Young, J.W., Chadburn, A., et al. (2009). Priming of protective T cell responses against virus-induced tumors in mice with human immune system components. The Journal of experimental medicine *206*, 1423-1434. 10.1084/jem.20081720.
187. Haque, T., Johannessen, I., Dombagoda, D., Sengupta, C., Burns, D.M., Bird, P., Hale, G., Mieli-Vergani, G., and Crawford, D.H. (2006). A mouse monoclonal antibody against Epstein-Barr virus envelope glycoprotein 350 prevents infection both in vitro and in vivo. The Journal of infectious diseases *194*, 584-587. 10.1086/505912.
188. Rivailler, P., Jiang, H., Cho, Y.G., Quink, C., and Wang, F. (2002). Complete nucleotide sequence of the rhesus lymphocryptovirus: genetic validation for an Epstein-Barr virus animal model. Journal of virology *76*, 421-426.
189. Carville, A., and Mansfield, K.G. (2008). Comparative pathobiology of macaque lymphocryptoviruses. Comparative medicine *58*, 57-67.
190. Wu, L., and Hutt-Fletcher, L.M. (2007). Compatibility of the gH homologues of Epstein-Barr virus and related lymphocryptoviruses. The Journal of general virology *88*, 2129-2136. 10.1099/vir.0.82949-0.
191. Herrman, M., Muhe, J., Quink, C., and Wang, F. (2015). Epstein-Barr Virus gp350 Can Functionally Replace the Rhesus Lymphocryptovirus Major Membrane Glycoprotein and Does Not Restrict Infection of Rhesus Macaques. Journal of virology *90*, 1222-1230. 10.1128/JVI.02531-15.
192. Snijder, J., Ortego, M.S., Weidle, C., Stuart, A.B., Gray, M.D., McElrath, M.J., Pancera, M., Veesler, D., and McGuire, A.T. (2018). An Antibody Targeting the Fusion Machinery Neutralizes Dual-Tropic Infection and Defines a Site of Vulnerability on Epstein-Barr Virus. Immunity *48*, 799-811 e799. 10.1016/j.immuni.2018.03.026.
193. Wu, X., Yang, Z.Y., Li, Y., Hogerkorp, C.M., Schief, W.R., Seaman, M.S., Zhou, T., Schmidt, S.D., Wu, L., Xu, L., et al. (2010). Rational design of envelope identifies broadly neutralizing human monoclonal antibodies to HIV-1. Science *329*, 856-861. 10.1126/science.1187659.
194. Sathiyamoorthy, K., Jiang, J., Mohl, B.S., Chen, J., Zhou, Z.H., Longnecker, R., and Jardetzky, T.S. (2017). Inhibition of EBV-mediated membrane fusion by anti-gHgL antibodies. Proceedings of

the National Academy of Sciences of the United States of America *114*, E8703-e8710. 10.1073/pnas.1704661114.

195. Tiller, T., Busse, C.E., and Wardemann, H. (2009). Cloning and expression of murine Ig genes from single B cells. Journal of immunological methods *350*, 183-193. 10.1016/j.jim.2009.08.009.
196. Tangye, S.G., Palendira, U., and Edwards, E.S. (2017). Human immunity against EBV-lessons from the clinic. The Journal of experimental medicine *214*, 269-283. 10.1084/jem.20161846.
197. Omerovic, J., and Longnecker, R. (2007). Functional homology of gHs and gLs from EBV-related gamma-herpesviruses for EBV-induced membrane fusion. Virology *365*, 157-165. 10.1016/j.virol.2007.03.054.
198. Rao, P., Jiang, H., and Wang, F. (2000). Cloning of the rhesus lymphocryptovirus viral capsid antigen and Epstein-Barr virus-encoded small RNA homologues and use in diagnosis of acute and persistent infections. Journal of clinical microbiology *38*, 3219-3225.
199. Moutschen, M., Leonard, P., Sokal, E.M., Smets, F., Haumont, M., Mazzu, P., Bollen, A., Denamur, F., Peeters, P., Dubin, G., and Denis, M. (2007). Phase I/II studies to evaluate safety and immunogenicity of a recombinant gp350 Epstein-Barr virus vaccine in healthy adults. Vaccine *25*, 4697-4705. 10.1016/j.vaccine.2007.04.008.
200. Cui, X., Cao, Z., Chen, Q., Arjunaraja, S., Snow, A.L., and Snapper, C.M. (2016). Rabbits immunized with Epstein-Barr virus gH/gL or gB recombinant proteins elicit higher serum virus neutralizing activity than gp350. Vaccine *34*, 4050-4055. 10.1016/j.vaccine.2016.06.021.
201. Delecluse, H.J., Hilsendegen, T., Pich, D., Zeidler, R., and Hammerschmidt, W. (1998). Propagation and recovery of intact, infectious Epstein-Barr virus from prokaryotic to human cells. Proceedings of the National Academy of Sciences of the United States of America *95*, 8245-8250.
202. Kalla, M., Göbel, C., and Hammerschmidt, W. (2012). The lytic phase of epstein-barr virus requires a viral genome with 5-methylcytosine residues in CpG sites. Journal of virology *86*, 447-458. 10.1128/JVI.06314-11.
203. Pattabhi, S., Lotti, S.N., Berger, M.P., Singh, S., Lux, C.T., Jacoby, K., Lee, C., Negre, O., Scharenberg, A.M., and Rawlings, D.J. (2019). In Vivo Outcome of Homology-Directed Repair at the HBB Gene in HSC Using Alternative Donor Template Delivery Methods. Molecular therapy. Nucleic acids *17*, 277-288. 10.1016/j.omtn.2019.05.025.
204. Kimura, H., Morita, M., Yabuta, Y., Kuzushima, K., Kato, K., Kojima, S., Matsuyama, T., and Morishima, T. (1999). Quantitative analysis of Epstein-Barr virus load by using a real-time PCR assay. Journal of clinical microbiology *37*, 132-136.
205. McGuire, A.T., Gray, M.D., Dosenovic, P., Gitlin, A.D., Freund, N.T., Petersen, J., Correnti, C., Johnsen, W., Kegel, R., Stuart, A.B., et al. (2016). Specifically modified Env immunogens activate B-cell precursors of broadly neutralizing HIV-1 antibodies in transgenic mice. Nature communications *7*, 10618. 10.1038/ncomms10618.
206. Plate, A.E., Smajlovic, J., Jardetzky, T.S., and Longnecker, R. (2009). Functional analysis of glycoprotein L (gL) from rhesus lymphocryptovirus in Epstein-Barr virus-mediated cell fusion indicates a direct role of gL in gB-induced membrane fusion. Journal of virology *83*, 7678-7689. 10.1128/JVI.00457-09.
207. Okuma, K., Nakamura, M., Nakano, S., Niho, Y., and Matsuura, Y. (1999). Host range of human T-cell leukemia virus type I analyzed by a cell fusion-dependent reporter gene activation assay. Virology *254*, 235-244. 10.1006/viro.1998.9530.
208. Omerovic, J., Lev, L., and Longnecker, R. (2005). The amino terminus of Epstein-Barr virus glycoprotein gH is important for fusion with epithelial and B cells. Journal of virology *79*, 12408-12415. 10.1128/JVI.79.19.12408-12415.2005.

209. Nikitin, P.A., Yan, C.M., Forte, E., Bocedi, A., Tourigny, J.P., White, R.E., Allday, M.J., Patel, A., Dave, S.S., Kim, W., et al. (2010). An ATM/Chk2-mediated DNA damage-responsive signaling pathway suppresses Epstein-Barr virus transformation of primary human B cells. Cell host & microbe *8*, 510-522. 10.1016/j.chom.2010.11.004.
210. Muhe, J., and Wang, F. (2015). Host Range Restriction of Epstein-Barr Virus and Related Lymphocryptoviruses. Journal of virology *89*, 9133-9136. 10.1128/jvi.01235-15.